Development of a 2-Mode AWD E-REV Powertrain and Real-Time Optimization-Based Control System

by

Jeffrey James Waldner
B. Eng, University of Victoria, 2009

A Thesis Submitted in Partial Fulfillment
of the Requirements for the Degree of

MASTER OF APPLIED SCIENCE

in the Department of Mechanical Engineering

University of Victoria

Supervisory Committee

Development of a 2-Mode AWD E-REV Powertrain and Real-Time Optimization-Based Control System

by

Jeffrey James Waldner
B. Eng, University of Victoria, 2009

Supervisory Committee

Dr. Zuomin Dong (Department of Mechanical Engineering)
Supervisor

Dr. Curran Crawford (Department of Mechanical Engineering)
Member

Dr. Nick Dechev (Department of Mechanical Engineering)
Member

Abstract

Supervisory Committee

Dr. Zuomin Dong (Department of Mechanical Engineering)

Supervisor

Dr. Curran Crawford (Department of Mechanical Engineering)

Member

Dr. Nick Dechev (Department of Mechanical Engineering)

Member

Increasing environmental, economic, and political concerns regarding the consumption of fossil fuels have highlighted the need for more efficient and alternative energy solutions. Hybrid electric vehicles represent a near-term opportunity for reducing liquid fossil fuel consumption and green-house gas emissions in the transportation industry, and as a result, many automotive manufacturers have invested heavily in hybrid vehicle development. The increased complexity of hybrid electric vehicles over standard internal combustion engine-powered vehicles has subsequently placed significant emphasis on development of advanced control methods geared towards efficient energy management.

Real-time optimization-based methods represent the current state-of-the-art in terms of hybrid vehicle control and energy management. This thesis summarizes the development of an optimization-based real-time control system – which determines the optimal instantaneous system operating point, including gear, traction split between front rear axles, and engine speed and torque – and its application to an all-wheel drive extended-range electric vehicle that uses a General Motor's front-wheel drive 2-Mode electronic continuously variable transmission and an additional rear traction motor. The real-time

control system was developed and validated using a plant model and preliminarily tested in the vehicle using a four-wheel drive chassis dynamometer.

Results of simulation and in-vehicle testing demonstrate engine operation focused on high-efficiency operating regions and minimal use of the rear traction motor. Further testing revealed that a rule-based traction split system may be sufficient to replace the optimization-based traction split determination, and that the limited rear traction motor use was not a function of the motor itself, but rather an inherent result of the selected architecture.

Table of Contents

List of Tables

List of Figures

List of Abbreviations

AER
All-electric range

AWD
All-wheel drive

CAN
Controller Area Network

CS
Charge sustaining

CD
Charge depleting

DOE
US Department of Energy

DOF
Degrees of freedom

ECM
Equivalent circuit model

ECMS
Equivalent consumption minimization strategy

ECVT
Electric continuously variable transmission

EF
Equivalency factor

E-REV
Extended-range electric vehicle

ESS
Energy storage system

FD
Final drive or differential

FWD

Front-wheel drive

GM
General Motors

GHG
Greenhouse gas

HEV
Hybrid electric vehicle

HOS
Hybrid operating selection

ICE
Internal combustion engine

LFF
Liquid fossil fuels

MABX
dSPACE MicroAutoBox

MG
Electric motor/generator

PEC
Petroleum energy consumption

PHEV
Plug-in hybrid electric vehicle

PSD
Power-splitting device

RMS
Root-mean-square

RTM
Rear traction motor

SOC
State of charge

TPIM
Transmission power inverter module

UF
SAE J1711 Utility factor

VDP
Vehicle development process

WTW
Well-to-wheel

CHAPTER 1 Introduction

1.1. A Call for Action

Financial, environmental, supply, and other concerns regarding the use of fossil-fuels have risen to alarming prominence over the past decade. In 2009, the United States' net imports of crude oil and petroleum products reached 9.7 million barrels each day [1]. Increasing concerns over the availability of oil and political unrest in some oil producing countries has pushed the average cost of gasoline in the United States of America (US) up from $1.51 USD/gallon in 2000 to $2.79 USD/gallon in 2010, and the upward trend is continuing [2]. At the same time, mounting scientific evidence points to anthropogenic greenhouse gas (GHG) and other emissions as a likely cause of global climate change, rising sea levels, and several other troubling global issues [3].

The transportation sector consumed 74% of US petroleum resources in 2009 while renewable sources made up only 6% of transportation sector energy consumption [1]. As a result, this sector has been under increasing public and regulatory pressure to reduce petroleum energy consumption (PEC). In response, automotive manufacturers have placed significant resources into the development of hybrid and alternative fuel vehicles, which have the ability to significantly reduce fuel consumption.

1.2. The Hybrid Vehicle Solution

Traditional internal combustion engine (ICE) vehicles rely only on liquid fossil fuels (LFF) for propulsion. Because this single power source must supply the entirety of propulsive power for the vehicle, it is often required to operate in an inefficient manner for a significant amount time. Hybrid vehicles, which combine two or more power sources, can reduce petroleum fuel consumption through an appropriate, efficiency-based

blend of these multiple power sources, kinetic energy recovery methods such as regenerative braking, and/or direct displacement of petroleum fuel.

Though hybrid vehicles can use a variety of alternative energy sources, such as hydrogen, hybrid electric vehicles (HEVs) present the best opportunity for current use over other sources for several reasons including: pre-existing electrical infrastructure; existing electrical storage system (ESS) technology, especially with recent improvements such as lithium-ion batteries; and well-developed and efficient energy conversion devices (electric motors or MGs, for motor/generator).

Standard HEVs, which derive all net propulsive power from LFF and achieve increased efficiency through a blending approach, have been in development and in the consumer market for many years. For example, the Toyota Prius and Honda Insight were released in the late 1990s. Recently, and coinciding with the aforementioned improvements in ESS technology, next-generation hybrid vehicles such as plug-in hybrids (PHEVs) and extended-range electric vehicles (E-REVs) – which have the ability to displace LFF through onboard storage of electricity from the grid – as well as fully electric vehicles (EV) are under development. PHEVs typically have some all-electric capability, but frequently use a blended strategy to deliver propulsive power requests until ESS depletion. E-REVs are characterized by larger electric components, and are capable of full performance as an electric vehicle. Both vehicle types operate as a standard HEV upon ESS depletion. The portion of driving during which a PHEV or E-REV uses stored electrical energy, depleting the ESS to a low value, is called the charge depleting (CD) mode; subsequent operation is called charge sustaining (CS). The characteristics of various classes of hybrid vehicles are summarized in Table 1-1.

Table 1-1: Characteristics of Hybrid Vehicles

Class	Net Power Source	All-Electric Capability
HEV	LFF	Limited/None
PHEV	LFF/Electricity	Mild
E-REV	LFF/Electricity	Full
EV	Electricity	Full

The development of next generation hybrid vehicles was highlighted first by the release of PHEV conversion kits, such as the Hymotion kit developed by A123 Systems for the Toyota Prius, and more recently the release of the first consumer E-REV by GM in 2010, the Chevrolet Volt, which can operate for up to 60 km in electric-only mode.

1.3. Challenges in Hybrid Vehicle Development

The transition to hybrid vehicles represents a significant increase in vehicle complexity that affects all aspects of development. The vehicle design and powertrain selection process requires rigorous investigation and simulation in order to determine the most appropriate combination of ICE, MG(s), and ESS based on desired vehicle operating characteristics such as performance and fuel economy. The addition of electric drive components and the ESS increases packaging difficulty and the associated increase in mass affects vehicle dynamics and handling. Measures also have to be taken to ensure that high voltage electrical systems are safe and will remain so in the event of a crash.

Perhaps most importantly, advanced control systems are required not only to ensure smooth and effective blending of power from multiple powertrain sources, but also to take advantage of the flexibility of the hybrid powertrain in order to maximize system efficiency. This development area has received a significant amount of attention from both industry and academia due to its importance and complexity, and is the focus of this research.

1.4. EcoCAR: The NeXt Challenge

EcoCAR: The NeXt Challenge (EcoCAR Challenge) was a collegiate student design competition – held over the 2008-09, 2009-10, and 2010-11 academic years – that challenged teams from 16 universities across North America to re-engineer a donated vehicle into a hybrid, with the goals of improving fuel economy and minimizing vehicle emissions while retaining performance and consumer appeal. Sponsored primarily by the US Department of Energy (DOE) and General Motors (GM), and managed by the US DOE's Argonne National Laboratory, the ultimate goal of the program is to train the next generation of automotive engineers for careers in the hybrid vehicle industry.

The University of Victoria, British Columbia, Canada (UVic) was awarded participation in the program in 2008. Through this program, UVic developed an advanced, all-wheel drive (AWD) hybrid vehicle based on a form of the GM 2-Mode transmission, an electronic continuously variable transmission (ECVT) representing the cutting edge of commercially available hybrid technology. The car, which is the platform upon which this thesis focuses, is shown below competing at the EcoCAR Challenge final competition.

Figure 1-1: UVic EcoCAR Competing in EcoCAR Challenge Finals

In addition, through the EcoCAR program UVic established a state-of-the-art hybrid vehicle research and testing facility, and fostered a significant amount of graduate-level research on hybrid vehicle technology.

1.5. Research Problem

Increasingly complex hybrid vehicle powertrains require equally complex control systems in order to achieve optimal operation. The UVic EcoCAR vehicle is no exception: combining a large ESS with an ICE, 2-Mode transmission, and a large electric motor on the rear axle, it is an advanced hybrid vehicle with a flexible powertrain that offers significant opportunities for reduced fuel consumption using advanced control methods. The goals of this work are to:

1. Investigate current hybrid vehicle control strategies;
2. Summarize the UVic EcoCAR vehicle powertrain architecture, the architecture selection process, and UVic's progress through the vehicle development, including vehicle modeling and simulation;
3. Examine the operation and capabilities of the GM 2-Mode transmission in the context of the UVic EcoCAR vehicle;
4. Apply an advanced, real-time optimization-based control strategy to the UVic EcoCAR vehicle;
5. Examine the efficacy of the control strategy from the perspective of fuel economy, performance, drivability, and consumer acceptability; and
6. Perform initial in-vehicle testing to validate the operation of the control system.

The development of a real-time optimization strategy for the UVic EcoCAR vehicle is based on previous research at UVic involving a real-time optimization strategy for the 2-

Mode system alone [4]. This research expands the strategy for use in an AWD vehicle and addresses the issues associated with this expansion.

1.6. Organization of the Thesis

Chapter 2 discusses the primary hybrid vehicle powertrain component configurations, provides an overview of the UVic EcoCAR powertrain architecture selection process, and summarizes the literature regarding hybrid vehicle control strategies.

Chapter 3 provides an in-depth analysis of the UVic vehicle's most advanced powertrain component: the GM 2-Mode transmission.

Chapter 4 traces UVic's path through the vehicle development process and presents the simulation model used during algorithm development.

Chapter 5 discussed the organization and development of the selected real-time control strategy, as applied to the UVic EcoCAR vehicle, while Chapter 6 examines the algorithm in practice and the effects of varying algorithm parameters on fuel economy, performance, and drivability.

Finally, Chapter 7 compares the performance of the algorithm against vehicles using alternative powertrain control methods, and the last chapter provides a summary of this work and offers recommendations for future research and development.

CHAPTER 2 Background

2.1. Hybrid Vehicle Powertrain Architectures

There are several types of hybrid vehicle, though the most common and the focus of this research combines an ICE with one or more MG and an ESS. Though their classification in terms of electrification varies based on the size of the onboard ESS and MG(s), HEVs of all classifications are based on the architectures summarized in the following sections and take advantage of the following technologies to improve overall fuel efficiency:

- *Engine idle-stop* - Larger MGs provide more control over and faster ICE starting, as compared to standard ICE starters, thus allowing the ICE to be stopped at low vehicle speeds without affecting consumer acceptability or drive quality. The ESS can also supply auxiliary electrical loads more readily than the 12 volt battery found in conventional ICE vehicles.
- *Regenerative braking* - The MGs can recapture kinetic energy from the vehicle during deceleration events.
- *Efficient ICE operation* - The ICE can operate in more efficient regions by decoupling ICE speed and/or torque from axle speed and/or torque.

In general, PHEVs and EREVs are better equipped to take advantage of the latter two benefits as compared to standard HEVs; their larger ESSs are typically associated with not only more energy storage, but also larger power transfer capabilities. This means they are more capable of absorbing larger influxes of power during regenerative braking, and, for short periods of time if necessary, may also source more electric power – which improves flexibility in terms of ICE operation.

The primary hybrid vehicle powertrain component configurations/architectures are series, parallel, and power-split, which are discussed in turn below.

2.1.1. Series

Series HEVs provide fully electric vehicle propulsion using a traction MG and couple an ICE to a pure generator to source electric power. The series configuration is shown in Figure 2-1.

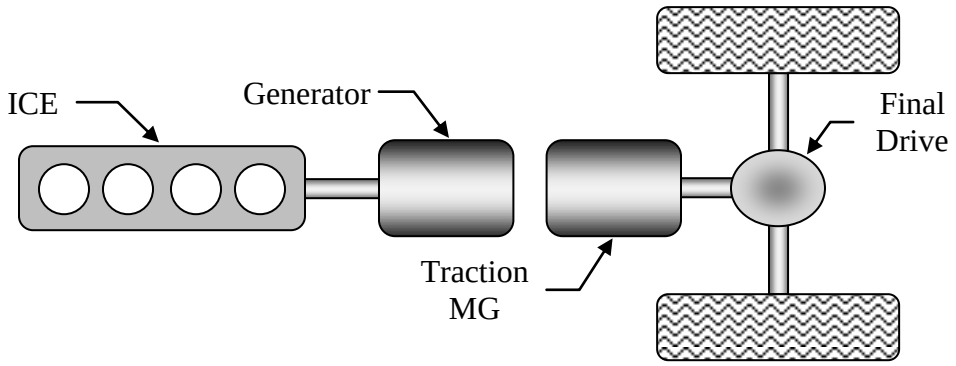

Figure 2-1: Series Configuration

The primary benefit of the series HEV is the ability to operate the ICE at its most optimal point at all times. Additionally, series HEVs offer simplified vehicle speed and torque control due to the use of a single propulsive torque source [5], and reduced packaging and integration complexity since the ICE and generator are mechanically independent from the remainder of the powertrain and a single-reduction transaxle coupling the traction MG to the wheels typically replaces a geared transmission.

However, series architectures have several significant drawbacks. Foremost, the lack of a mechanical power path to the wheels results in high electro-mechanical energy conversion losses, since all propulsive power is converted first from mechanical ICE power to electrical power, and then back again. Additionally, two MGs are needed, one

of which must be large enough to provide significant propulsive power. This often adds weight and significant cost to the vehicle. Finally, though the series architecture can be highly efficient for certain applications, its efficiency for high average power applications, such as propelling a vehicle up grades or at highway speeds, is notably low compared to other architectures [6].

Another point worth addressing is the common misconception that ICEs for series HEVs may be much smaller than for other configurations, which is not necessarily the case. Series vehicles do have a slight advantage in this regard over configurations that couple ICE speed to vehicle speed: since ICE speed in a series configuration is completely decoupled from vehicle speed, the ICE can operate at maximum power levels at any time regardless of vehicle speed. Conversely, the maximum power output of an ICE coupled to the drivetrain of a vehicle is a function of the vehicle's speed and the gear ratio of the transmission. However, in any standard HEV, or a PHEV or EREV with a depleted battery, the net power for a given trip is supplied by the ICE, since ESS state of charger (SOC) must be maintained. Therefore, assuming the need to maintain the utility of standard ICE vehicles, the ICE in any HEV must be sized to meet the maximum average required power output of the vehicle, say traveling up a grade for a long period of time [7]. Otherwise, there exists the risk of either depleting the ESS or stranding the driver on trips with high average power requirements. This limit places an absolute minimum on the ICE size for any HEV configuration, including the series configuration.

2.1.2. Parallel

Parallel HEVs have both an ICE and a MG mechanically coupled to the vehicle's drivetrain, a flexible arrangement which allows both sources to contribute to vehicle propulsion. The parallel configuration is shown in Figure 2-2.

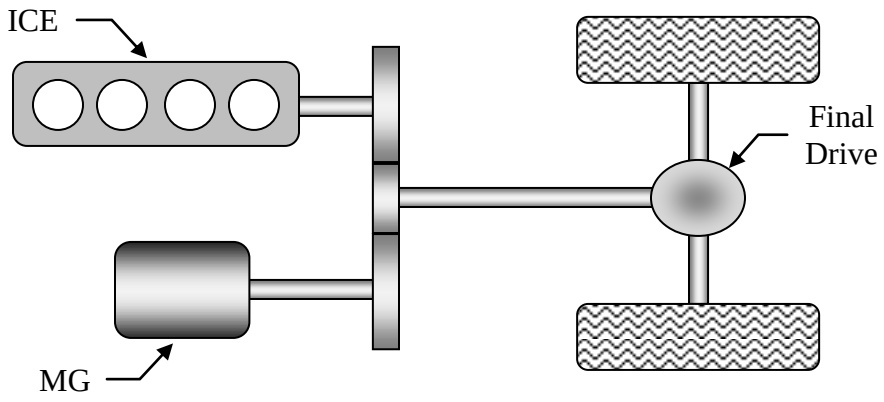

Figure 2-2: Parallel Configuration

Motor/generators in the parallel architecture come in a wide variety of sizes, down to so-called micro-parallel designs that include an MG of only a few kilowatts [6]. Parallel HEVs offer flexibility in terms of power management, as the MG, ICE, or both can deliver torque to the road, and the MG can act as a generator when necessary to maintain ESS SOC. Energy conversion losses are reduced as compared to the series architecture since both the MG and ICE are directly coupled to the powertrain, and parallel HEVs are also more efficient for higher average power applications than series configurations [6]. Furthermore, the use of only one MG in a parallel configuration reduces component costs, though the need for a transmission in a parallel configuration offsets any weight savings that are obtained through the use of only one MG.

Parallel HEVs are also not without drawbacks, the most notable being that ICE speed is coupled to vehicle speed; this significantly reduces the range of available operating

efficiencies of the ICE, which makes the power-split architecture more desirable. Additionally, if an all-electric mode is desired, the ICE must either be decoupled from the drivetrain or placed in a state where it can freewheel without significant losses. Finally, the multiple traction power sources and mechanical power path to the wheels require more complex integration and packaging, and more advanced control algorithms than a series architecture.

2.1.3. Power-split

Power-split HEVs, also called parallel/series HEVs, combine an ICE with two MGs and one or more power-splitting devices (PSDs), most often planetary gears, in such a way that results in a very flexible system. The 'split' terminology is derived from the fact that input/ICE power to the transmission is divided by a PSD between electrical and mechanical power paths within the transmission. An example of simple power-split configuration is shown in Figure 2-3.

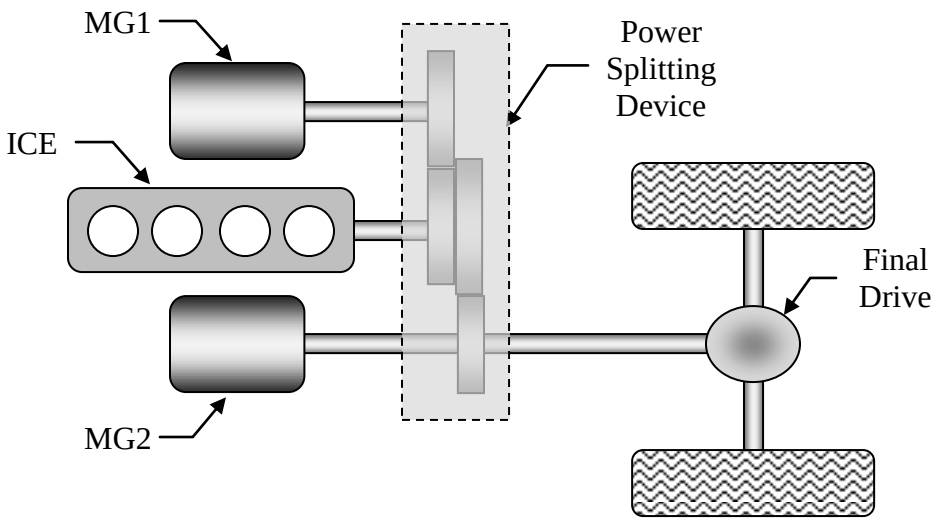

Figure 2-3: Powersplit Configuration

In general, power-split HEVs combine elements of series and parallel HEVs. The configuration of their electric powertrain components and PSD(s) result in an ECVT. An ECVT allows for the decoupling of both ICE speed and torque from vehicle speed and torque, thus providing the opportunity for increased ICE operating efficiency. There are numerous power-split architectures, as described by Wishart, Zhou, and Dong [6] and Miller [8], though they can be broadly classified as single-mode or multi-mode.

A single-mode ECVT uses one PSD that connects the ICE and MG1 to the transmission output, which is shared by MG2. In this configuration, MG1 converts a fraction of ICE power to electrical energy to be either stored in the ESS or used by MG2, while the remainder of ICE power is transferred to the transmission output. MG2 may add or subtract torque from the output to meet the power demands of the vehicle and/or ESS. At any given/constant output speed, the speed of MG1 and the ICE are linked; therefore, it is possible to control the speed of the ICE (preferably shifting it towards a region of higher efficiency) by controlling the speed of MG1. This is the configuration used in the Toyota Hybird System, now called Hybrid Synergy Drive.

At high vehicle speeds, however, and depending on PSD gear ratios and component operating parameters, single-mode architectures can suffer from low efficiency as a result of power recirculation. A description of the cause of this inefficiency is provided by Wishart *et al*. [6] and will also be discussed in §3.1. In order to address this issue, multi-mode power-split configurations were developed.

Multi-mode configurations build on the single mode configuration, but add one or more PSDs and also require the use of mechanical clutches to control the speeds of various components of the PSDs. The result of this increase in complexity is the ability to

operate in more than one continuously variable mode. The first mode (used at lower speeds) is virtually the same as the configuration described above, while the additional mode(s) improve overall transmission efficiency at higher vehicle speeds. This is the basis of 2-Mode technology, a dual mode ECVT configuration developed by GM.

A more detailed discussion of ECVTs and the GM 2-Mode transmission is given in Chapter 3.

2.2. UVic EcoCAR Powertrain Architecture Selection

The University of Victoria EcoCAR vehicle has been termed a 2-Mode Plus All-Wheel Drive E-REV. The vehicle and primary powertrain components are shown in Figure 2-4.

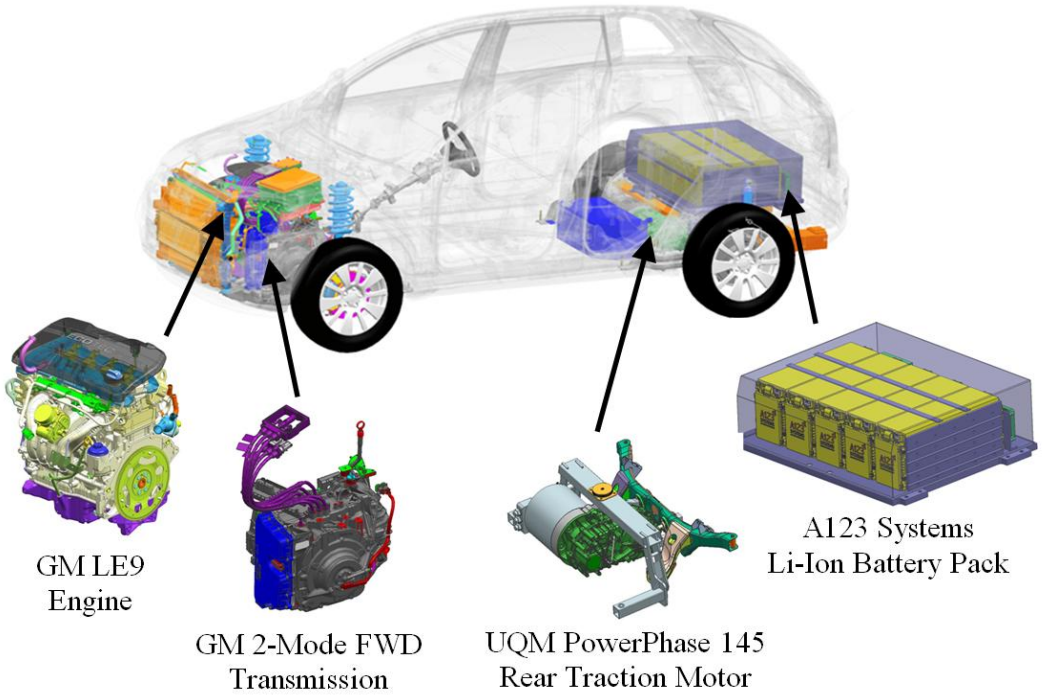

Figure 2-4: UVic EcoCAR Powertrain Components

Vehicle and powertrain component specifications are summarized in Table 2-1.

Table 2-1: UVic EcoCAR Vehicle and Powertrain Component Specifications

Component	Specifications
Vehicle	2009 Saturn VUE
GM 2-Mode FWD Trans	2 x 55 kW Electric Motors
GM 2.4L LE9 ICE (E85)	131 kW @ 5800 rpm 230 Nm @ 5000 rpm
UQM PowerPhase 145 RTM	145/85 kW (Peak/Cont) 400 Nm Peak
A123 Systems ESS	Lithium Iron Phosphate Chemistry 21.1 kWh 363 V

Selection was driven by the rules and scoring criteria of the competition, which are closely aligned to the goals of the automotive industry as a whole; mainly, reducing GHG emissions and petroleum energy consumption, and improving vehicle fuel economy without sacrificing performance and safety. To frame this discussion regarding architecture selection, Table 2-4 gives a breakdown of the percentage of points allocated to various metrics in the third year of competition.

Table 2-2: EcoCAR Challenge Scoring Summary

Event	Percentage of Total Points
Braking Distance	1.5
Towing Capability	1.5
Max Lane Change Speed	2.0
Autocross Event	2.5
Acceleration	4.0
Drive Quality	4.5
Dynamic Consumer Acceptability	5.0
Static Consumer Acceptability	9.0
Criteria Tailpipe Emissions	10.5
Fuel Economy	10.5
Petroleum Energy Consumption	10.5
WTW GHG Emissions	10.5
TOTAL (Driven Events)	**72**
Non-Driven Events	28

Events related to fuel economy and petroleum consumption make up 42% of points for the competition. These metrics can be heavily dependent on the architecture selected, and

underscore the need to select an architecture that offers the best opportunity to minimize fuel consumption. With this in mind, the following sections provide a high-level overview of architecture selection; more detailed information can be found in a published paper regarding the selection process [9].

It should be noted that while some external factors were considered, such as impacts on the electricity grid due to charging, the primary focus was meeting competition requirements while pushing the envelope of hybrid vehicle research. Therefore, several factors external to the performance of the vehicle, such as cost or the merits of various methods of production for alternative fuels, were not heavily weighted in selection.

2.2.1. Fuel Selection

An analysis was performed using GHGenius [10] to assess upstream GHG emissions of five fuels: 10% ethanol (E10, standard gasoline in North America), 85% ethanol (E85), 20% biodiesel (B20), hydrogen, and electricity. GHG emissions per kWh of electricity were provided by competition organizers, and were based on a weighted average of the Canadian and American electricity mix. Results of the analysis for each fuel, before energy conversion efficiencies, are summarized in Table 2-3.

Table 2-3: Fuel WTW GHG Emissions Analysis Results

Metric	E10	E85	B20	Hydrogen	Electricity
PEC (kWh petroleum per kWh)	99.31 %	23.32 %	86.42 %	1.47 %	7.85 %
Total GHG ($g\ CO^2$ per kWh)	304.96	234.66	248.32	397.50	699.18
Normalized PEC (vs Electricity)	12.65	2.97	11.01	0.57	1.0
Normalized GHGs (vs E85)	1.30	1.00	1.06	1.69	2.98

While hydrogen was included in the analysis, it was ruled out as a possible fuel due to a lack of infrastructure at UVic. Therefore, with B20 conversion efficiencies only slightly higher than for E85 and both fuels being essentially equal in terms of GHG emissions, E85 offered significant advantages in terms of PEC and was selected. Of note is that, while GHG values for electricity are high, electricity is converted to propulsive energy much more efficiently than liquid fuels.

2.2.2. The Utility Factor and Electrical Component Sizing

The utility factor (UF) is based on real-world data collected by the National Household Travel Survey of the US Department of Transportation [11] and defined by Society of Automotive Engineers (SAE) Standard J5841 [12]. The UF is a tool that can be used to determine the fuel economy of PHEVs using SAE Standard J1711 [13]. Essentially, the UF represents the fraction of drivers who on average drive a given distance or less each day. From the perspective of PHEVs and E-REVs, then, the UF may be interpreted as the fraction of drivers whose average daily driving needs would be satisfied by the respective CD range of the vehicle. The UF curve used in EcoCAR Challenge scoring is given in Figure 2-5.

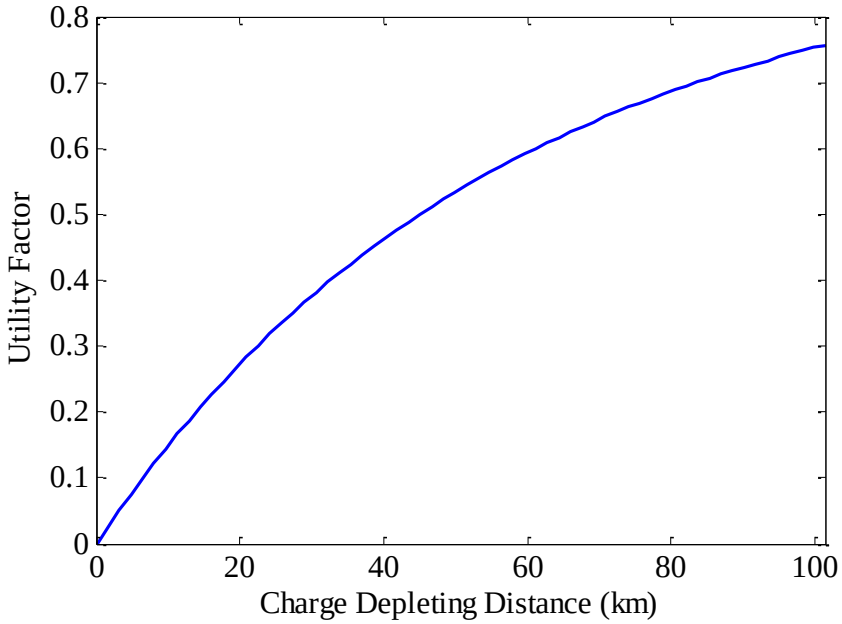

Figure 2-5: EcoCAR Challenge Utility Factor Curve

The calculation of fuel consumption (FC) is performed using Equation 2-1.

$$FC_{UF} = UF \times FC_{CD} + (1 - UF) \times FC_{CS} \qquad 2\text{-}1$$

Based on Equation 2-1 and the UF curve, a fully electric CD mode requiring a faster discharge of electrical energy will result in a lower net fuel economy than a CD mode requiring a slower discharge of electric energy combined with blended power from the ICE. To demonstrate, Figure 2-6 shows a theoretical example of UF-weighted fuel consumption for a vehicle with a possible 60 km all-electric range (AER) and a CS fuel economy of 8 L/100km that, instead of using a fully electric CD mode, uses a blended strategy to achieve various CD ranges.

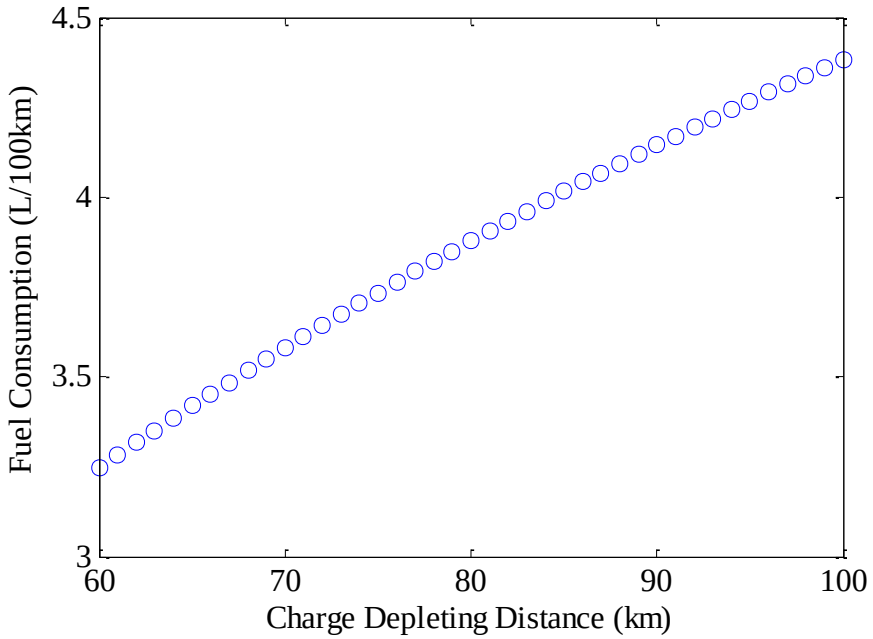

Figure 2-6: UF-Weighted Fuel Consumption with Increasing CD Distances

This analysis affects component selection in two ways: first, a true AER is desired, meaning that selected electrical components should be capable of providing full propulsive power to the vehicle; and, second, the ESS should both be capable of providing this power and be sufficiently large so as to achieve a high UF. Further analysis of ESS size versus fuel economy, PEC, and GHG emissions showed diminishing gains in fuel economy and PEC and increasing GHG emissions with increasing ESS sizes. This analysis, coupled with potential packaging and integration constraints, put a feasible limit of approximately 250 kg on battery size, assuming lithium-ion chemistry.

2.2.3. Powertrain Component Selection

An analysis of propulsive requirements for a 2009 Saturn VUE over three standard US Environmental Protection Agency drive cycles [14] that encompass city (Urban Dynamometer Driving Schedule, UDDS), highway (Highway Fuel Economy

Test, HWFET), and aggressive (US06) driving was conducted to determine vehicle propulsive power requirements. The results are shown in Table 2-4.

Table 2-4: Vehicle Power Requirements for Standard Drive Cycles

Drive Cycle	Avg/Peak Propulsive Power	Avg/Peak Braking Power
UDDS	10.02 kW / 45.2 kW	8.1 kW / 28.5 kW
HWFET	19.1 kW / 38.3 kW	9.9 kW / 38.6 kW
US06	33.3 kW / 118.2 kW	19.6 kW / 67.1 kW

Three different architectures were selected for further analysis using Argonne National Laboratory's Powertrain Systems Analysis Toolkit (PSAT) [15]: a 2-Mode plus rear traction motor (RTM) configuration, a rear-wheel drive series configuration, and a parallel belted alternator/starter with RTM configuration.

Ultimately, while all scored relatively on par with regards to performance, fuel economy and GHG emissions, the 2-Mode plus configuration was selected due to the 2-Mode's flexibility in terms of ICE operation and ability to blend high levels of electric and mechanical power. The 2-Mode system was further analyzed in PSAT with two different RTMs: UQM's PowerPhase 125 and 145. While both gave the vehicle the ability to complete all three standard drive cycles, the 145 kW MG was selected because it offered no decrease in efficiency with only a slight increase in size.

Several ICEs were also investigated, with the LE9 being selected due to its high operating efficiency, well-matched maximum efficiency power band, and its flex-fuel capabilities, meaning that no modifications were required in order for it to operate on E85.

Competition battery sponsor/supplier A123 Systems provided each team in the competition a choice between lithium-ion ESSs of either 21.3 kWh or 12.5 kWh. After negotiations with a Canadian battery manufacturer were unsuccessful, the 21.3 kWh, 360

V A123 ESS was selected. Weighing roughly 200 kg, with a maximum (10-second)/continuous output power of 192/63 kW, it not only met power output requirements necessary to achieve full all-electric performance on the US06 cycle, but also was on par with the aforementioned sizing analysis.

It was felt that this unique combination of components provided the UVic Team with a high-potential and flexible powertrain architecture and few limitations throughout the competition. In order to achieve this potential, an advanced control strategy was required; the following section examines various strategies used for HEV control.

2.3. Hybrid Vehicle Control Strategies

Managing energy transfer in increasingly complex and flexible hybrid power trains is a challenging task that has cultivated a significant amount of research. Many solutions of varying complexity have been developed, and were recently summarized several times [16-18]. The following sections present and discuss the most commonly used control strategies for hybrid vehicles.

Control strategies are generally classified in two broad groups: rule-based strategies and optimization-based strategies, each with two primary sub-groups, as shown in Figure 2-7.

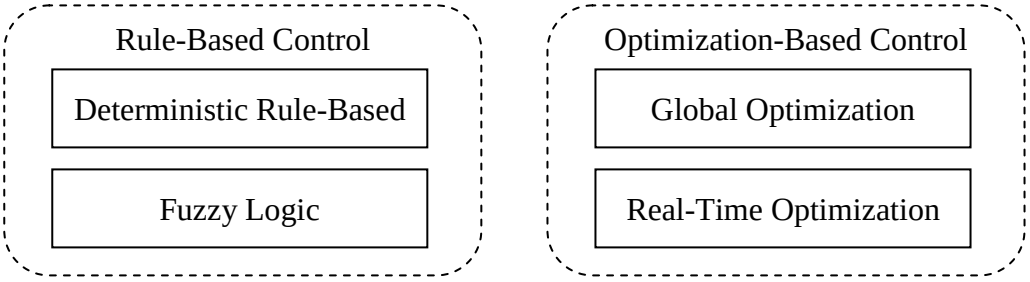

Figure 2-7: Common HEV Control Strategy Classifications

2.3.1. Rule-Based

Rule-based strategies rely on a pre-determined set of system operating guidelines typically informed by engineering intuition, performance requirements, system constraints, and/or mathematical models. While rules themselves can be inherently simple, 'if-then-else'-type commands for example, the system as a whole can become complex based on its requirements, which most likely include minimizing fuel consumption, and maximizing performance, drivability, safety, and component longevity.

One difficulty associated with rule-based systems is their typical inflexibility or inadaptability. While these systems can be tuned to achieve near-optimal efficiency on a given drive cycle, such tuning may cause them to fall far short of optimal operation on a different drive cycle. As such, rules must typically be relaxed and designed in such a way as to ensure desired operation across the full range of vehicle operating conditions. This relaxing of rules, though, may result in broadly sub-optimal performance as the rules may not focus on optimizing the complete drive train under the given operating conditions [18]. While fuzzy logic systems are more adaptable to change than deterministic systems, they too are based on pre-determined rules, and can suffer from the same faults as deterministic systems. Further description and several examples of each category are given below.

Deterministic

The simplest example of a deterministic operating strategy is termed 'thermostat control', whereby ESS SOC is maintained using ICE on/off control, and when on the ICE operates at its peak efficiency (imagine a saw-toothed SOC profile over time, with SOC falling when the ICE is off, and rising when on). This strategy is deficient in that it does

not match input and output power, which results in increased power transfer losses and decreased component lifetimes. More complex deterministic strategies essentially build on the thermostat concept with additional rules and operating conditions regarding ICE on/off logic and operation.

The most notable of these strategies is the power or load follower, used by early versions of the Toyota Prius and Honda Insight [16]. In this strategy the ICE provides net propulsive power, but is shifted to more favorable operating regions through the decoupling of ICE torque (and speed in the case of the Prius) from the wheels using a MG. Typically included in this strategy are a set of ICE operating rules based on the current state of the ESS and the vehicle power demand. Cheng *et al*. [19], for example, implemented a grid-based rule system for an ECVT-based hybrid that used various sets of rules based on the vehicle operating point. A representative grid is shown in Figure 2-8.

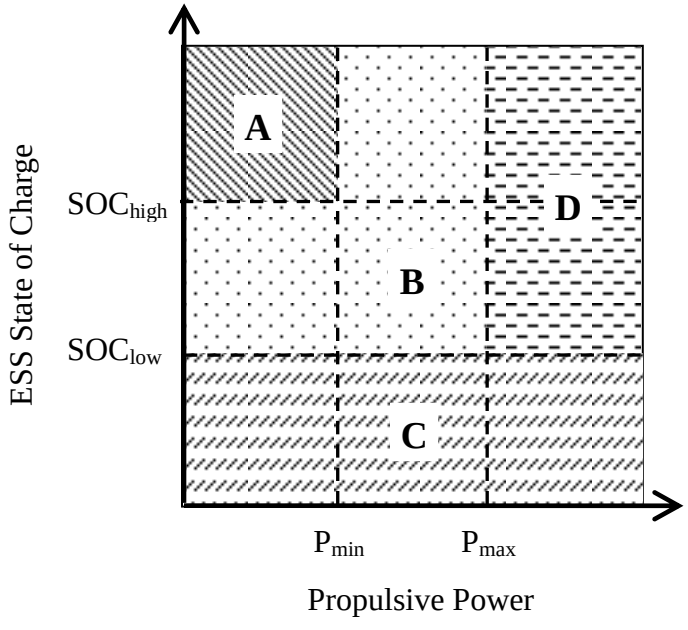

Figure 2-8: Example of Rule-Based ICE On/Off Control [19]

Regions of the grid are used to define ICE on/off logic, and ICE and MG operating rules within each section were developed based on prior knowledge of ICE operating efficiency. For example, in region A of Figure 2-8, which corresponds to low power demand and high SOC, the ICE is commanded off. In region C, the SOC is below the minimum threshold and the ICE must be operating to recharge the ESS. Based on this strategy, the authors report a 37% improvement in fuel economy over a conventional ICE-powered vehicle of the same body type.

Similarly, Chen *et al*. [20], developed a rule-based power blending control strategy for a four wheel drive series/parallel HEV (with all-electric rear traction), with a rule system based on ICE speed and vehicle power requirements; a replicated rule grid is given in Figure 2-9.

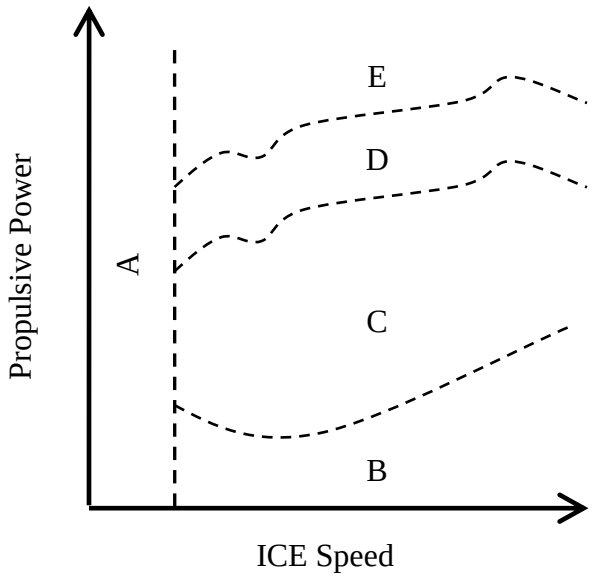

Figure 2-9: Example of Rule-Based Power Blending Strategy [20]

Once again, ICE operation is informed by knowledge of ICE operating efficiency. For example, in Area A of Figure 2-9 where ICE speed would be low, it remains off, while in

region C where ICE operation is most efficient, the vehicle is propelled by the ICE alone. This study reports a 14% increase in fuel economy over the matching conventional vehicle.

Fuzzy Logic

Fuzzy logic was developed as an alternative to classical logic in which objects or items have distinct membership or non-membership in a set. Items in a fuzzy set can have varying degrees of membership, as is the case often in the real world. A simple example from the MathWorks' fuzzy logic tutorial [21] is given in Figure 2-10.

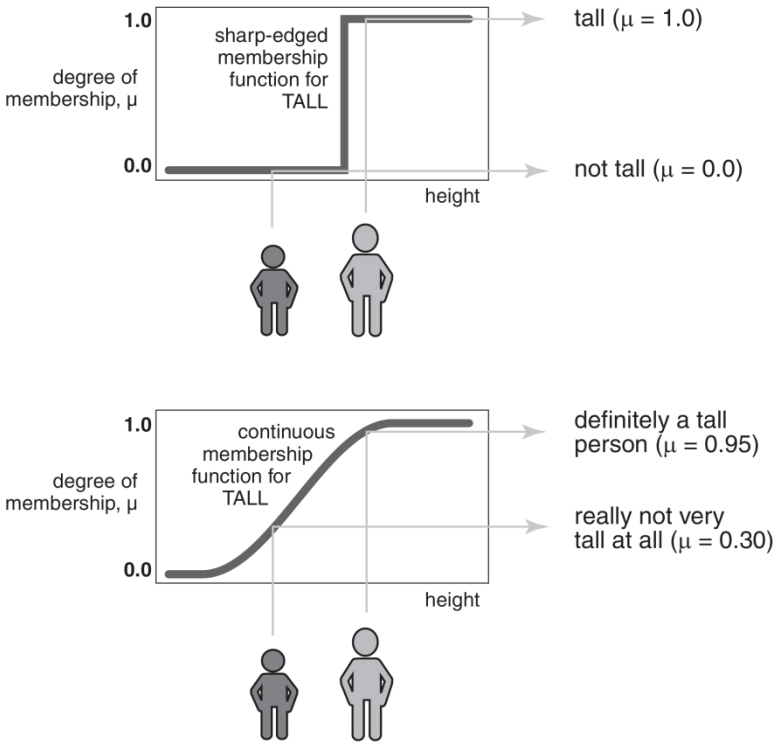

Figure 2-10: Membership in Deterministic (Top) and Fuzzy (Bottom) Sets [21]

Clearly, there is no strict divide between tall and not-tall people; analogously, many of the operating rules of an HEV do not necessarily need to be strict and the efficiency of the vehicle as a whole can be increased as a result of this relaxation or tolerance inherent

to fuzzy logic. In addition to this, a wide variety of membership functions are available, and a single fuzzy controller can have multiple inputs and outputs. Fuzzy logic systems are similar to rule-based systems in that the membership functions and actions in the system are typically based on user knowledge and experience; however, methods also exist that allow for the development or training of a fuzzy controller based on the use of captured input and output data, similar to the training of a neural network [22].

The use of fuzzy logic has additional benefits that include: adaptability to imprecise measurements or inputs and component variations; robustness in modeling and controlling non-linear systems; and the ability to modify membership functions on the fly in order to adapt to different situations [16, 18].

Examples of the application of fuzzy logic to HEV control systems resulting in increased fuel economy compared to a similar standard ICE-powered vehicle [23, 24] or similar HEVs with purely deterministic strategies [25, 26] are abundant, which firmly demonstrates the applicability of fuzzy logic systems to HEVs.

A good example of the capability of fuzzy logic and the various means by which controllers are constructed is the work done by Anderson *et al*. [27], who first developed a fuzzy controller for a power-split vehicle based on their own knowledge and experience, and then improved it by including mathematical models for fuel consumption. Using the 2005 Toyota Prius as a baseline vehicle, the authors developed a fuzzy controller that modulated the torque provided by the MGs based on the speed of the vehicle, the driver's torque demand, and the ESS SOC. The initial rule base was developed by intuition and tuned using simulation, but only achieved an unadjusted fuel economy on a standard drive cycle of 4.80 L/100 km, as compared to the 3.92 L/100 km

achieved by the Toyota Prius on the same cycle. In order to improve fuel economy, the authors introduced a mathematical rule-base that performed a simple optimization for ICE operation based on the ratio of available ESS energy to required tractive power, which they termed *E*. This modification yielded a fuel economy of 4.27 L/100 km: an improvement, but still not on par with the Toyota Prius. The term 'optimization' is used loosely here, as the authors were not optimizing component operation directly for fuel economy, but instead were doing so indirectly through the parameter *E*.

Though the results of the previous example did not meet the benchmark fuel consumption values of the Toyota Prius, the process itself was enlightening. It demonstrated the potential for fuzzy logic in HEV control systems, especially when combined with some form of optimization, but also the difficulty in designing a controller based on knowledge alone. Even in the second version of the controller developed by Anderson *et al*., the optimization was based on an intuitive quantity, rather than on the direct minimum for the system; it is assumed that a control strategy based on direct optimization may indeed meet the benchmark fuel economy in this study. This leads us to a discussion of optimization-based strategies and their potential in HEV applications.

2.3.2. Optimization-Based

The distinction between the primary sub-groups of optimization-based control strategies is that global optimization (GO) strategies are not suitable for on-board use, while real-time strategies (as the name implies) are suitable. Optimization problems rely on the development and minimization of an objective function for a desired parameter, such as fuel consumption or tailpipe emissions. They differ from rule-based strategies in that they typically *directly* determine the most efficient system operating point based on

component data or mathematical relationships for component operation. For example, optimization-based methods may take directly into account ICE, MG, ESS, and driveline efficiencies as well as tailpipe emissions when searching for and selecting the most optimal system operating point. This type of behavior cannot be replicated by a strictly rule-based system, especially when human knowledge/intuition is the sole method for rule creation. Optimization-based methods still require some input from the designer, most frequently in the form of constraints on the optimization itself (such as component operating constraints) or on the application of the solution to the system.

Global Optimization

GO-based methods generally use offline optimization to determine optimal system operating parameters over a known drive cycle. This is typically very time consuming and also requires prior knowledge of the drive cycle, meaning that these methods cannot be implemented in practice. Instead, they are used to determine a performance benchmark for a given vehicle, optimize certain vehicle parameters for a given drive cycle, and/or inform the development of alternate control strategies, such as fuzzy logic.

For example, Perez *et al*. [28] used dynamic programming to optimize the power flow in a series hybrid vehicle based on a simplified mathematical model of the vehicle. The result of the optimization was a time-based solution for the desired ICE operating points throughout the cycle in order to minimize fuel consumption. This is a slightly different approach as compared to that taken by Montazeri-Gh *et al*. [29], who used the genetic algorithm to optimize five control variables for a parallel hybrid vehicle to achieve optimal performance over three cycles. These variables included the upper and lower ESS SOC boundaries, the speed below which the vehicle should operate in all-electric

mode, and the torque load that should be placed on the ICE when on in order to charge the batteries. Thus, the result of the optimization was not direct ICE operation, but a set of parameters that have a direct effect on ICE operation. The authors performed several additional optimizations to reduce various specific emissions components (CO_x, NO_x, for example) and noted that concurrent minimization of all objectives was not possible: minimizing one objective resulted in a net increase of other objectives above their absolute minimum levels. While the authors report a 27% improvement in fuel consumption for one cycle over a standard ICE-powered vehicle, for example, they note that optimal parameters are different for each cycle, and thus, results of one optimization are not applicable to all driving conditions. Many similar studies, such as [30], [31], and [32], have yielded similar positive results, though all suffer from this same caveat. This is quite problematic and limits the practical use of this type of global optimization approach.

Perhaps a more promising and flexible approach is the use of global optimization to train or inform the development of fuzzy controllers and neural networks. Shichun *et al*. [33] used the genetic algorithm to tune the membership functions of a fuzzy controller for two standard drive cycles, which resulted in fuel consumption improvements of roughly 2% over the un-tuned fuzzy controller. Chang-jun *et al*. [34] trained a neural network using the genetic algorithm for a standard drive cycle and showed a 7% decrease in fuel consumption over a previously employed fuzzy approach. While both of these approaches may be more flexible than the parameter-based approach discussed in the previous paragraph, they may still result in sub-optimal control for situations that lie outside of the operating conditions that were used for training (if such conditions exist),

or may depend on the efficacy of training. As well, in these cases, training was based specifically on the standard driving cycles selected during each study, with separate training events occurring for each cycle. An additional downside to the use of neural networks is that the controller is not transparent, meaning that it is very difficult for a user to alter the performance of the network without additional training; this is in contrast to fuzzy logic, where users could more easily modify controller membership functions.

Real-Time Optimization

Real-time optimization differs from the global variety in that the optimization is performed on-board the vehicle, at discrete time intervals while driving. One of the primary challenges of real-time control is the lack of prior knowledge of the drive cycle, meaning that true optimal control cannot be implemented. The goal instead is to achieve sub-optimal control that approaches the efficiency of optimal control by optimizing powertrain operation at discrete time intervals. Another large barrier is that real-time strategies are typically very computationally expensive, and the development of an efficient and accurate optimization algorithm for implementation in practice is difficult. Finally, because vehicles are very dynamic systems, applying the results of separate, instantaneous optimizations yielded by real-time strategies at each discrete time step can be difficult and can affect drivability, as optimal operating points can change frequently and by large margins.

One of the most prominent real-time optimization methods is the equivalent consumption minimization strategy (ECMS), or some form thereof, popularized by Paginelli *et al*. [35]. The ECMS weights electrical energy consumption with an equivalency factor (EF) to set it on par with liquid fuel consumption and allow for the

determination and minimization of an equivalent fuel consumption that encompasses both electric and liquid fuel consumption. In other words, at each time step, the EF allows for the determination of an equivalent fuel consumption for a series of possible powertrain operating points (*ie*: different blends of ICE and electric power), after which optimization techniques can be used to determine the operating point which results in minimum equivalent consumption. Paginelli *et al*. originally used a static EF, but found that each drive cycle possessed a different average EF, which causes problems for SOC control over different drive cycles. As such, an additional variable called 'sensibility' was added to weight the objective function appropriately to maintain the target SOC. The authors reported a 17% decrease in fuel consumption with the use of the ECMS. The authors also mention that the method used had not yet been applied in real time, which is telling of the difficulty required to do so.

Subsequent work on ECMS-type algorithms, such as that found in [36] and [37], involved methods for implementing of a dynamic EF that replaced the sensibility term above and which also resulted in SOC control over all drive cycles. The authors of [36], for example, implement a PI controller based on current versus target SOC in order to change the EF and keep SOC within a target window. This work was followed by more advanced methods of EF modulation.

As mentioned, every drive cycle has a distinct overall EF, which is a function of the efficiencies of electrical and fuel energy conversion in the vehicle's powertrain throughout the cycle. The same can actually be said for any specific time window within a given cycle. This fact led researchers to develop methods to modify the EF based on current or past driving trends. Musardo *et al*. [38] introduced the adaptive ECMS

algorithm, which changes the EF based on past and predicted vehicle speed data. The authors note, however, that the use of GPS is a requirement to determine road grade, which is not captured by vehicle speed data, but does affect vehicle power requirements.

2.4. Summary

Optimization-based methods represent the cutting edge of HEV control and offer significant promise for the reduction of fuel consumption, especially with the increasing complexity of hybrid powertrains. The UVic EcoCAR, which possesses an advanced E-REV architecture and a flexible powertrain is an excellent candidate vehicle for the implementation of a real-time control strategy.

Within the context of the aforementioned challenges of real-time optimal control, this work will focus primarily on the application of an ECMS-based real-time control strategy to the 2-Mode Plus architecture of the UVic EcoCAR vehicle in practice, and will address issues such as the integration and operation of the UVic control system, the computational demand of the selected algorithm, drivability, and component longevity. Algorithm development, which is summarized in Chapter 5, is based heavily on a real-time algorithm for a front-wheel drive (FWD) 2-Mode system that was developed by a previous graduate student at UVic [4].

CHAPTER 3 ECVT and Powertrain System Analysis

This chapter will provide an overview of fundamental ECVT operation, followed by an in-depth analysis of the GM 2-Mode transmission. The following nomenclature will be used throughout this chapter:

r_x = number ring gear teeth divided by number sun gear teeth, where x is used for multiple PSDs

ω_{ice} = speed of the ICE

ω_{mga} = speed of MGA

ω_{mgb} = speed of MGB

ω_{out} = speed of the output, prior to the final drive

T_{ice} = ICE speed

T_{mga} = MGA torque

T_{mgb} = MGB torque

T_{out} = output torque, prior to the final drive

3.1. ECVT Fundamentals

3.1.1. The Planetary Gear Set

The core of the ECVT as well as conventional automatic transmissions is the planetary gear set, a PSD consisting of gears arranged as shown in Figure 3-1. Planetary gear sets are used in transmission applications due to their ability to transfer large amounts of torque and achieve high gear ratios in relatively compact spaces, and the fact that they have three mechanical ports: ring, planet carrier, and sun.

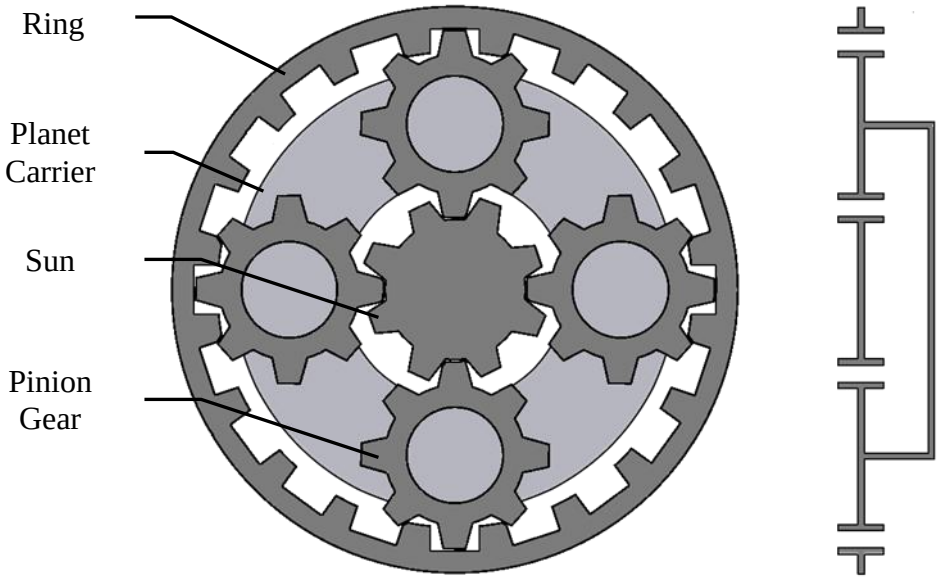

Figure 3-1: Planetary Gear Set

The speed and steady state torque relationships between the ring, planet carrier, and sun components of a planetary gear set are listed in Equations 3-1 3-4. Torques at the ports of a planetary gear set are also balanced, as per Equation 3-5.

$$(r+1)\cdot\omega_c - \omega_s - r\cdot\omega_r = 0 \quad \text{3-1}$$

$$T_r = \frac{T_c}{1+1/r} \quad \text{3-2}$$

$$T_s = \frac{T_c}{r+1} \quad \text{3-3}$$

$$T_s = (1/r)\cdot T_r \quad \text{3-4}$$

$$T_c = T_s + T_r \quad \text{3-5}$$

Here, the subscripts *c*, *r*, and *s* denote planet carrier, ring gear, and sun gear, respectively.

Note that the torque at one mechanical port defines the torque at the remaining two ports, while the speed at two ports must be known to define the speed at the third.

Planetary gear sets can be simply represented using a lever diagram. Three nodes on a lever diagram represent the sun, planet, and ring gears; the distance between the nodes represents the gear ratio between the various components, while the horizontal displacement from a defined zero axis represents component speeds, as illustrated in Figure 3-2.

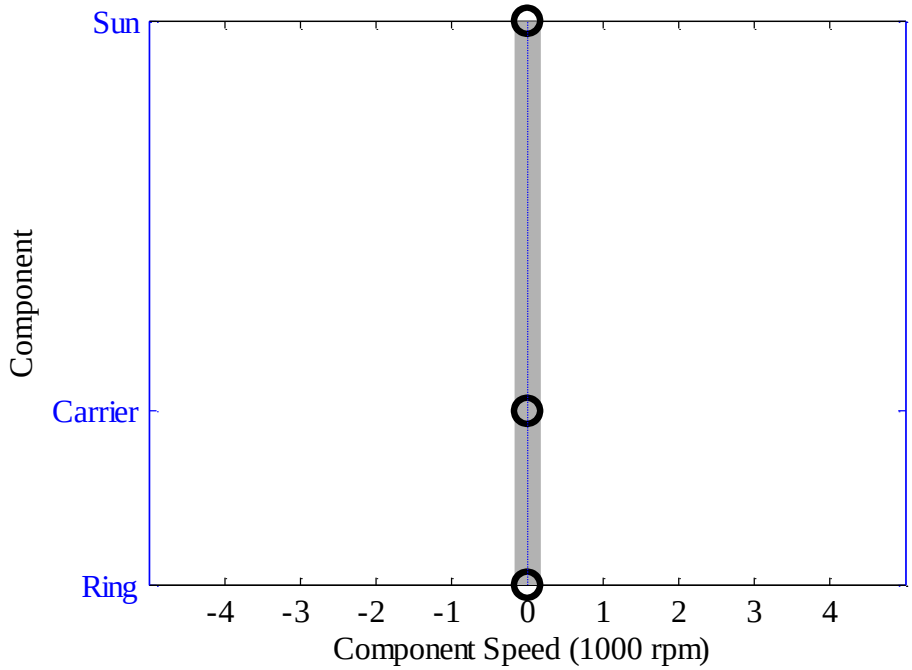

Figure 3-2: Lever Diagram Representation of a Planetary Gear

Ring, carrier, and sun components will be referred to from here on by R, C, and S, respectively. The following section provides an example of the application of the lever diagram and fundamental planetary gear equations in a single-mode ECVT.

3.1.2. Single Mode ECVT Example

Figure 3-3 shows the arrangement of a typical single mode ECVT, with the ICE connected to planet carrier, one MG (MGA) connected to the sun, and the final drive (FD) with a second MG (MGB) connected to the ring.

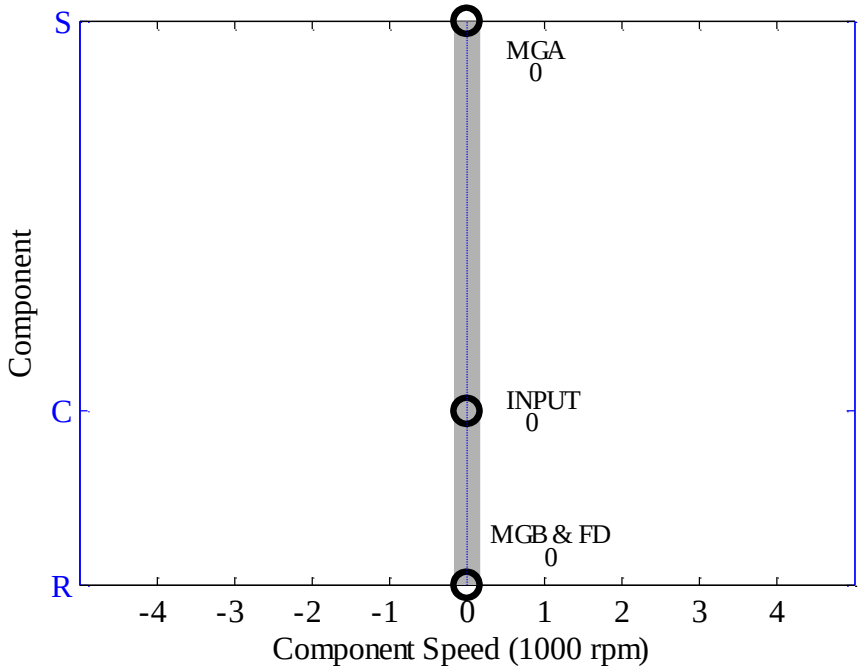

Figure 3-3: Single Mode ECVT Configuration

The speed relation between the sun gear and planet carrier means that at any given vehicle speed, the speed of the ICE can be varied by changing the speed of MGA. While MGB provides propulsive power to aid the ICE, MGA acts as a generator, converting its share of ICE energy to electrical energy that is used by MGB and/or charges the ESS. Thus, both ICE speed and torque are decoupled from road speed and torque. The output torque equation of a single-mode ECVT is given in Equation 3-6.

$$T_{out} =\cdot \frac{T_{ice}}{(1+1/r)} + T_{mgb} \qquad 3\text{-}6$$

ICE speed is controlled using MGA, as per Equation 3-7, where the transmission output speed is defined by road speed.

$$\cdot\, \omega_{ice} = \frac{\omega_{mga} + r \cdot \omega_{out}}{(r+1)} \qquad 3\text{-}7$$

Figure 3-4 provides an example of an all-electric launch, whereby the ICE remains off at low vehicle speeds. Here, MGA speed is negative so as to maintain zero ICE speed.

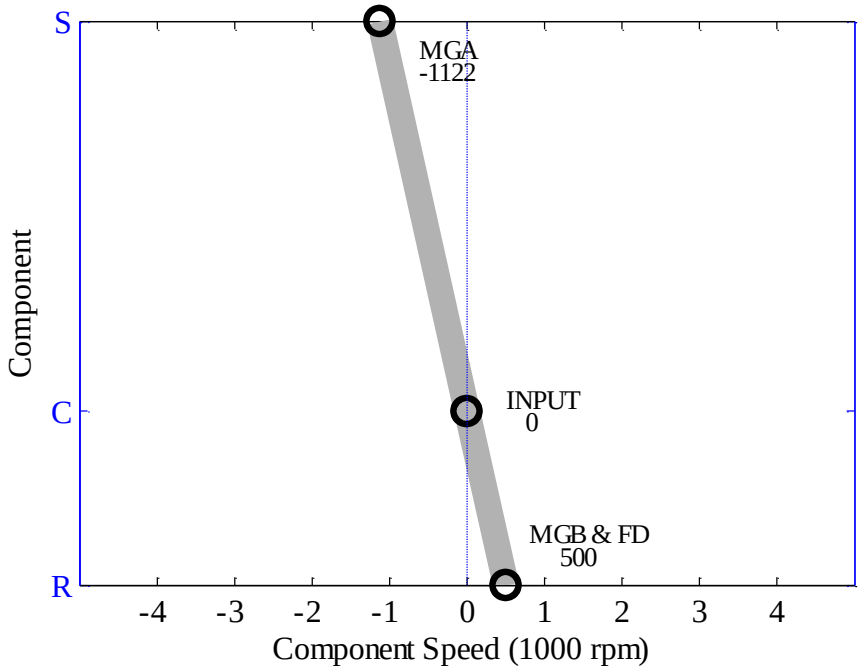

Figure 3-4: Single Mode ECVT All-Electric Operation

In Figure 3-5, while vehicle speed has not changed, MGA speed has been increased in order to start the ICE.

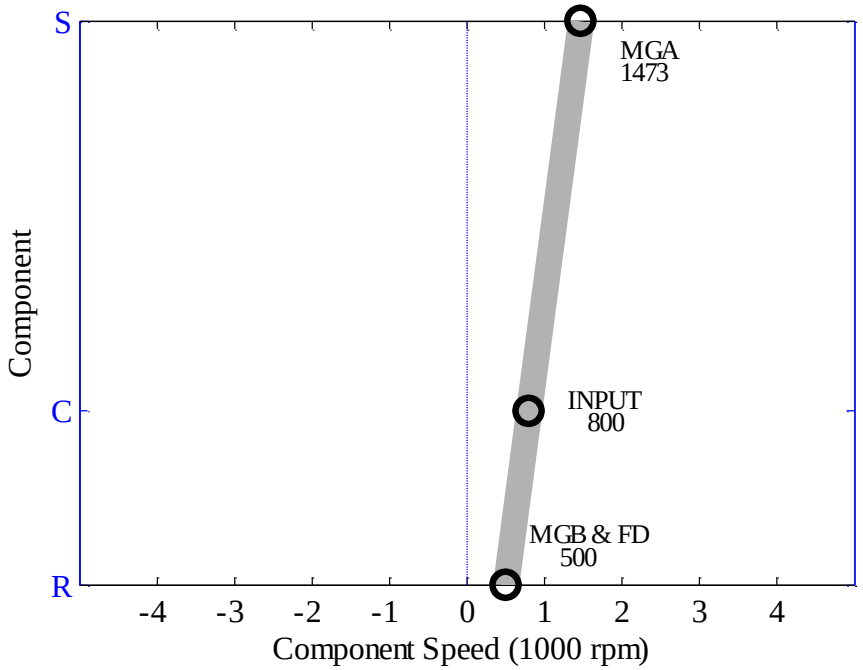

Figure 3-5: Single-Mode ECVT Rolling ICE Start

3.1.3. The Mechanical Point

Recall that a an ECVT transmission is also called a power-split, referring to the fact that ICE power is split between mechanical and electrical power paths to the wheels. A mechanical point is a point at which the power through the electrical path becomes zero, which, in the case of the ECVT used in the above examples, corresponds to the point at which MGA reaches zero speed during operation; see Figure 3-6.

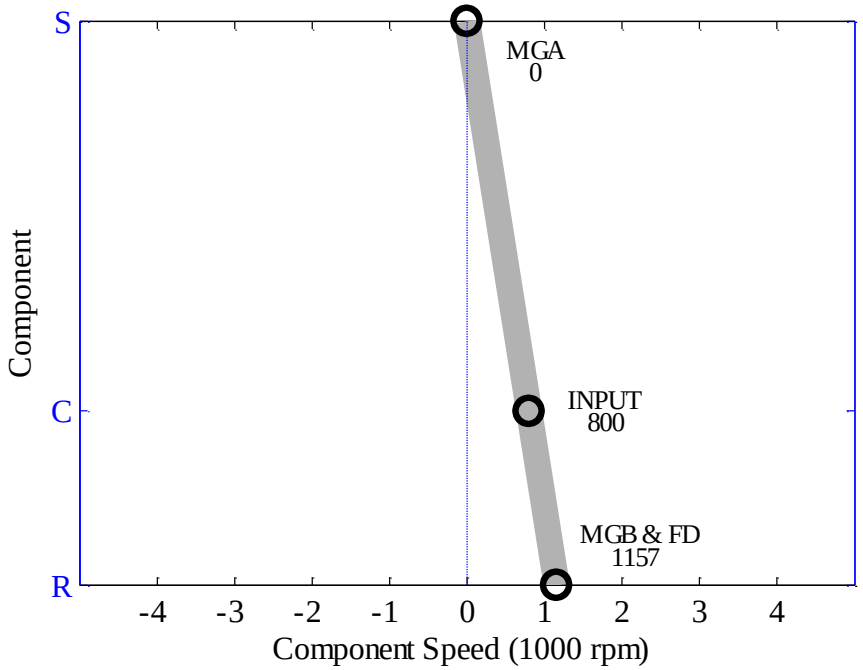

Figure 3-6: Single-Mode ECVT Mechanical Point

As the mechanical power path through the transmission is more efficient than the electrical path, operation at these points is desirable. Operation above the mechanical point decreases in efficiency rapidly, as above this point in our example the speed of MGA becomes negative and the roles of MGA and MGB reverse. Observe that MGA must apply a negative reaction torque at the sun gear to balance the torque from the ICE (see Equation 3-3), thus resulting in net power consumption when MGA speed is negative. MGB then acts as a generator and supplies power to MGA. This effect is called power recirculation, and drastically reduces transmission efficiency above the mechanical point. This is illustrated by Figure 3-7, where a constant ICE speed of 800 rpm has been assumed, and a planetary gear ratio (r) of 2.24 is used. The point at which MGA and MGB power meet at the x-axis, just above 40 km/h here, is the mechanical point.

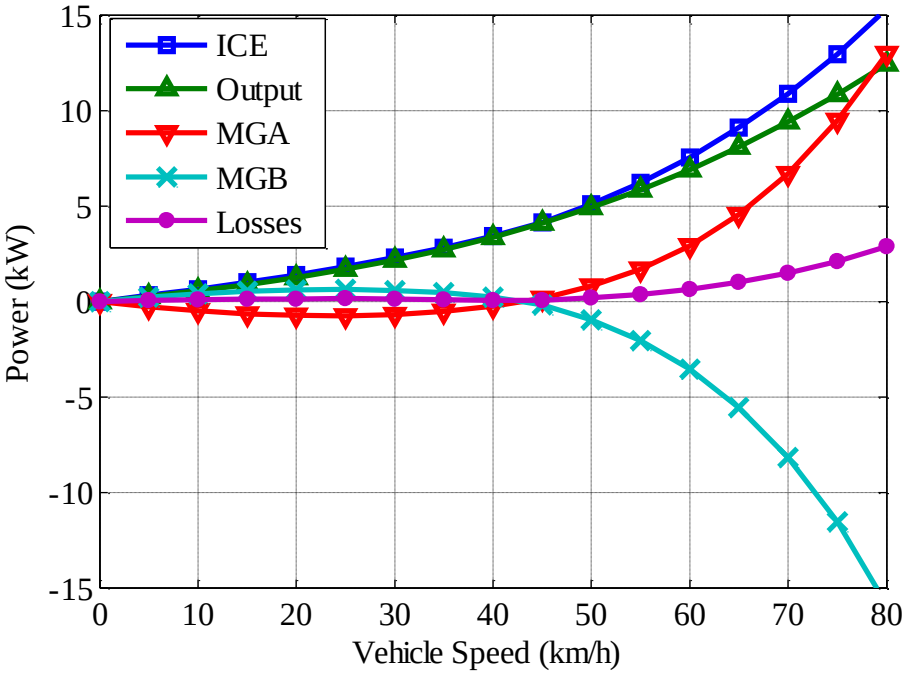

Figure 3-7: Mechanical Point Power Flow - 800 rpm @ Input

Increasing the speed of the ICE increases the vehicle speed at which the mechanical point is reached, as shown in Figure 3-8, where ICE speed has been set to 1200 rpm.

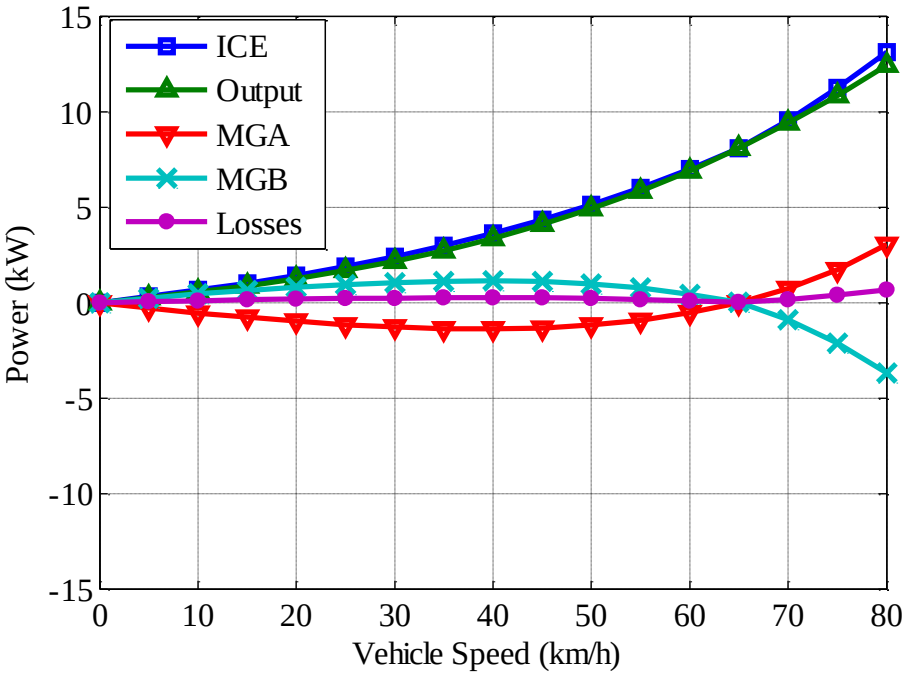

Figure 3-8: Mechanical Point Power Flow - 1200 rpm @ Input

It should be noted, though, that in some cases, ICE speed can be below the mechanical point without power recirculation occurring. In this case, MGA could be receiving electrical power only from the ESS, while MGB does not generate power. In general though, this is rare, and the mechanical point in a single-mode ECVT essentially sets a lower bound on ICE speed based on the speed of the vehicle. This has the potential to reduce overall efficiency at high vehicle speeds, and was perhaps a major factor in the development of multi-mode ECVTs such as the GM 2-Mode transmission.

3.2. The GM 2-Mode Transmission

The GM 2MT70 combines two MGs and two PSDs, at the input and output of the transmission, with four clutches. The result is a system with two ECVT modes and four fixed gears. Table 3-1 summarizes relevant system information.

Table 3-1: GM 2MT70 Specifications

Motor A Power	55 kW
Motor B Power	55 kW
PSD 1 Ratio	2.36 (compound); 1.36 (simple)
PSD 2 Ratio	2.24 (simple)

The 2-Mode system increases vehicle efficiency in two primary ways: introducing a second ECVT mode with an additional mechanical point that allows for lower ICE speeds at high vehicle speeds, and introducing fixed gears that each result in a parallel hybrid configuration. Figure 3-9 provides an overview of the transmission.

Note first that the input PSD is actually a compound planetary gear set, which can be represented as a simple planetary gear set by switching the connectivity of the planet carrier and ring gear and subtracting one from the compound gear ratio; the simple ratio is listed in Table 3-1. This simplified from of the input PSD is reflected in Figure 3-9

and used from this point forward for parallelism with the output PSD. A review of the component layouts and kinematics of the 2-Mode transmission can be found here [39].

Note the following notation for Figure 3-9:

SX = sun gear, where X represents PSD number

CX = planet carrier, where X represents PSD number

RX = ring gear, where X represents PSD number

CXXX = clutch, where XXX represents clutch nomenclature as discussed below

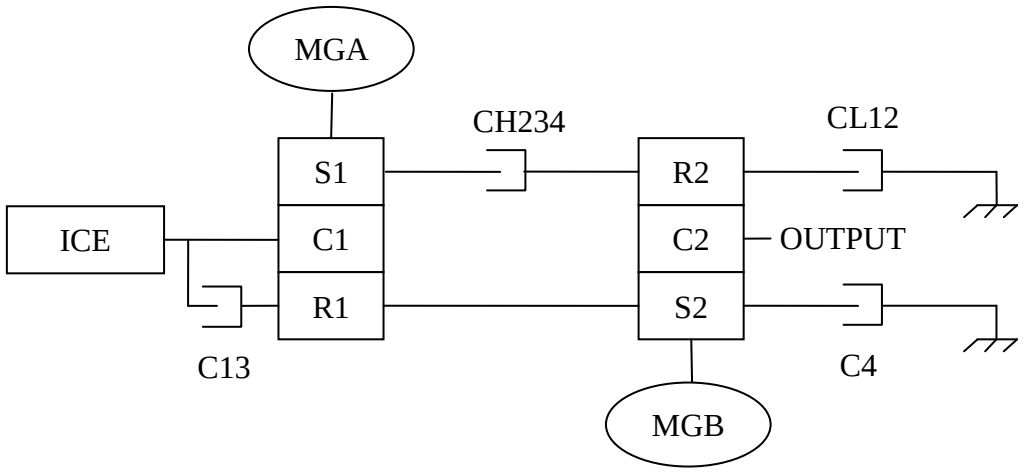

Figure 3-9: GM 2MT70 Simple Planetary Layout

Clutch nomenclature in Figure 3-9 represents the gears or modes for which each clutch is activated/closed, where numbers represent fixed gears and L and H represent Mode 1 (or low ECVT mode) and Mode 2 (or high ECVT mode), respectively. Table 3-2 summarizes clutch activation for all transmission operating states as well as which MGs are connected in parallel for each fixed gear.

Table 3-2: 2MT70 Clutch Activation Table

State	C13	CL12	CH234	C4	Parallel MG
Mode 1		X			-
Mode 2			X		-
Fixed Gear 1 (FG1)	X	X			MGA + MGB
Fixed Gear 2 (FG2)		X	X		MGB
Fixed Gear 3 (FG3)	X		X		MGA + MGB
Fixed Gear 4 (FG4)			X	X	MGA
Neutral					-

MGB and MGA are clutched to ground in FG2 and FG4, respectively, whereas both MGs are available to add or subtract propulsive power in FG1 and FG3.

Also of note is that fixed gears are actually subsets of one or both of the modes in terms of operating region, having been subjected to a constraint (by the activation an additional clutch) that the ICE operate at a fixed speed relative to vehicle speed. This will be demonstrated clearly throughout § 3.3.

3.2.1. Synchronous Shift Execution

The 2MT70 was designed to make synchronous shifts between states, meaning that the relative speed between the sides of a clutch to be activated is brought to zero before activation. Clutches designed for synchronous use are smaller, lighter, cheaper, and are subject to less wear than clutches designed for slip (a drive clutch in a manual transmission for example). The trade-off is that some controls effort must be expended to bring the two sides of a clutch to zero relative speed, and that not all transitions between states can be made. More specifically, transitions between fixed gears must pass through an ECVT mode, because only in these modes are the relative speeds of some components within the transmission variable. The transition between Mode 1 and 2 also passes through a fixed gear.

As an example, let us examine this transition between Modes. Table 3-3 is a subset of Table 3-2 that contains only states related to this transition.

Table 3-3: 2MT70 Clutch Activation Table - FG2 Subset

State	C13	CL12	CH234	C4
Mode 1		X		
FG2		X	X	
Mode 2			X	

As is evident from Table 3-3, FG2 is a subset of Mode 1 and Mode 2 in terms of available operating regions. In the transition from Mode 1 to Mode 2, the relative speed of CH234 is brought to zero by changing the speed of MGA, which also changes ICE speed. CH234 is then activated, placing the transmission in FG2, after which CL12 is deactivated. The amount of time spent in FG2 is very short, essentially the time between full activation of CH234 and deactivation of CL12.

Further examination of Table 3-2 reveals that Mode 1 is also a subset of FG1, and Mode 2 is a subset of FG3 and FG4. Figure 3-10 is a shift map demonstrating the possible state transitions in the 2MT70. Any transition between states that are not directly connected must travel through all intermediary steps.

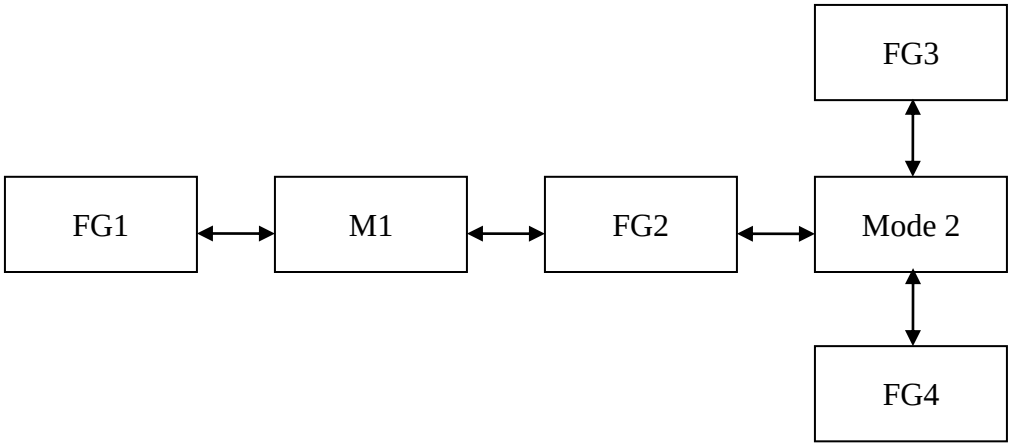

Figure 3-10: 2MT70 Shift Transition Map

3.3. Vehicle Operational Analysis

The following sections will now examine each mode and gear of the transmission in greater detail and also take into consideration the effect of the RTM on propulsion capability. Operating equations and then lever diagrams were developed based on the configuration of the 2-Mode components outlined in Figure 3-9, and the fundamental planetary gear set equations presented in § 3.1.1.

Note the symbols below, which are used in the lever diagrams in the following sections:

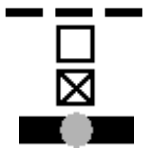

Shaft
Open Clutch
Closed Clutch
Locked Planetary Gear Set (Clutch C13)

When the closed clutch symbol appears over a node on a lever, it represents the node being clutched to ground.

3.3.1. ECVT Mode 1

The Mode 1 configuration is essentially the same as the single-mode ECVT outlined in §3.1.2, except that the output PSD adds an additional gear reduction before the FD. Note the parallels of Figure 3-11 below, which depicts Mode 1 operation at low vehicle speeds and an ICE speed (INPUT) of 800 rpm, with the same scenario for single-mode ECVT of Figure 3-5. The ‘OUTPUT’ represents the output of the transmission before the FD.

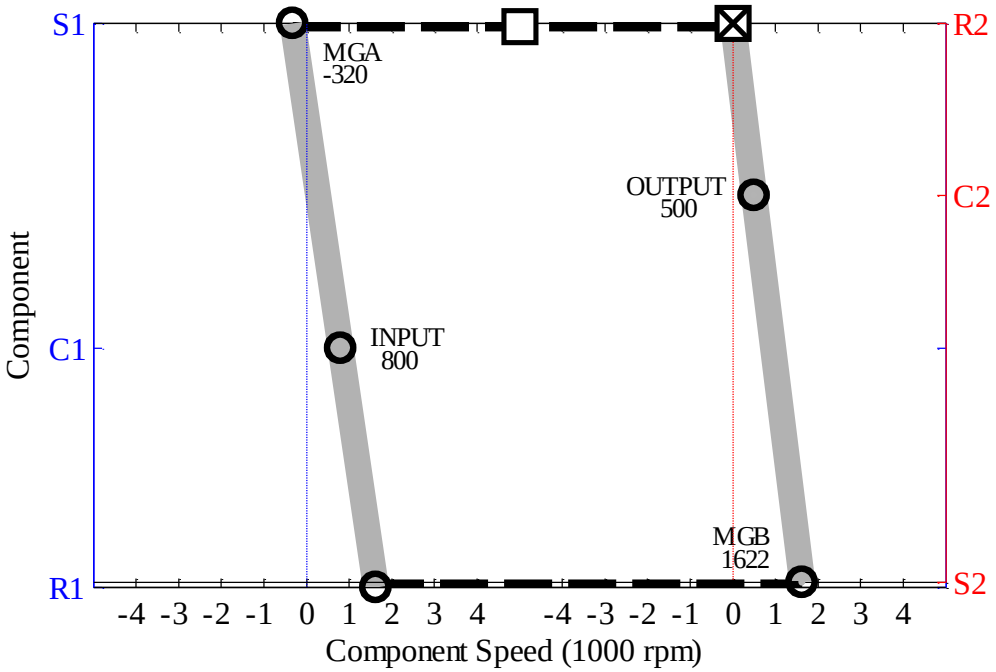

Figure 3-11: Mode 1 ICE On

Similarly, the ICE can remain off at low vehicle speeds by increasing the speed of MGA in the negative direction, as shown in Figure 3-12.

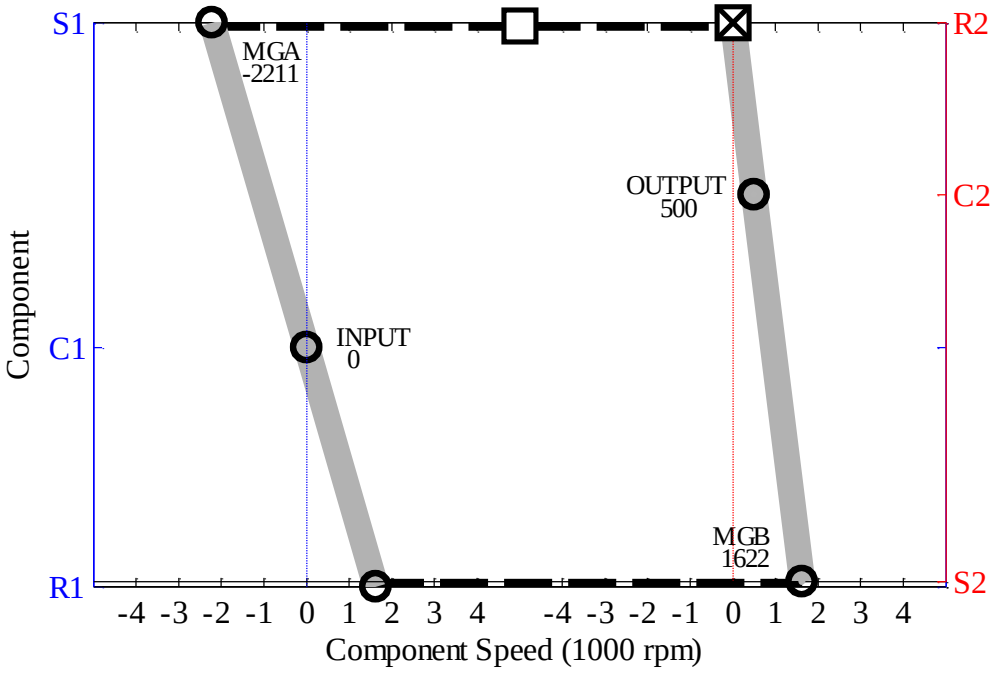

Figure 3-12: Mode 1 All-Electric Operation

Equations 3-8, 3-9, and 3-10 are the governing equations for output torque and ICE speed in Mode 1.

$$T_{out} = (r_2 + 1) \cdot \left(T_{mgb} + \frac{T_{ice}}{(1 + {}^{1}/_{r_1})} \right) \quad 3\text{-}8$$

$$T_{mga} = -\frac{T_{ice}}{(r_1 + 1)} \quad 3\text{-}9$$

$$\omega_{ice} = \frac{r_1 \cdot \omega_{out}(r_2 + 1) + \omega_{mga}}{(r + 1)} \quad 3\text{-}10$$

Figure 3-13 plots the ICE speed at which the mechanical point in Mode 1 is reached as a function of vehicle speed.

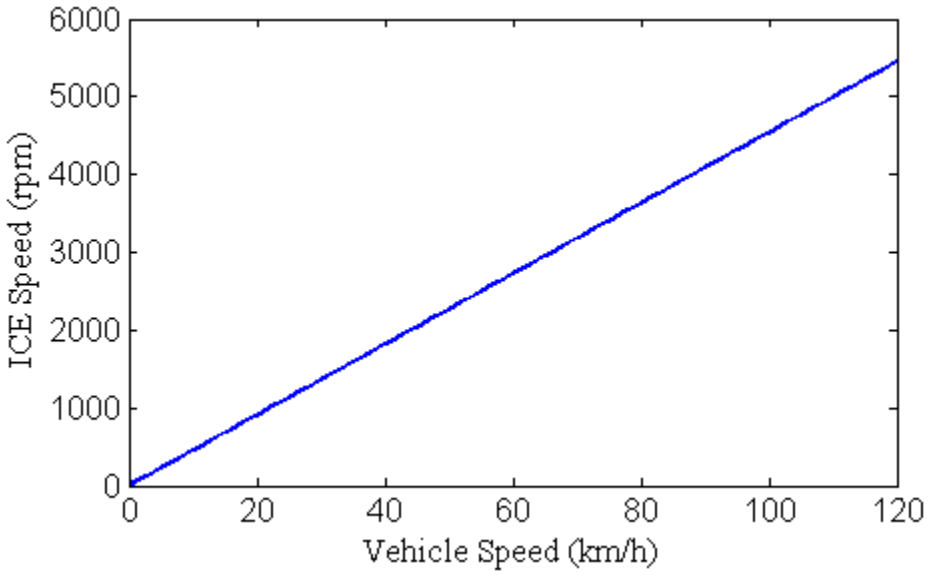

Figure 3-13: Mode 1 Mechanical Point

The region below the line in Figure 3-13 is the area in which power recirculation occurs, and should be avoided. So, Mode 1 is not suitable for high speed driving, since to avoid inefficient regions of transmission operation, the ICE must operate an in inefficient region.

Finally, the maximum axle torque capability of Mode 1 after the FD (or at the wheels) is illustrated in Figure 3-14 as a function of ICE and vehicle speed. Axle torque capabilities for each gear are given because they aid in an understanding of the gear selection process, which will be addressed later in the thesis. Basically, if the axle torque requested by the driver exceeds the output torque capability of a gear, operation in that gear is ruled out; conversely, any gear that is capable of meeting output torque requests is a candidate gear, and an appropriate gear selection method must be used.

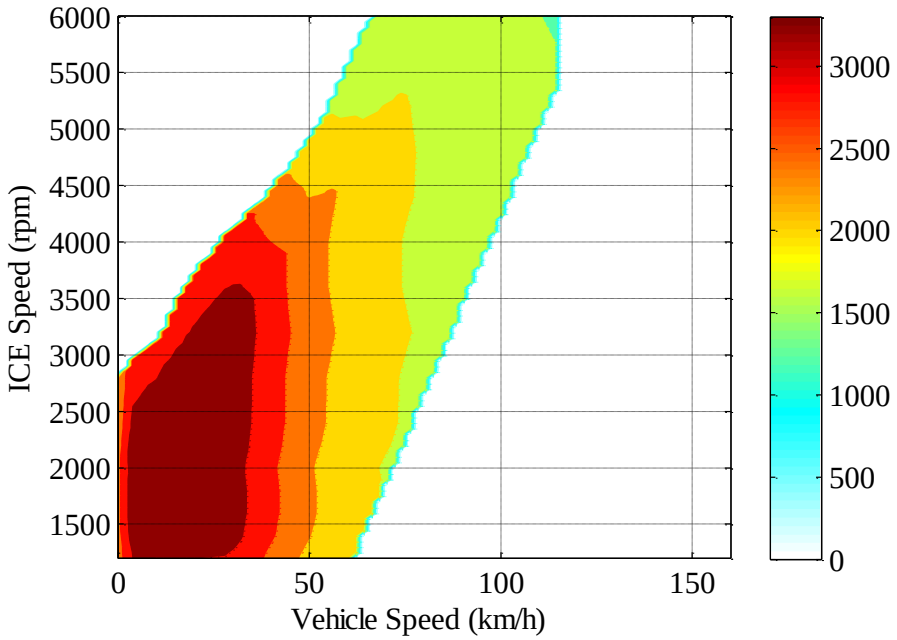

Figure 3-14: Mode 1 Max Axle Torque Capacity (Nm)

The axle torque capability of Mode 1 is heavily influenced by the torque capability of MGB, as it aids the ICE in propulsion. The minimum bound on ICE speed as vehicle speed increases is a result of the maximum speed limit of a pinion gear in the first PSD.

It should be noted for this figure and subsequent similar figures in the following sections that battery power levels are not considered in these plots, and thus, some regions of the plot will result in high levels of electrical power use.

3.3.2. ECVT Mode 2

Whereas in Mode 1 MGB speed was fixed by road speed according to the ratio of the output PSD, neither MG is constrained by road speed in Mode 2. Instead, the balance of MG speeds at a given output speed determines the speed of the ICE, and either of the MGs can be brought to zero speed at a given output speed. The lever diagram of Figure 3-15 depicts Mode 2 operation.

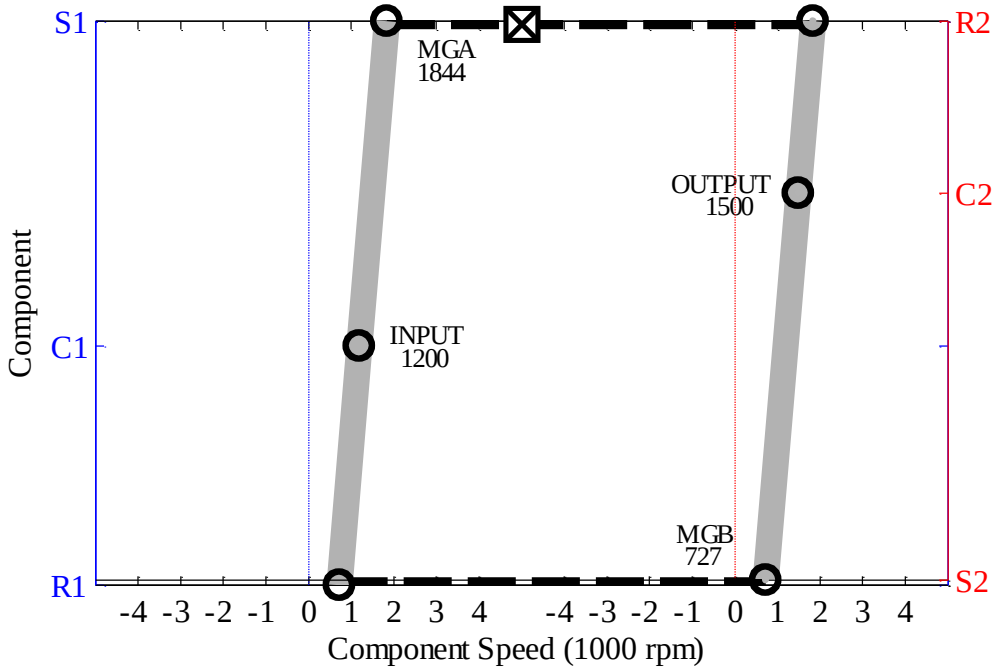

Figure 3-15: Mode 2 Operation

Because both MGs can be brought to zero speed, Mode 2 has two mechanical points, though the point at which MGA speed is zero is shared with Mode 1 as the synchronous shift point between the two modes. The second mechanical point is illustrated in Figure 3-16.

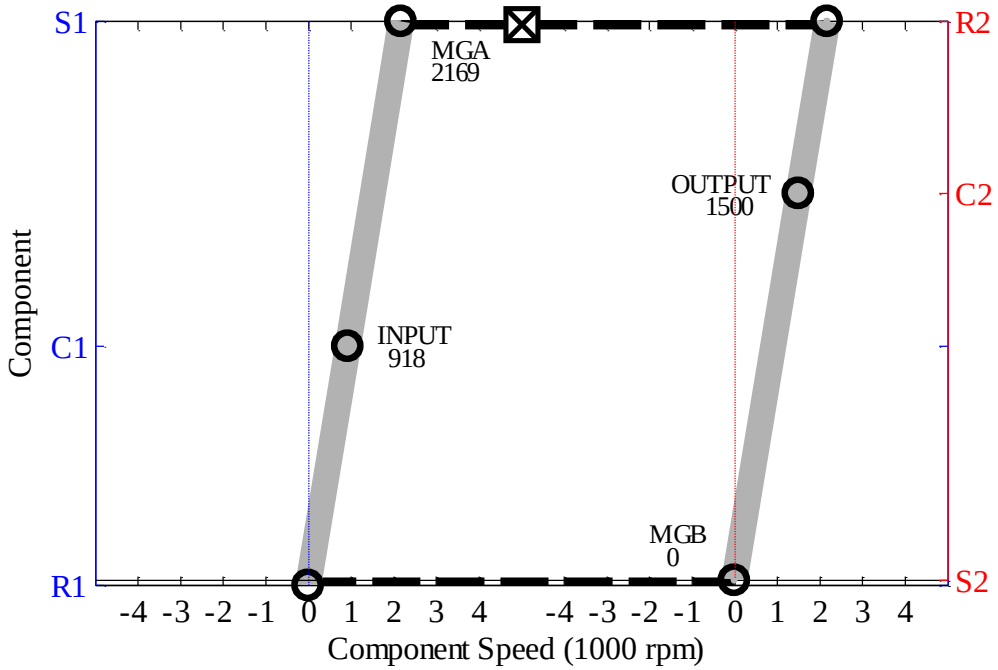

Figure 3-16: Mode 2 MGB Mechanical Point

Equations 3-11 and 3-12 are the governing equations for output torque and ICE speed in Mode 2.

$$T_{out} = \left({}^{1}/_{r_2} + 1\right) \cdot \left(T_{mga} + \frac{T_{ice}}{r_1 + 1}\right) = (r_2 + 1) \cdot \left(T_{mgb} + \frac{T_{ice}}{{}^{1}/_{r_1} + 1}\right) \quad 3\text{-}11$$

$$\omega_{ice} = \frac{\omega_{mga} + r_1 \cdot \omega_{mgb}}{r_1 + 1} \quad 3\text{-}12$$

The torques of MGA and MGB must balance at steady state, so Equation 3-12 yields the constraint of Equation 3-13.

$$T_{mga} = r_2 \cdot T_{mgb} + (r_1 r_2 - 1) \cdot \left(\frac{T_{ice}}{r_1 + 1}\right) \quad 3\text{-}13$$

Figure 3-17 plots both mechanical points in Mode 2 as a function of vehicle speed.

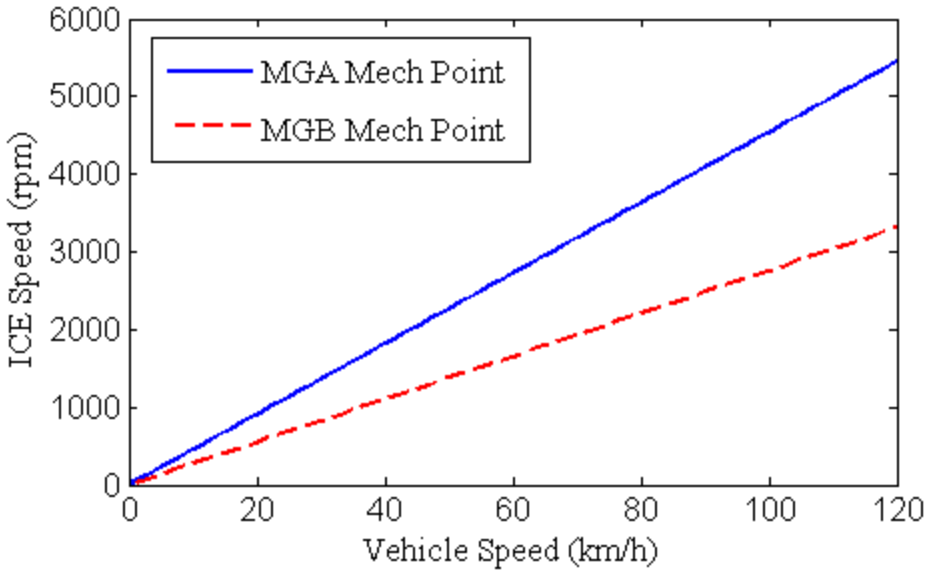

Figure 3-17: Mode 2 Mechanical Points

It can clearly be seen that the second mechanical point offers a more desirable ICE operating range at higher vehicle speeds, and was intended to improve fuel economy at highway cruising speeds.

The axle torque capability of Mode 2 is illustrated in Figure 3-18.

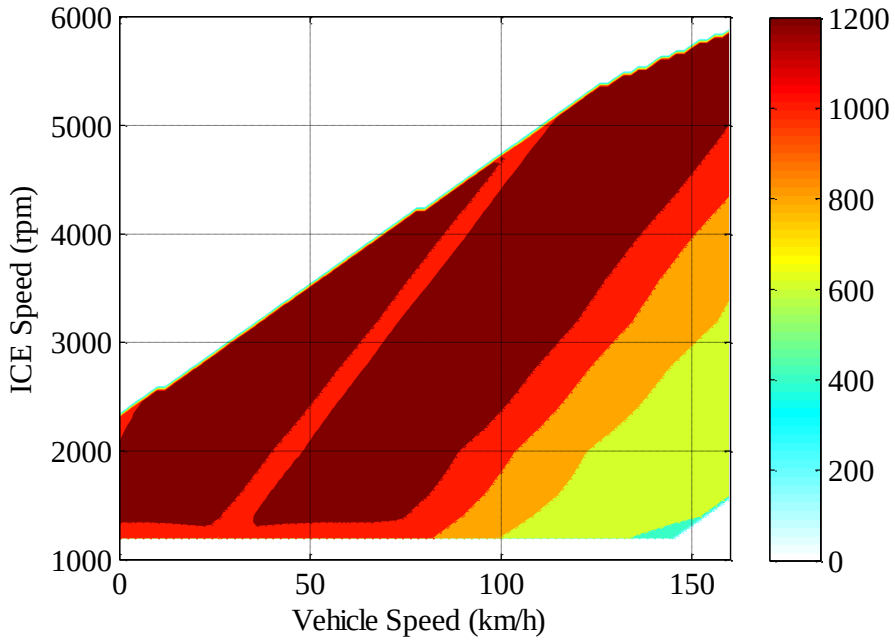

Figure 3-18: Mode 2 Max Axle Torque Capacity (Nm)

3.3.3. Fixed Gear 1

The transition to FG1 is accomplished by bringing MGA speed to MGB speed and activating clutch C13, thus making the entire planetary gear rotate as one unit. FG1 operation is illustrated in Figure 3-19.

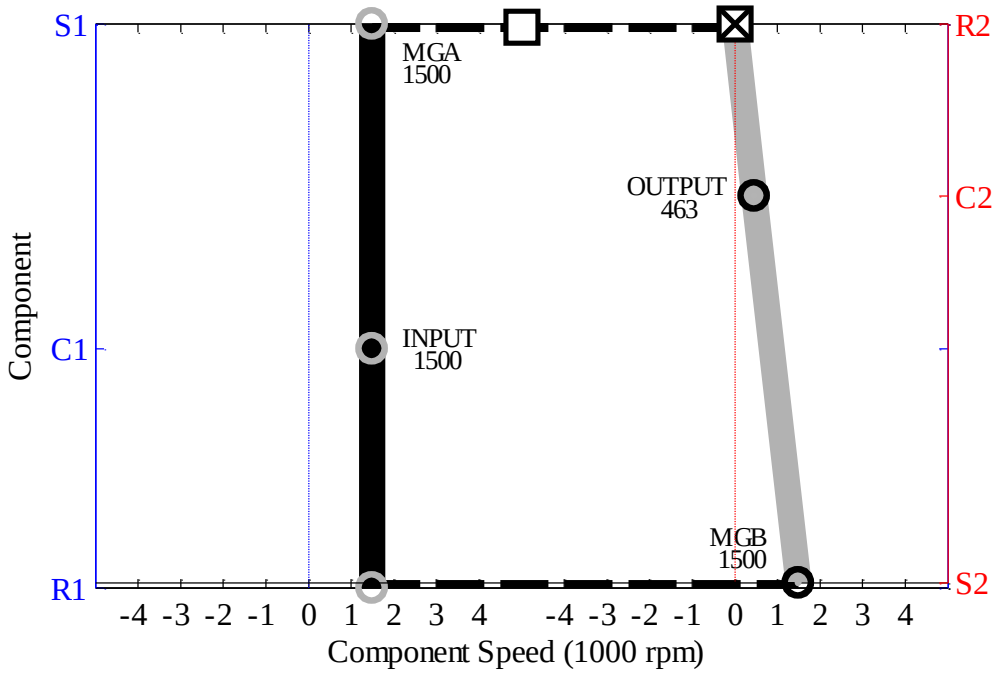

Figure 3-19: FG1 Operation

In FG1, both MGA and MGB can aid in propulsion, and transmission output torque is governed by Equation 3-14. The fixed transmission ratio is given in Equation 3-15.

$$T_{out} = (r_2 + 1) \cdot \left(T_{ice} + T_{mga} + T_{mgb}\right) \quad 3\text{-}14$$

$$\omega_{ice} = (r_2 + 1) \cdot \omega_{out} = 3.24 \cdot \omega_{out} \quad 3\text{-}15$$

FG1 is the subset of Mode 1 whereby MGA speed is equal to MGB speed. However, because C13 locks the input PSD, FG1 is not subject to the constraint that MGA balance ICE torque to maintain ICE speed, therefore allowing MGA to aid propulsion and resulting in much higher output capability as compared to Mode 1. Figure 3-20 plots FG1 output torque capability as well as the maximum output torque capability of Mode 1 as a function of only vehicle speed.

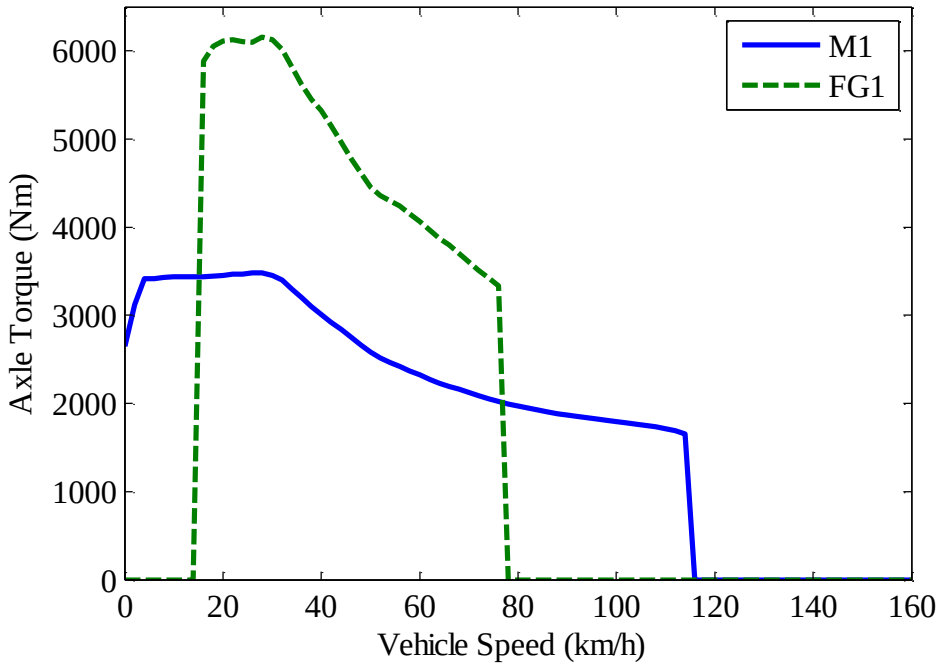

Figure 3-20: FG1 & M1 Max Axle Torque Capability

The sharp rises and drops in axle torque capability are the result of lower and upper ICE speed limitations. In these diagrams, the minimum 1200 rpm ICE speed limit has been used.

3.3.4. Fixed Gear 2

FG2 is the synchronous shift point between Modes 1 and 2, with both clutches CL12 and CH234 activated; see Figure 3-21. In this parallel configuration, MGA is clutched to ground, and so only MGB can aid in propulsion.

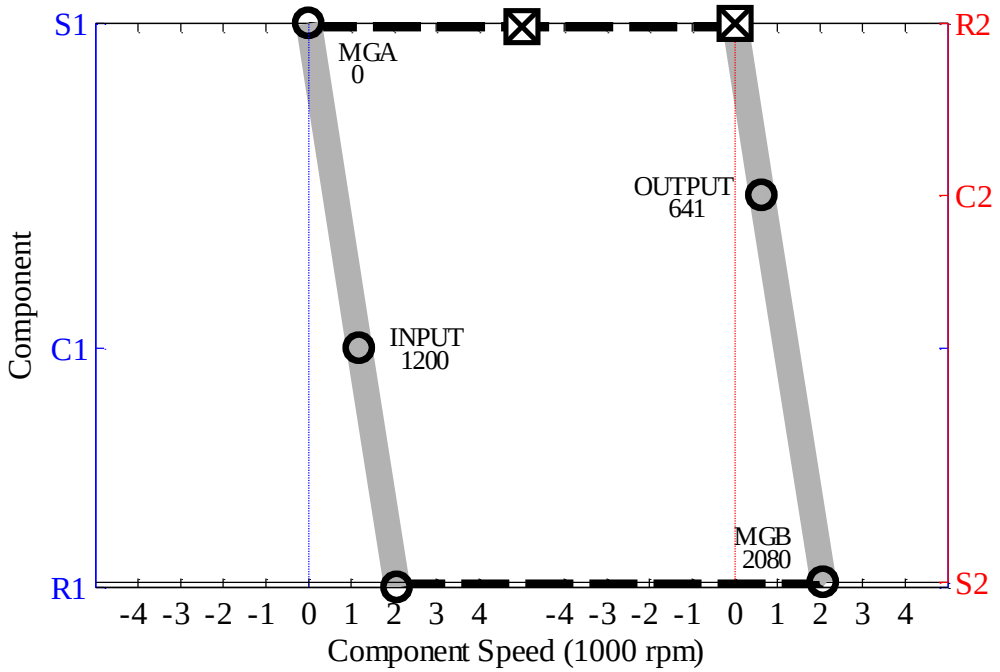

Figure 3-21: FG2 Operation

The FG2 torque equation and speed ratio for are given in Equations 3-16 and 3-17.

$$T_{out} = (r_2 + 1) \cdot \left(T_{mgb} + \frac{T_{ice}}{1 + {}^{1}/_{r_1}} \right) \qquad 3\text{-}16$$

$$\omega_{ice} = {}^{r_1 \cdot (r_2 + 1)}\Big/_{(r_1 + 1)} \cdot \omega_{out} = 1.87 \cdot \omega_{out} \qquad 3\text{-}17$$

The torque capability of FG2 is actually equal to the torque capability of Mode 1 along the mechanical point line shown in Figure 3-13, as MGA speed in FG2 is always zero. This operating line is also shared by Mode 2, as demonstrated in §3.2.1. Figure 3-22 illustrates the output capacity of FG2, as well as Mode 1 and Mode 2.

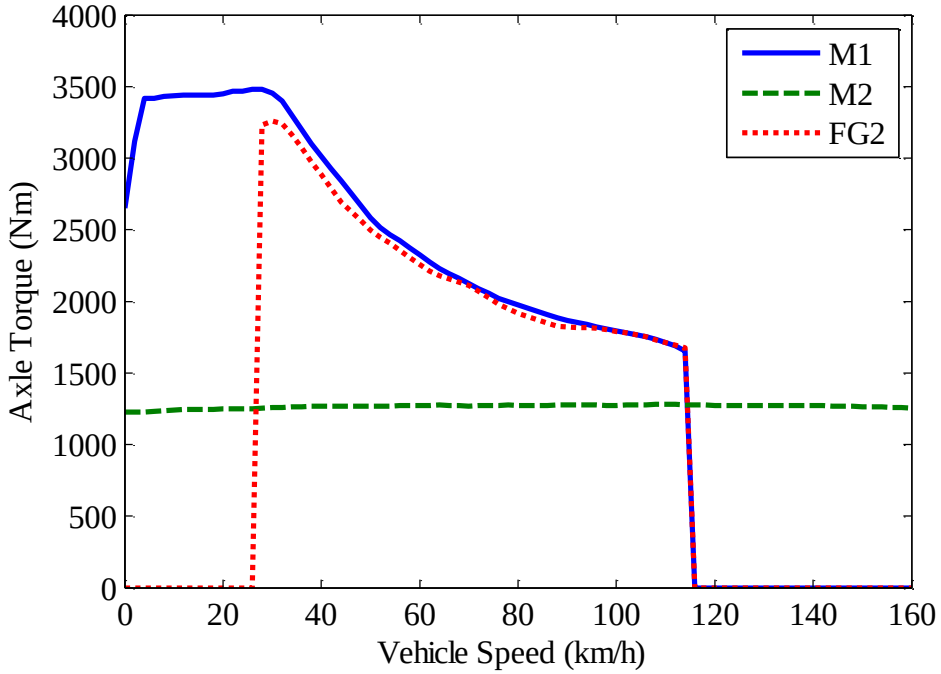

Figure 3-22: M1, M2 & FG2 Max Axle Torque Capability

Mode 1 is capable of marginally higher output capacity at a given vehicle speed as compared to FG2 because ICE speed can be varied at that vehicle speed in order to move the ICE into a region of higher torque capability. The output capability of Mode 2 along this mechanical point is much lower than FG2 and Mode 1, as Mode 2 is subject to the constraint that MG torques must balance each other.

3.3.5. Fixed Gear 3

In FG3, the speed of all components is equal to the transmission output, as clutches C13 and CH234 lock the rotational speeds of both planetary gear sets together, as demonstrated in Figure 3-23.

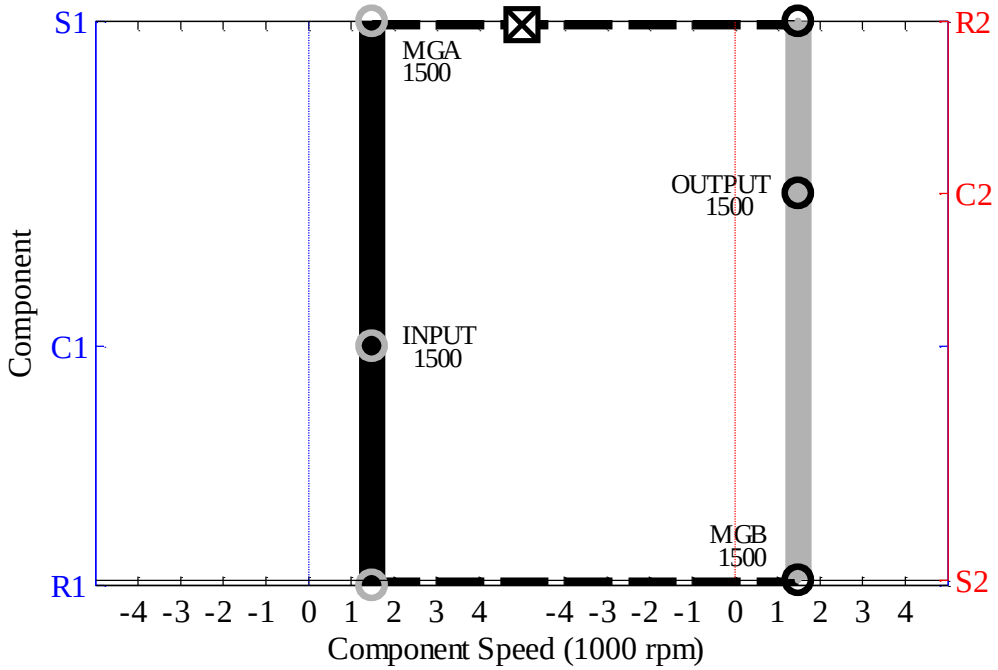

Figure 3-23: FG3 Operation

Output torque and speed ratio equations for FG3 are given in Equations 3-18 and 3-19.

$$T_{out} = T_{ice} + T_{mga} + T_{mgb} \quad 3\text{-}18$$

$$\omega_{ice} = \omega_{out} \quad 3\text{-}19$$

The operating points of FG3 are within the domain of Mode 2, lying along the line at which output speed is equal to input speed. Once again though, the output torque capability of Mode 2 is limited compared to FG3 by the requirement that the motor torques must balance each other at steady state. The maximum output capacity of FG3 and Mode 2 are shown in Figure 3-24 as a function of vehicle speed.

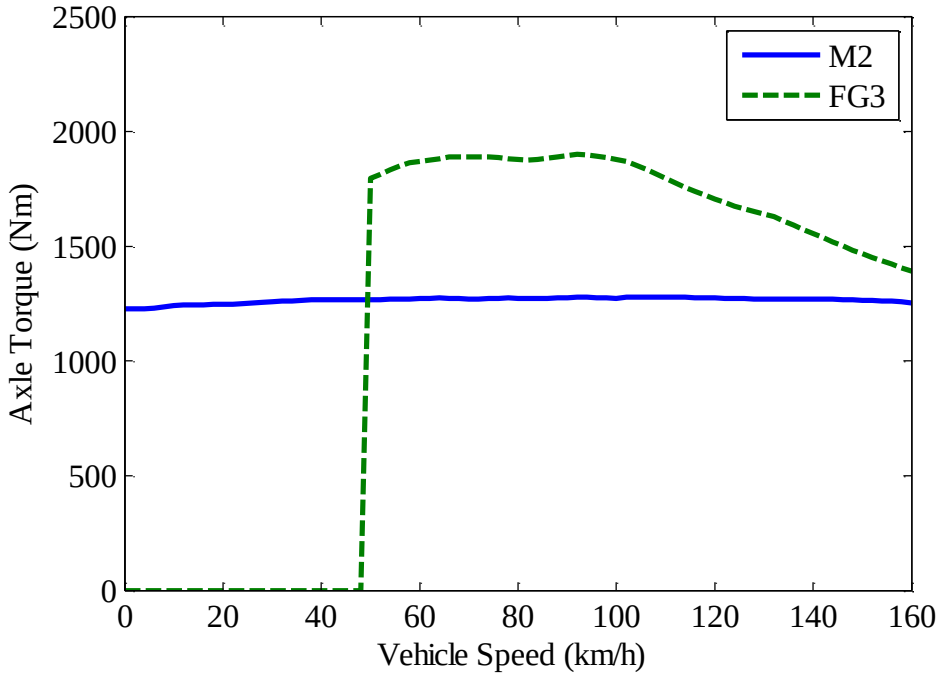

Figure 3-24: M2 & FG3 Max Axle Torque Capability

3.3.6. Fixed Gear 4

The transition from Mode 2 to FG4 is completed by bringing ICE speed to the second mechanical point at the current vehicle speed (meaning MGB speed is zero) and activating C4. A lever diagram of FG4 is shown in Figure 3-25.

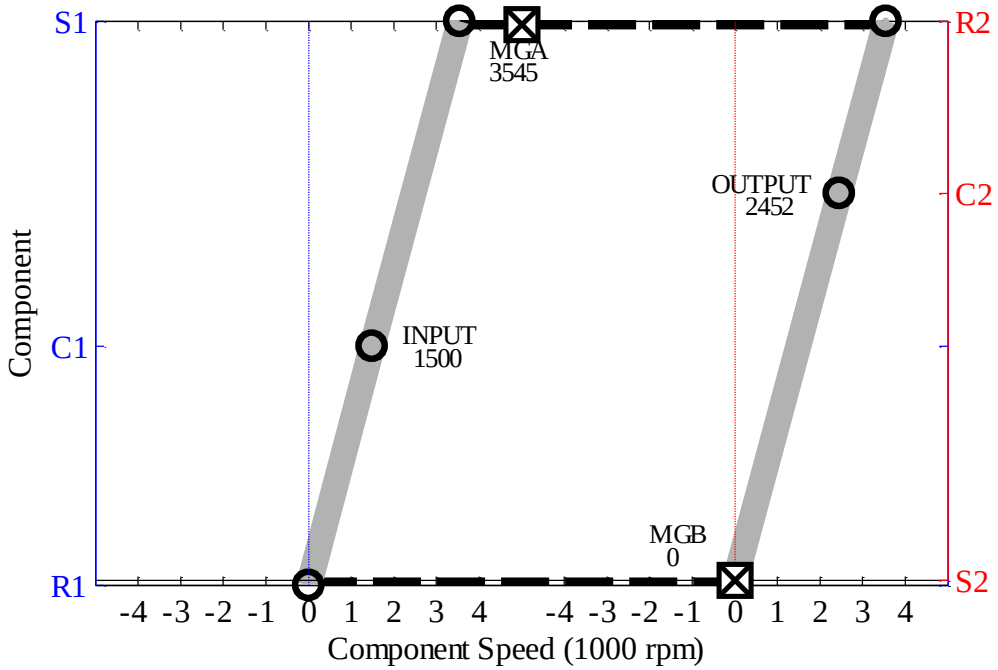

Figure 3-25: FG4 Operation

The output torque equation and speed ratio for this gear are given in Equations 3-20 and 3-21.

$$T_{out} = \left({}^{1}/_{r_2} + 1\right) \cdot \left(\frac{T_{ice}}{r_1 + 1} + T_{mga}\right) \qquad 3\text{-}20$$

$$\omega_{ice} = {}^{(r_2 + 1)}\Big/_{r_2 \cdot (r_1 + 1)} \cdot \omega_{out} = 0.61 \cdot \omega_{out} \qquad 3\text{-}21$$

The output torque capability of FG4 lies along the line of the second mechanical point within the operation space of Mode 2. Here, as in the case of FG2 and Mode 1, Mode 2 is capable of higher output torque at some vehicle speeds than FG4, as ICE speed can be adjusted to more powerful regions when the transmission is operating in Mode 2. The capabilities of FG4 and Mode 2 as a function of vehicle speed are shown in Figure 3-26.

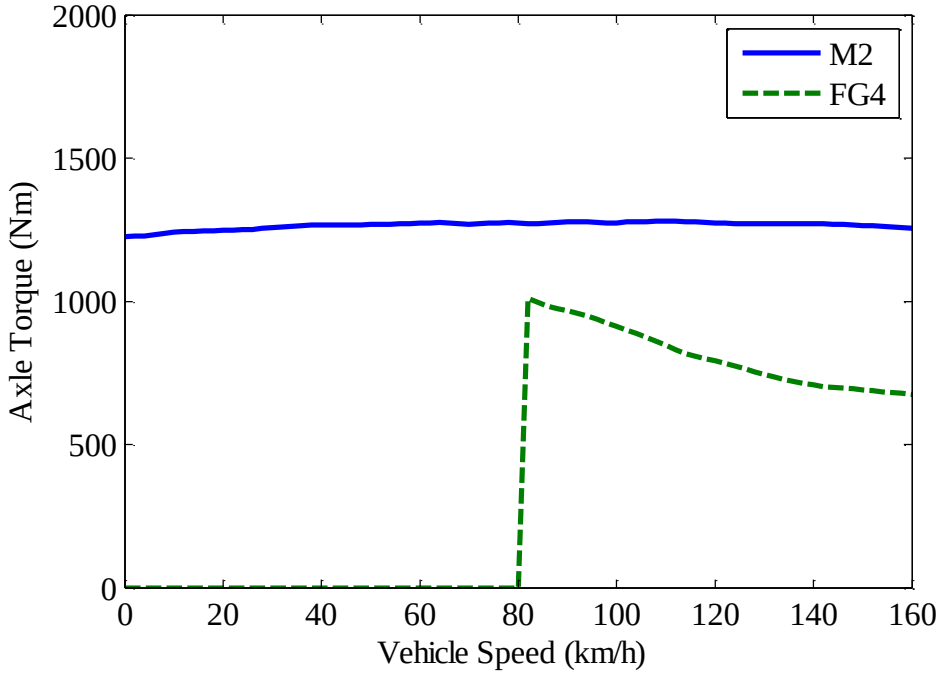

Figure 3-26: M2 & FG4 Max Axle Torque Capacity

3.3.7. 2-Mode Plus Rear Traction Motor

The RTM is connected to the rear axle by a single-reduction transaxle with a gear ratio of 8.28 to 1. This high ratio means that the RTM can supply large amounts of axle torque, as shown in Figure 3-27; however, this ratio also means that the maximum RTM speed limit of 8000 rpm is reached at roughly 125 km/h (discussed further in §4.4), and the continuous torque capability of the RTM at highway speeds is limited.

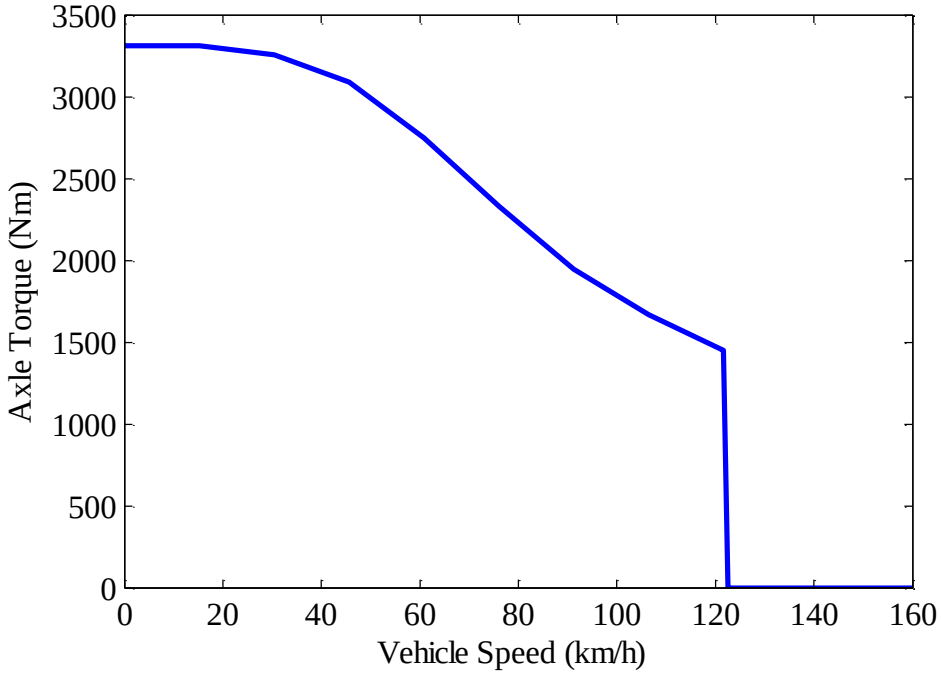

Figure 3-27: RTM Max Axle Torque Capability

CHAPTER 4 Vehicle Development and Modeling

The EcoCAR Challenge provides a unique platform for collaboration between academia and industry with the goal of furthering the development of HEV technology. The three year EcoCAR vehicle development process (VDP), as summarized in Table 4-1, is modeled on the development process of major automotive manufacturers.

Table 4-1: EcoCAR Vehicle Development Process

YEAR & OBJECTIVE	MECHANICAL	ELECTRICAL	CONTROLS
Year 1: Design	Lifecycle analysis, vehicle architecture selection and performance modeling		
	CAD - Component	Define Electrical Requirements	Control System Design
	CAD - Routing and Integrations	HIL Design/Setup	Simple Control and MIL / Prelim HIL
Year 2: Mule Vehicle	Finalized Component Selection		
	Vehicle Modification	Vehicle Harness / Systems Design	HIL Finalization & Communication Setup
	Component Integration	Vehicle Harness Setup	HIL Testing - Safety and Fault Mitigation Implementation
Year 3: Optimization & Refinement	Controls Integration and Vehicle Troubleshooting		
	Aerodynamics and Lightweighting	Refinement and Optimization	Refinement and Optimization
	99% Buyoff - Vehicle Ready for Production		

A significant portion of time and resources during vehicle development are spent on control system development – especially when considering hybrids – and EcoCAR is no exception. HEVS are highly complex mechatronic systems whose proper operation relies not only on individual powertrain components, but also heavily on an advanced network of electronic controllers that must work seamlessly to ensure a reliable, safe, and efficient system. In turn, these control systems must undergo significant amounts of testing both before and after integration in the vehicle. The automotive industry therefore relies on a

process that uses model-based design (MBD) in the development and testing of vehicles. This process is outlined in Figure 4-1, which is termed the V-diagram.

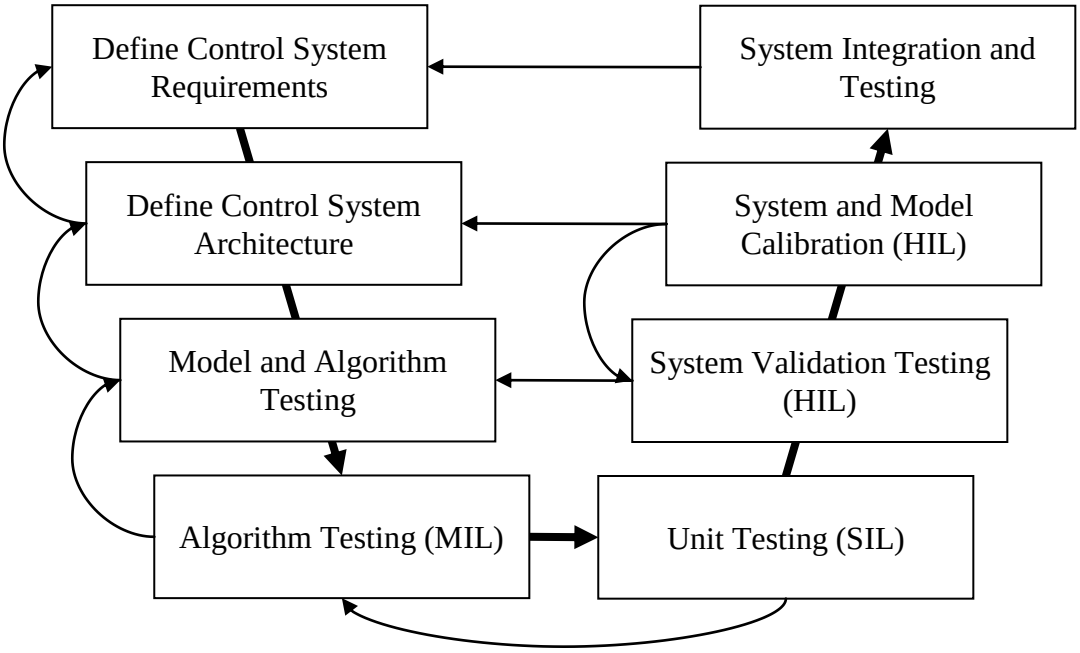

Figure 4-1: Control Development V-Diagram

The following sections outline UVic EcoCAR's progress through the V-diagram steps, including integration of UVic's control system hardware and software into the VUE platform, the process of MBD, the modelling work done by UVic and in the development of this thesis work. It is important to note here that a number of UVic EcoCAR Team members played a role in the vehicle development process; the author is not attempting to take credit for all of this work, but summarize the work of many.

4.1. Control System Integration

Integrating non-stock components into a HEV can be challenging from a mechanical standpoint, but is more daunting from a controls hardware and software perspective. This is primarily due to the significant amount of information transferred between vehicle

components and the fact that production vehicles have been finely tuned to operate with their intended components. Fortunately, the integration process was supported by GM, who provided human and intellectual resources, and modified software where necessary. The following sections briefly discuss the control hardware and software architecture for the UVic EcoCAR; more detailed information can be found in a published paper on the topic [40].

4.1.1. Control System Harware Architecture

Figure 4-2 shows the control hardware architecture of the stock GM 2-Mode transmission and the system as modified by UVic.

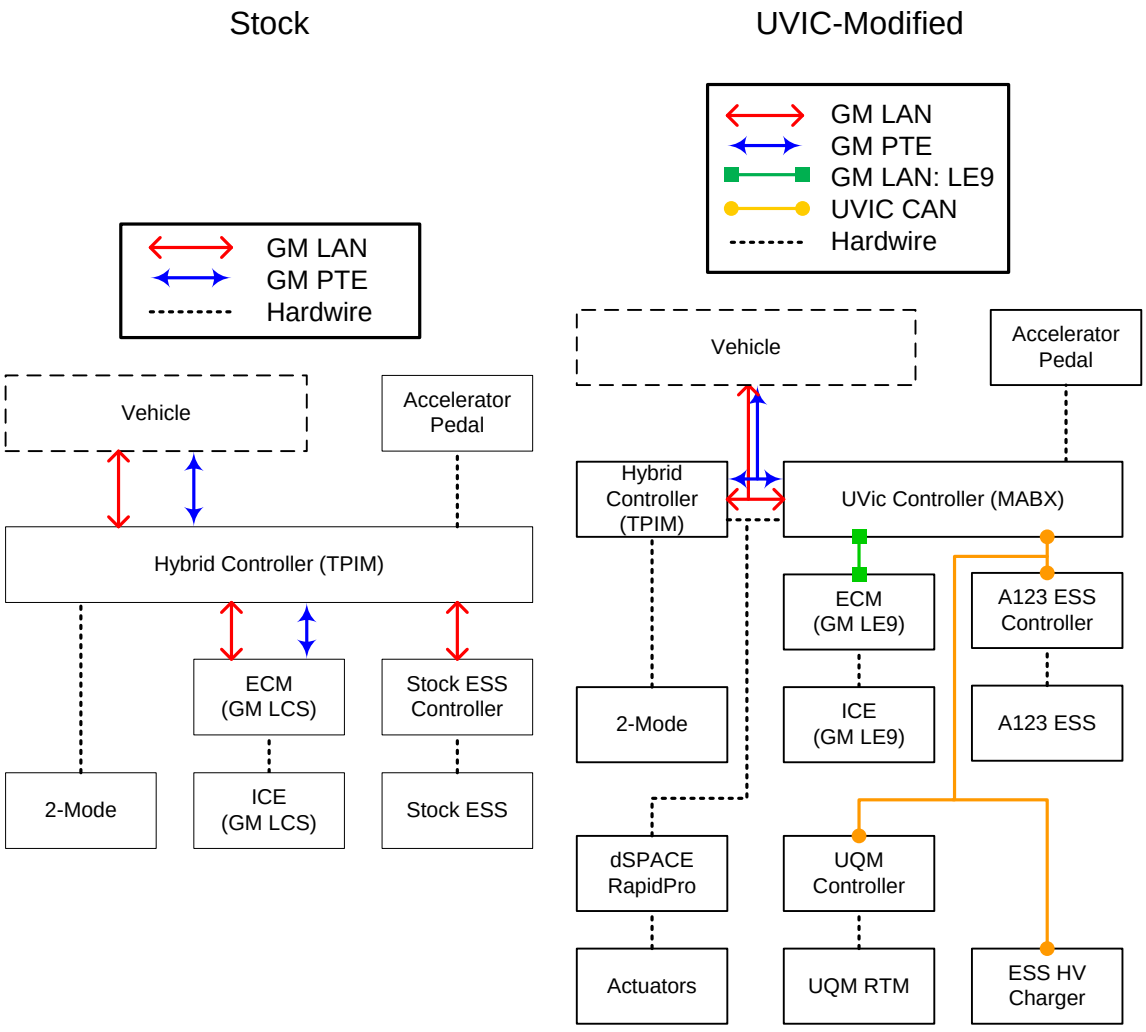

Figure 4-2: Stock GM 2-Mode (Left) and UVic EcoCAR (Right) Control Hardware Architecture [40]

In the stock vehicle, the Transmission Power Inverter Module (TPIM) acts as the supervisory controller, which interprets driver input, determines operation of the system, and communicates with hybrid components using two controller area network (CAN) buses/channels.

The UVic control architecture uses a dSPACE MicroAutoBox 2 (MABX) [41] as the supervisory controller combined with a modified TPIM. This modified TPIM allows the the MABX to assume supervisory control of the system and issue high level commands

such as desired ICE operation, desired gear, and desired axle torque, via a special software interface introduced by GM specifically for EcoCAR. The TPIM still performs many of the lower-level processes required in the vehicle, such as MG and clutch control, which would be nearly impossible for a student team to implement.

In addition to assuming supervisory control of the system, the MABX also plays a pivotal role in translating and relaying messages across four CAN channels – both stock channels, as well as a channel for the LE9 ICE and a channel for UVic-added components. Messages must be translated to meet the controller requirements for each respective powertrain component. For example, messages from the A123 ESS must be sent to the TPIM in the same format as those sent from the stock ESS. Additional components, such as sensors, ESS coolant pumps, and the HV ESS charger are also controlled by the MABX with the help of a dSPACE RapidPro, a system of high- and low-side drivers.

4.1.2. Control System Software Architecture

With this hardware architecture in mind, a modular control system software architecture was developed for the UVic system, as shown in Figure 4-3. Dotted lines represent hierarchical logic levels in the controller and solid rectangles represent controller subsystems.

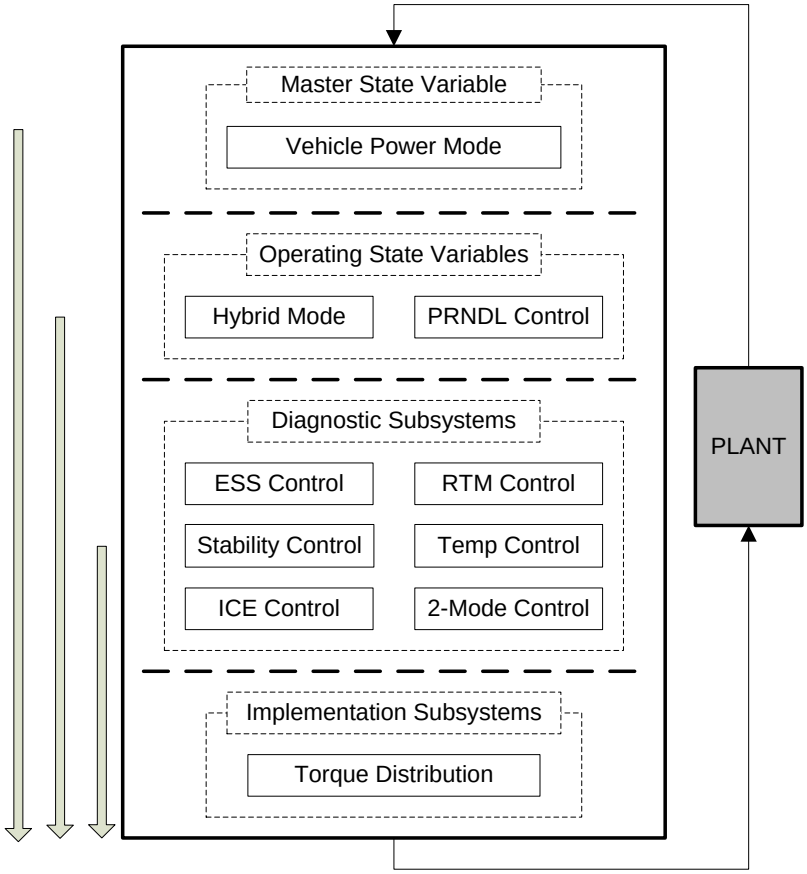

Figure 4-3: UVic Control Software Architecture [40]

The UVic control system was designed and organized in a hierarchical fashion based on the functional roles for which it was intended, and the function of the system is bound tightly to the functions of vehicle and existing control system. Subsystems higher in the hierarchy enforce vehicle operating states and define the function of the remaining subsystems.

The highest layer in the hierarchy is the 'Vehicle Power Mode' subsystem, which takes input from the vehicle regarding its current operational state – this is essentially the on/off switch for the vehicle, based on key position. The second level, the 'Operating State Variables', further define system operation: the 'PRNDL Control' subsystem (an acronym for the gear positions on an automatic shifter – Park, Reverse, etc.) enables or

disables propulsive power and determines torque direction, while the ‘Hybrid Mode’ subsystem commands either CD or CS modes. The hybrid mode subsystem also houses the majority of decision making subsystems in the controller, including those that determine the desired ICE speed and torque, and gear.

The ‘Diagnostic’ subsystems communicate heavily with the vehicle and UVic-added components to perform the necessary message translation for signals that transition across CAN buses, assess the state of their respective systems, and inform operation of other control subsystems. For example, the ‘RTM Control’ subsystem monitors the temperature of the RTM and inverter coolant loop, the torque limits of the motor, and a number of diagnostic CAN messages sent by the RTM in order to determine the extent to which the RTM can be used. Diagnostic information is used by systems at different levels in the control hierarchy to inform operating decisions on both long- and short-term scales.

Finally, the ‘Torque Distribution’ subsystem applies power to the wheels based on the driver’s request and information from other subsystems. For example, the ‘Stability’ subsystem is intended to monitor wheel slip and ensure that torque is distributed safely and effectively between axles; it therefore imposes limits on axle torque that the ‘Torque Distribution’ subsystem adheres to during operation, regardless of the driver’s torque request.

4.2. The Model-Based Design Process

Like the automotive industry, the EcoCAR Challenge places a large emphasis on MBD in its vehicle development process. MBD is a methodology first widely adopted in the automotive industry (though now used by many others) that relies on the development and use of mathematical system models that allow developers to design complex systems

quickly, efficiently, and safely. The use of a mathematical model means that development of various aspects of the system, such as a controller, can begin earlier and proceed more quickly without the need to have the physical system present. As the products developed by the automotive and other industries increase in complexity – take hybrid vehicles, for example – MBD helps to reduce time-to market, reduce development costs, and improve product quality [42]. For example, MBD is used heavily in the automotive industry not only for the development of control strategies, as it is applied in this work, but also for the equally important development of on-board diagnostics and fault/failure mitigation [43]. Even aside from the fact that the development of a model is typically much less expensive than the development of a physical prototype, beginning the development process earlier provides significant benefits.

4.2.1. Model-, Software-, and Hardware-in-the-Loop

There are several stages in the MBD process as shown in the V-diagram: model-in-the-loop (MIL) testing, software-in-the-loop testing (SIL), and hardware-in-the-loop (HIL) testing.

MIL testing involves simulation of the plant and control software on a single platform, typically a PC, whereby communication protocols are usually not defined and aspects of the plant or control software may be simplified. The goal of MIL is to develop and test algorithms quickly and efficiently; a completely accurate representation of the plant may not be necessary or possible, especially at the early stages of development. The complexity of the plant and controller in MIL testing typically increase until a transition to SIL and HIL testing can be made.

SIL testing involves testing embedded code developed in MIL on individual controllers to verify its operation.With UVic EcoCAR developing only one controller, and with it being the supervisory controller for the system (meaning that feedback from the plant was ideally required to ensure proper operation), SIL testing in EcoCAR was brief.

HIL testing is the ultimate goal of the MDB process, whereby an accurate plant model and the corresponding control software operate on different hardware – a HIL simulator and the embedded controller to be used in the final product, respectively. Plant and controller communicate using methods intended for the final product (network and/or hardwired communication), and the HIL system emulates the final product to the degree that, from the perspective of the controller, it is essentially indistinguishable from the physical product. Figure 4-4 demonstrates the progression in EcoCAR from MIL to HIL to in-vehicle testing.

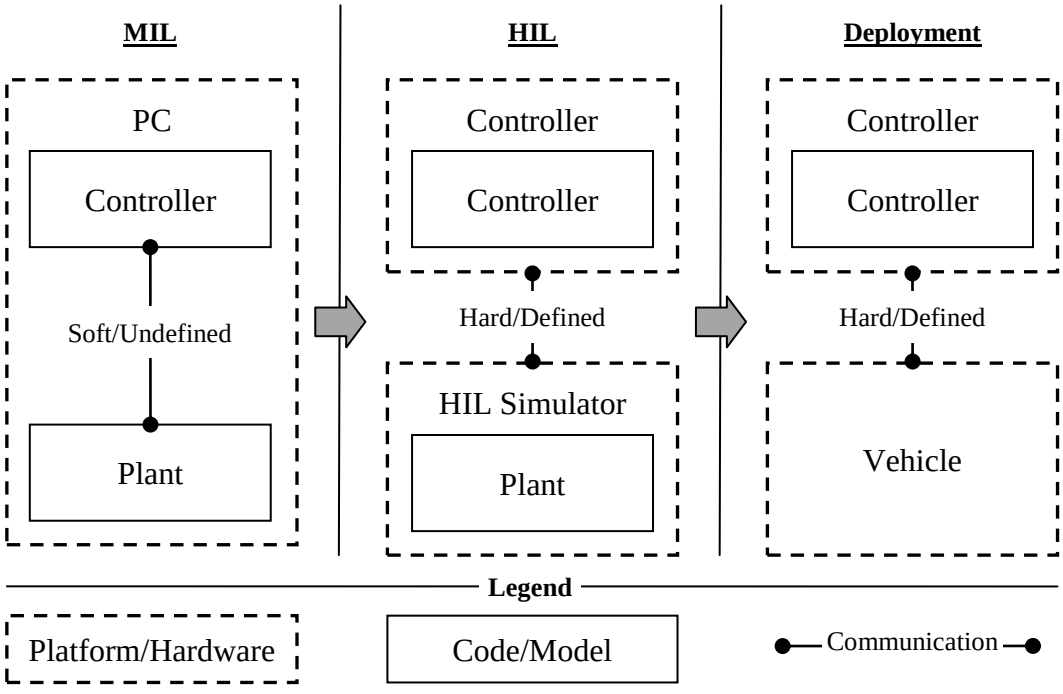

Figure 4-4: Progression Through MBD Process

4.2.2. HIL Testing and Fault Mitigation

As mentioned at the beginning of this section, an important use of HIL testing – in addition to the development of a control strategy – is the development of on-board diagnostics and remedial action, and safety systems in general. In this case, HIL systems not only allow for the development of safety systems earlier, but also increase the ease with which they can be tested. Especially when developing and testing remedial actions for component or vehicle failures, the benefits of use of a virtual model versus a physical component or vehicle are obvious. While the goal is to ultimately test all safety systems in the physical realm, the use of HIL testing prior to physical testing provides reasonable assurance that a safety measure will work properly when required.

The process of HIL failure testing in the automotive industry is frequently driven by the results of failure mode and effects analyses (FMEA) completed throughout the vehicle or control system design process. FMEA, reviewed in detail here [44], is a process used to determine, categorize, and resolve potential failures for a vehicle or individual vehicle components based on a systematic analysis of vehicle systems and their combined operation. Based on FMEA results, specific safety systems tests, including both the failure itself and the remedial actions, can be incorporated into a HIL model/system for testing. This process is highly iterative, and is illustrated in Figure 4-5.

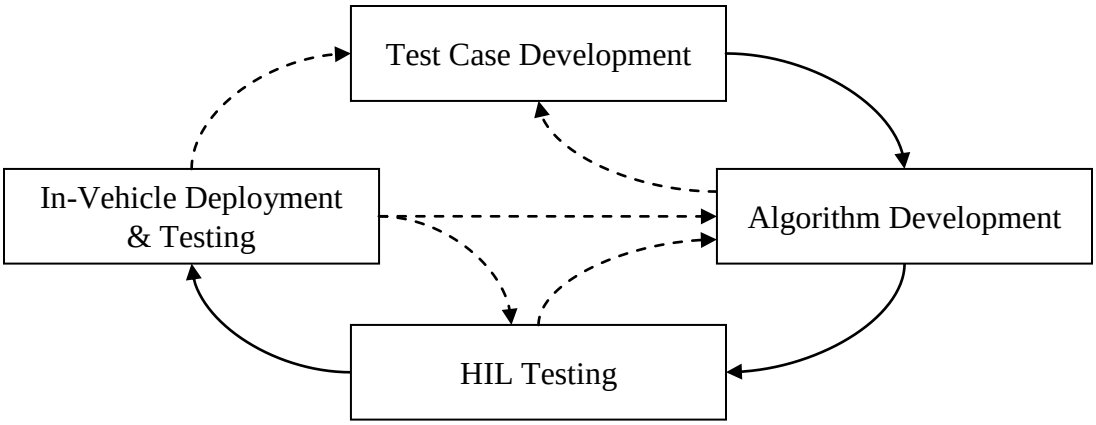

Figure 4-5: HIL Testing Strategy [40]

Once HIL testing is complete, in-vehicle testing may be performed, with results determining the necessity for additional testing.

Starting the control design process with a well-tuned, production vehicle had two primary effects on control system development and HIL testing. First, FMEA activities focused on systems added by teams and their interfaces with existing vehicle systems which greatly reduce the workload typically associated with completing a FMEA. Second, and more importantly with regards to this work, having little to no insight into the VUE design process and the intricacies of its stock control systems (EcoCAR teams did not have access to GM code or specific details regarding intended system operation) meant that much had to be learned through direct in-vehicle testing to proceed through control system development. In essence, some aspects of the HIL system were 'reverse-engineered' from the physical vehicle.

A full discussion of the Team's FMEA and HIL testing activities is beyond the scope of this work. However, it is worth noting the challenges associated with modifying a production vehicle, as in this case. Having little insight into the design and function of the vehicle, especially during the process of architecture selection, led to several difficulties

during the development of the selected architecture, which in turn, resulted in several vehicle limitations, which will be summarized following a discussion of the plant model used for control development.

4.3. Vehicle and Powertrain Modeling

This section summarizes the UVic vehicle and powertrain models used during control system development. Several UVic powertrain component models are based on manufacturer data that was supplied to the UVic team under a non-disclosure agreement, and as such, true data for such components will not be presented in this thesis. Exemplary data in the public domain will be given where applicable. Additionally, notable limitations of the model and their effects on model performance are noted.

It is worth mentioning again that a number of UVic EcoCAR Team members were involved in the modeling process. In general, each individual component models were developed by a small group of members, with the author overseeing model connectivity, tuning, and control development.

4.3.1. Vehicle and Driveline Model

The vehicle and driveline models were developed in Mathworks' Simulink® environment using SimDriveline, a part of the SimScape library, which is intended specifically for automotive modeling. Examples of several blocks in the library are shown in Figure 4-6.

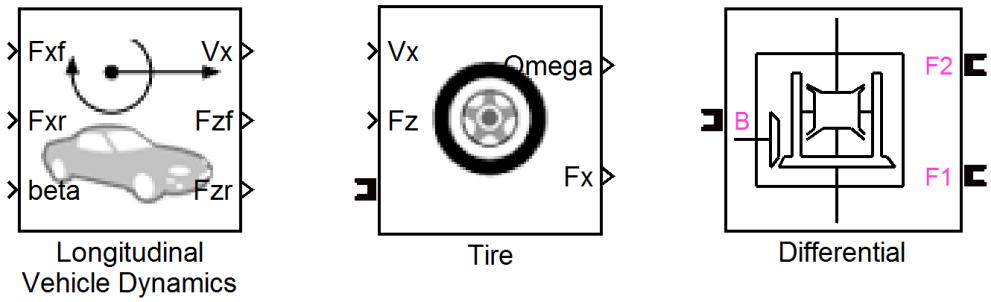

Figure 4-6: SimDriveline Component Models

While the SimDriveline library contains a component for modeling longitudinal vehicle dynamics, as shown above, deficiencies in the calculation of static and rolling friction pointed out by Wise [4], were remedied through the use of an additional term based on a simple glider model outlined in Figure 4-7.

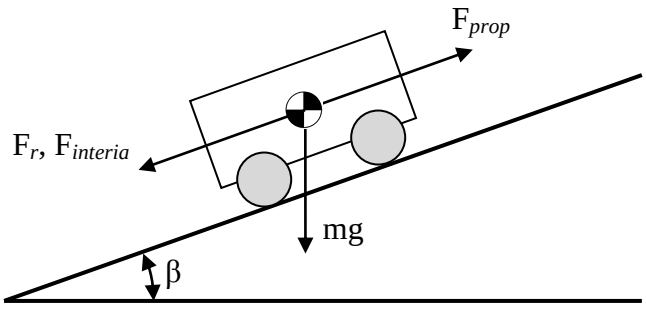

Figure 4-7: Vehicle Glider Model

The propulsive force in this model is governed by Equations 4-1 and 4-2.

$$F_{prop} = F_r + F_{inertia} + mg \cdot \sin\beta \qquad 4\text{-}1$$

$$F_r = F_0 + F_1 \cdot v + F_2 \cdot v^2 \qquad 4\text{-}2$$

Where:

F_{prop} = propulsive force

F_r = resistive force, including aerodynamic drag and rolling friction (F_0 = 180; F_1 = 4.863; F_2 = 0.551)

$F_{inertia}$ = inertial force due to acceleration of vehicle

v = vehicle velocity

The driveline, including wheels, half-shafts, front and rear differentials, as well as the 2-Mode transmission and RTM/transaxle shafts and gearing, were modeling using standard blocks from the SimDriveline library. Inertias for each component were based on data provided by manufacturers.

Limitations

The SimDriveline environment was developed to provide a simple and practical method to model vehicles and drivelines, and as such, the fidelity of some aspects of the model are relatively low. For example, no standard SimDriveline component exists for modeling lateral vehicle dynamics, and tire models are simplified. Additionally, shafts in the environment are stiff, meaning that there is no compliance in the drivetrain. These limitations make this model unsuitable for modeling driveline or tire dynamics, such as for the development of a traction control system, but the model is suitable for the type of testing done in this work – using standard drive cycles and assuming standard road conditions.

4.3.2. ICE Modeling

The characteristics of the LE9 ICE are given in Table 4-2.

Table 4-2: GM LE9 ICE Characteristics

Characteristic	Value
Cylinders	Inline 4
Displacement	2.38 L
Bore/Stroke	88/98 mm
Peak Power w/ E85 Fuel	131 kW @ 5800 rpm
Peak Torque w/ E85 Fuel	230 Nm @ 5000 rpm

GM provided an ICE brake specific fuel consumption (BSFC) map for normal operation using E85 fuel, which serves as the basis for this table-based model. An example of a BSFC map for a 1.6 L inline 4 ICE, taken from PSAT [15], is given in Figure 4-8. A BSFC map represents the ratio of fuel consumption to output power for an ICE (in this case grams of fuel per kWh of output energy), and simplifies comparisons across different ICEs.

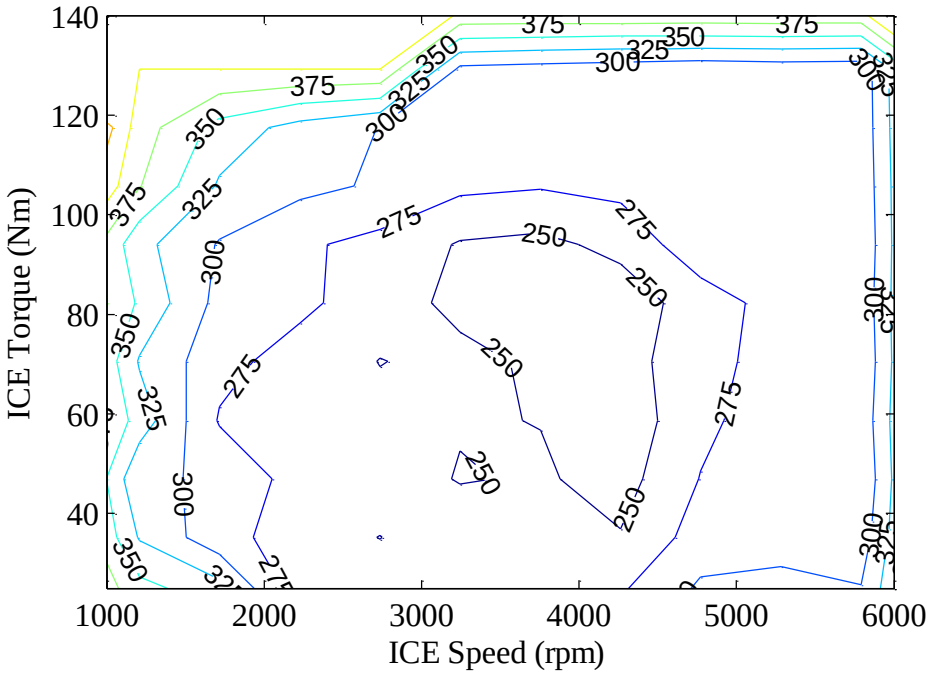

Figure 4-8: Example BSFC Map for 1.6 L ICE (g/kWh) [45]

The model essentially responds to torque commands up to its maximum torque limit at the current operating speed and with appropriate delay in the response, while the BSFC map is used to determine fuel consumption at the current operating point.

Limitations

Table-based models can be inaccurate when used in dynamic systems, as compared to well-tuned dynamic models. Additionally, data was provided only for operation at

standard running temperatures, and therefore, ICE performance during starting and during cold operation will not be accurately modeled.

4.3.3. MG Modeling

The model contains three MGs, two in the 2-Mode transmission along with the RTM. 2-Mode motor data is proprietary, but data for the RTM is summarized in Table 4-3.

Table 4-3: UQM PowerPhase 145 MG Characteristics [46]

Characteristic	Value
Motor Type	Permanent Magnet Synchronous AC
Min/Max Voltage	240 – 420 V
Peak/Continuous Torque	400/250 Nm
Peak Power	145 kW
Peak Efficiency	94%
Max Speed`	8000 rpm
Weight (w/ Inverter)	66 kg

Similar to the table-based model of the ICE, MG models respond to torque commands up to their maximum limit at the current operating speed, and with an appropriate (*ie*: very short) delay. Based on the output power of the MG, the total power consumption is calculated using table-based data for power loss. Figure 4-9 shows power loss data for the UQM 145. Power loss is used here, as opposed to efficiency, in order to account for losses at zero speed.

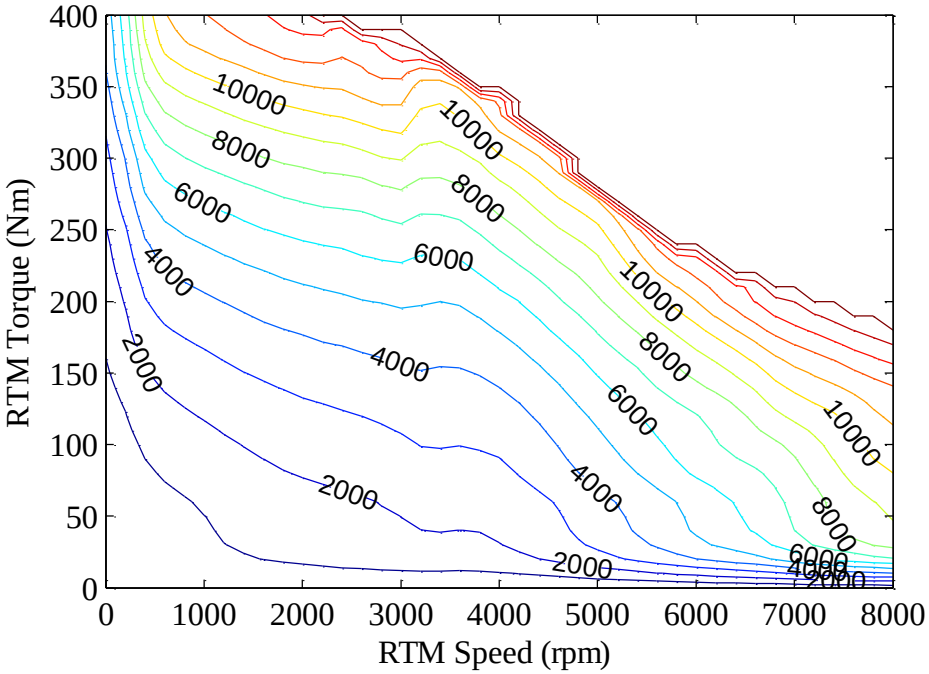

Figure 4-9: UQM Power Loss Map (kW)

As mentioned previously, the gearing and shafts associated with the 2-Mode transmission, UQM, and BorgWarner models were implemented in SimDriveline.

Transmission motor control and shift execution logic was developed by UVic, as this information was not provided by GM.

Limitations

Similar limitations apply to these table-based models as to the ICE model above regarding the use of tables. Additionally, data was provided for a single voltage, and thus, changes in power loss due to voltage sag and surge during operation – which are most likely small but are currently uncharacterized – will not be captured by the model.

4.3.4. ESS

The UVic EcoCAR ESS was developed by the UVic EcoCAR team using modules donate from A123 Systems, based on their AMP20 prismatic lithium-ion cells [47]. Characteristics of the ESS are given in Table 4-4.

Table 4-4: A123 ESS Characteristics

Characteristic	Value
Module Configuration	22 Series x 3 Parallel Cells
Pack Configuration	5 Series Modules
Voltage (Min/Nomimal/Max)	275/363/375 V
Capacity	21.1 kWh
Weight	210 kg

An equivalent circuit model (ECM) [48] of the ESS was developed, which is intended to more accurately model the dynamic characteristics of bus voltage during operation as compared to a table-based model. The basis of this model – an equivalent circuit based on a voltage source, an inline resistance (R_0), and two parallel RC components (R_1, C_1 and R_2, C_2) – is shown in Figure 4-10, though parameters will not be disclosed. The performance of the ECM was tuned in Simulink using the Parameter Estimation tool and real-world data from preliminary physical ESS testing.

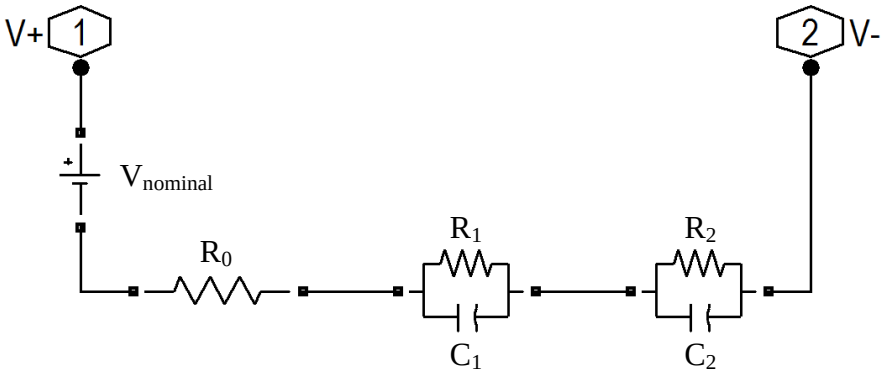

Figure 4-10: Equivalent Circuit Model of ESS

Resistive losses and heat generation were modeled based on tabular data for cell resistance provided by A123, and according to Equations 4-3 and 4-4 where *R* is pack resistance (not to be confused with the R values in Figure 4-10), *T* is pack temperature, and *I* is current.

$$R = f(T, SOC) \quad \text{4-3}$$

$$P_{heat} = I^2 \cdot R \quad \text{4-4}$$

Limitations

Modeling the dynamic sag/surge response of a lithium-ion battery is a difficult prospect, especially since its operation is dependent on the system to which it is connected. For example, a system with high capacitance (as is the case for the UVic EcoCAR, which has three MG inverters), may result in larger and more pronounced fluctuations in battery voltage. In general, however, this model offers good dynamic performance based on the ECM method.

4.3.5. Driver

The driver model converts a given desired speed profile into an appropriate axle torque request that is intended to ensure the vehicle meets the desired speed. The driver consists of three components, two of which are open loop, and one of which is closed loop, as shown in Figure 4-11.

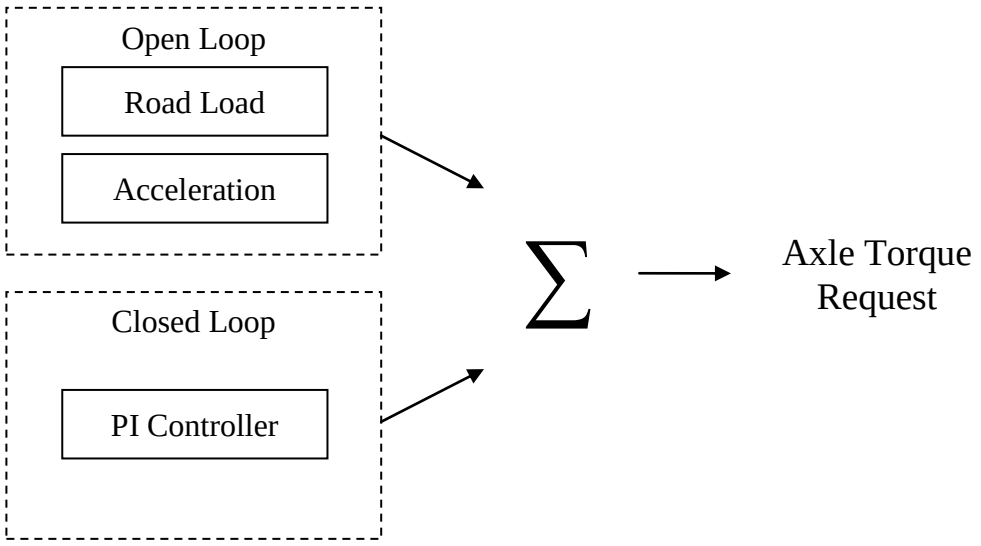

Figure 4-11: Driver Model Components

The ‘Road-Load’ open loop component produces a torque request that matches the aerodynamic and rolling losses of the vehicle at the desired speed. Concurrently, the ‘Acceleration’ component looks ahead in the desired speed profile and produces a torque request based on the difference between the present desired speed and the desired speed at a point 0.1 seconds in the future; this component in part accounts for the tractive force required to accelerate or decelerate the vehicle. Finally, the closed-loop ‘PI (proportional-integral) Controller” modifies the torque request of the vehicle based on the instantaneous difference between the actual and desired vehicle speed, ensuring that it meets the speed trace on a second to second basis.

Figure 4-12 displays the results of a model validation exercise: the difference between actual vehicle speed and desired vehicle speed over the course of the UDDS cycle.

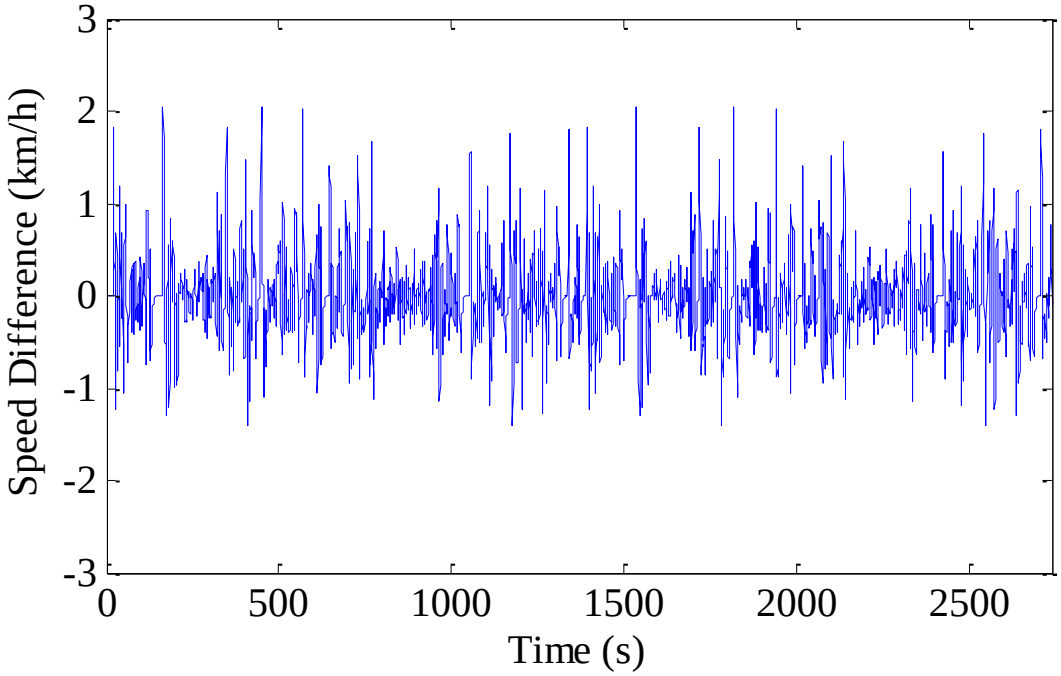

Figure 4-12: Driver Model Validation – Speed Difference for UDDS Cycle

The speed difference is rarely larger than 2 km/h, and marginally so, while the average speed difference over the course of the cycle is 0.29 km/h. While the error can be reduced by further tuning of the closed-loop driver component, attempting to reduce the speed error by too much can result in a volatile axle torque request that does not accurately reflect the response time of a human driver.

Limitations

Emulating a human driver is difficult, though in general, this method produces satisfactory results. Problems can arise when the vehicle is not capable of meeting the speed trace. This results in large driver torque requests that take time to correct once the vehicle meets the desired speed and can exceed the torque capabilities for the vehicle at some speeds (since torque output is a function of vehicle speed). This can result in overshoot when following a trace, but provisions have been made in the controller to account for torque requests that are greater than the capability of the vehicle.

4.3.6. Model Validation

In order to validate component operation in the model, and in light of the limitations listed in the previous sections, the overall performance of the model was compared to that of the actual vehicle. A velocity profile captured during preliminary vehicle testing, shown in Figure 4-13, was used as input to the model, and the results of both model and vehicle were compared.

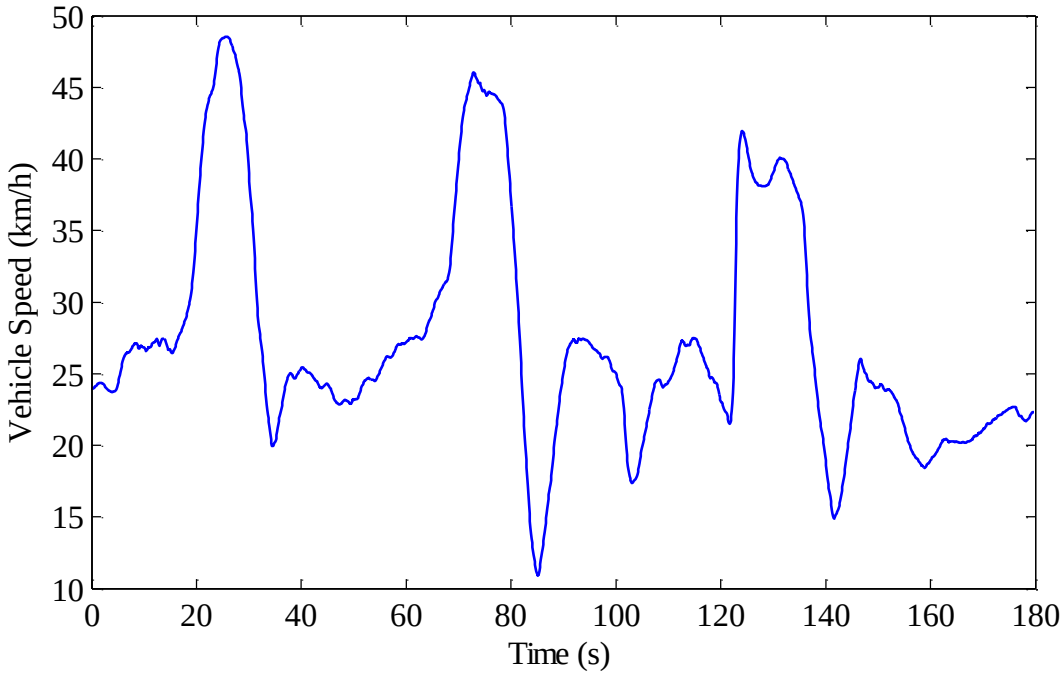

Figure 4-13: Model Validation – Speed Trace

The vehicle had a constant traction split of 0.5 during the validation cycle, and in order to ensure consistency across the results for the model and vehicle, ICE operation and gear selection during the cycle were also captured and used as request from the control system to the model. Without doing so, gauging the accuracy of ICE and transmission operation is difficult.

First, the accuracy of the vehicle dynamics model will be assessed; axle torque requirements to meet the speed trace are shown in Figure 4-14.

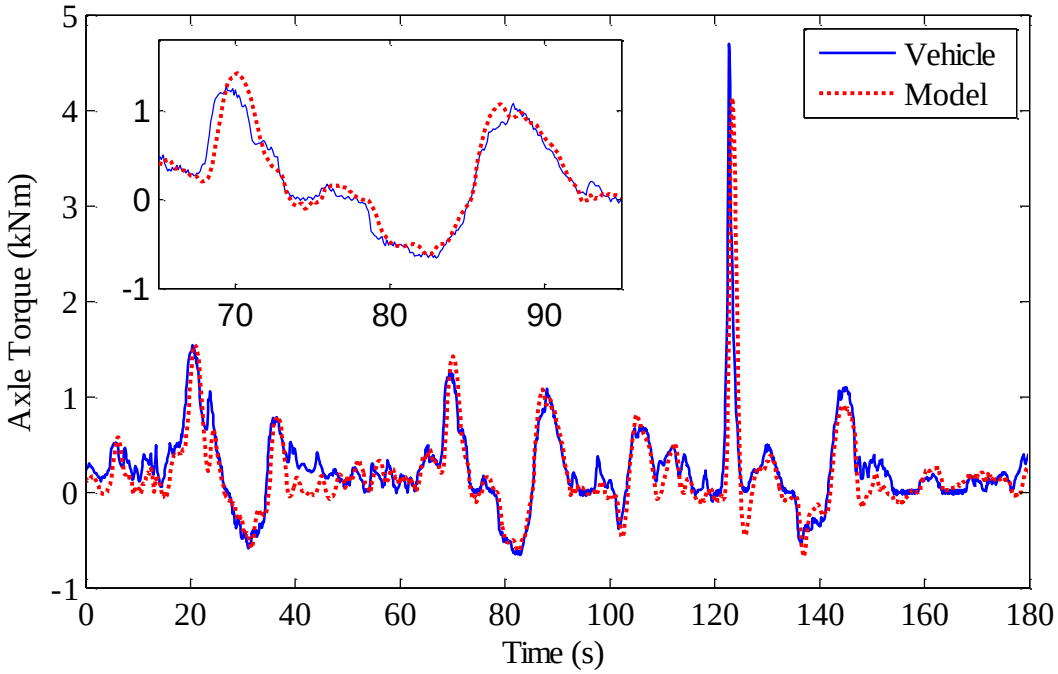

Figure 4-14: Model Validation – Axle Torque

Results are fairly consistent and the differences between the vehicle and model may in part be the result of the driver model. Emulating a human driver in simulation is difficult. Considering that output torque in the model is determined only by the speed profile input, not much more can be expected from a model of this fidelity.

As the ICE is look-up table-based, it will obey the torque request from the controller within its operation limits and with a slight delay. ICE speed, however, is controlled by 2-Mode, which is in turn controlled by the aforementioned UVic-developed transmission controller. Figure 4-15 compares ICE speed between model and vehicle.

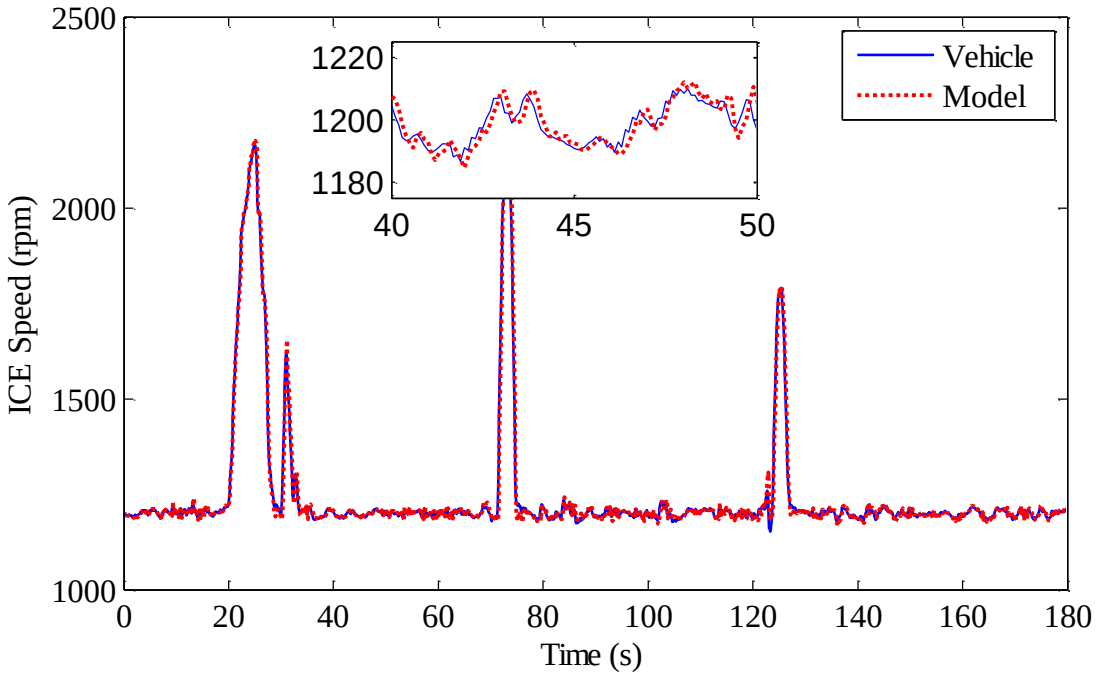

Figure 4-15: Model Validation – ICE Speed

ICE speed in the model very closely matches the true ICE speed, including the small fluctuations shown in the inset. The fact that the 2-Mode model is capable of controlling the ICE to such a degree confirms that the 2-Mode transmission model and controller are sound.

Figure 4-16 shows the fuel rate over the course of the cycle.

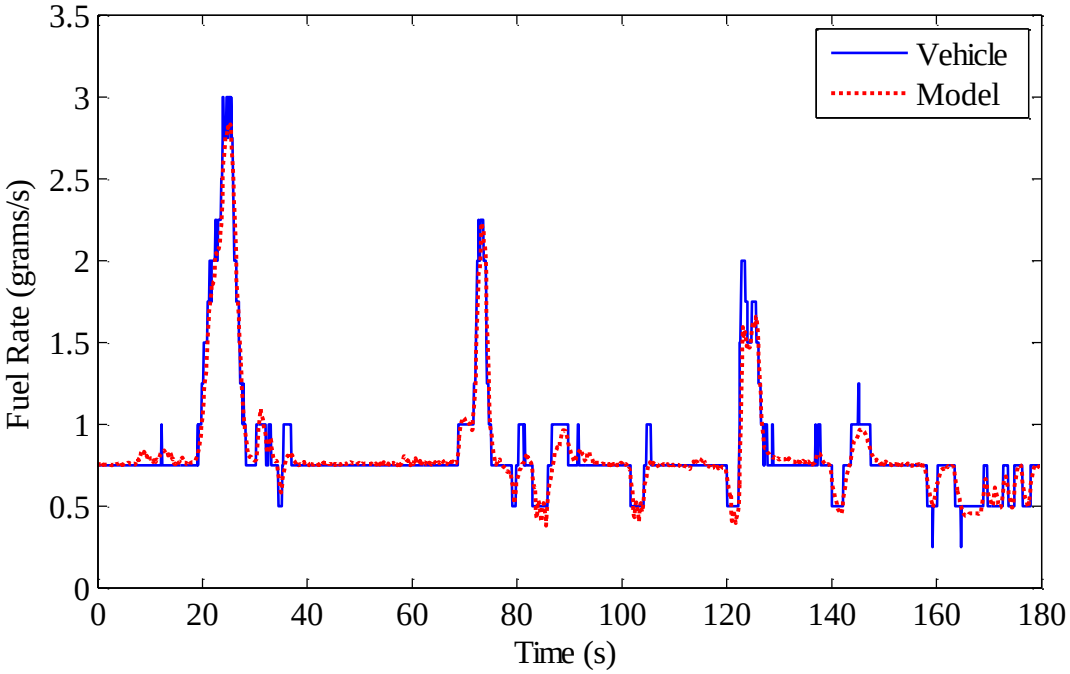

Figure 4-16: Model Validation – Fuel Rate

The fuel rate results are acceptable, though caution must be used in interpreting these results: as emissions testing equipment was not available, a low resolution (0.25 grams/s) CAN message from the ICE was used here for comparison. The total fuel use over the cycle differs by 1.4%, though the accuracy of this signal has not been verified and the low resolution of the signal also induces error in this calculation.

Figure 4-17 displays the ESS power throughout the cycle.

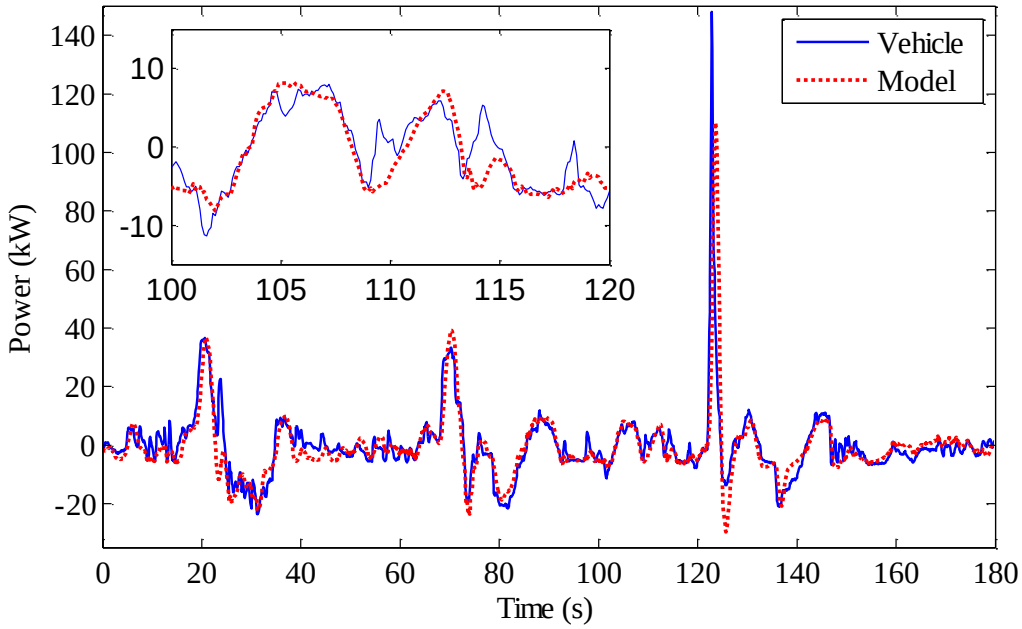

Figure 4-17: Model Validation – ESS Power

ESS power is a function of axle torque, and so it is difficult here to distinguish the error due to inaccuracies in the ESS model from the error due to differences between axle torque in the vehicle versus the model. In general, the equivalent circuit model shows good dynamic response, though modeling the dynamics of three MG inverters on a high-voltage bus is a difficult prospect; the inset shows that some of the oscillatory behavior present in the vehicle is lost in the model.

Overall, the results of model validation appear satisfactory, though caution must be used when interpreting results obtained from this model. This is especially true when considering fuel economy values, as no truly reliable validation of model results has occurred. Ideally, fuel economy and emissions data for standard drive cycles would be captured and compared to similar drive cycles in the simulation, but this is not possible at this time (see §7.3). Indeed, a degree of inconsistency is expected given that the components are primarily based on look-up tables and that the driveline was built in the

SimDriveline environment. As such, though the validation exercise appears promising, more emphasis should be placed on trends in the model rather than on actual fuel economy values.

4.4. Challenges in Control System and Powertrain Integration

Many challenges encountered during vehicle development were the result of either a lack of information available to UVic during the architecture selection process, or the modification of a system that had been finely tuned to meet its original design goals. These limitations affect the operation of the car and the scope of this work, as discussed in the following paragraphs.

The most significant issue relates to the fact that the 2-Mode transmission was developed for a pure hybrid application (as opposed to a PHEV or EREV application). It therefore does not possess a high speed all-electric mode of operation. It was believed at the time of selection that this limitation could be overcome through software changes provided by GM. While GM did supply 2-Mode transmissions with the custom control interface mentioned above, as development progressed it was determined that the proposed modifications were not possible. As a result, the ICE must remain spinning at speeds above 50 km/h. In order to obtain a fully-functional all-electric mode in the UVic architecture, the LE9 is placed in a spinning, un-fuelled state above this speed threshold, which affects CD AER, but does not affect CS operation. It should be noted, however, that GM has subsequently successfully modified the 2-Mode transmission hardware and software in order achieve high speed electric operation and thus adapt the transmission to a PHEV application [49].

Additional issues relate to the coupled 2-Mode/LE9 system. The system has a resonant frequency at an ICE speed of approximately 800 rpm, near the typical idle speed for the LE9, at which operation results in catastrophic failure. As such, a minimum ICE speed of 1200 rpm must be maintained. Additionally, while the engine control module in the stock vehicle was designed and programmed specifically for a 2-Mode application, the LE9 engine controller is intended for a standard ICE vehicle and therefore lacks several key features related to ICE starting and torque control. This lack of features is detrimental to ICE start/stop procedure as well as gear shifting. Though the specific details are beyond the scope of this description, the result is that engine idle-stop capabilities in CS mode have been disabled for stops shorter than 30 seconds to reduce the number of ICE starts, and that the vehicle uses only the ECVT modes during operation. While a workable solution is under development, this work respects this limitation.

Finally, the RTM is coupled to a BorgWarner 31-01 transaxle, one of the only available transaxles that met torque requirements during architecture selection. At the time of parts sourcing, only a single reduction 8.28:1 gear ratio was available, which places a top speed limit of 125 km/h on the vehicle.

These limitations do have a significant impact on the performance of the vehicle, but such limitations may be expected given the prototype status of the vehicle and the advanced architecture selected. In terms of scope, because of the limitations of the vehicle's CD mode – for which there is no remedy – this thesis focuses on the development of a CS strategy for the vehicle. Primarily, this is because developing a real-time, optimization-based controller to manage the UVic EcoCAR's CD mode does not constitute a contribution to the field of real-time control: such operating conditions are

atypical and would not be seen in industry. A real-time, optimization-based control strategy for AWD CS operation represents a meaningful contribution, and will build a solid foundation for future work. Though CS operation in the UVic EcoCAR vehicle also has several limitations, these limitations may be solved in the future and affect mainly system constraints. Thus, these limitations do not affect the legitimacy or applicability of this work to systems without such limitations.

CHAPTER 5 AWD 2-Mode Control Methodology

At a minimum, the control system must be designed to meet the following requirements:

1. Deliver the torque requested by the driver;
2. Maintain the SOC of the battery; and
3. Accomplish items 1 and 2 in the most efficient manner possible, while adhering to component operating constraints.

At the same time, the control system should be designed to address additional objectives related to driveability and component life, such as:

- Minimize ICE fluctuations that may be undesirable to the driver;
- Minimize the number of transmission shifts to an acceptable level;
- Control electric power draw to lengthen ESS lifetime; and
- Ensure a measure of repeatability with regards to vehicle operation.

Adhering to the points in both of the above lists can be difficult, not only because items in the latter are often at odds with those in the former, but also because items in the latter are more subjective in nature. For example, at certain times it may be desirable to draw very heavily from the ESS for propulsive power, say to meet the torque request of the driver or for reasons related to efficiency. However, doing so repeatedly over the life of the vehicle may result in accelerated ESS degradation, and thus, limits on ESS power draw may be observed despite the reduced performance.

5.1. Hybrid Operating Selection

The UVic EcoCAR architecture offers significant flexibility in terms of operating selection. In each ECVT mode the system has four degrees of freedom (DOF), two of

which – the transmission output torque and output speed – are typically defined by the driver's torque request and speed of the vehicle, respectively. Therefore, defining two additional component operating states within the transmission – one component torque and one component speed – fully defines the coupled transmission and ICE system. In each fixed gear, ICE speed is defined by the speed of the vehicle and the transmission ratio, and thus, only one degree of freedom – one component torque – is present in the system. In both cases, it is most intuitive to define the system using ICE operation. Thus, the decision variables for the 2-Modes system alone are ICE torque, ICE speed (in the ECVT modes), and gear. In addition, the large RTM can also source nearly all of the propulsive power required by the vehicle on most standard drive cycles. As such, an optimal control solution for energy management in this vehicle should also include provisions for determining the optimal traction split between front and rear axles.

The determination of these parameters will from here on be referred to as 'hybrid operating selection' or HOS. While any of the control strategies outlined in §2.1 could be implemented for HOS in this case, the development of a real-time operating strategy is desired not only because such strategies represent the cutting edge of current hybrid vehicle control development, but also because the intent of this work is to build on previous research conducted at UVic that resulted in the development of real-time control strategy for the 2-Mode transmission alone (*ie:* a FWD vehicle) based on the ECMS methodology [4].

The extension of ECMS to the UVic architecture increases the complexity and computational requirements of the problem, as the UVic architecture is AWD, making traction split a control variable as well. Additionally, the ultimate goal of this work is the

implementation of this algorithm on the vehicle, and as such, aspects of feasibility and drivability will be discussed.

5.2. Control Structure of HOS

For UVic to complete HOS for this vehicle, GM provided a modified software interface that excludes only GM's version of HOS, leaving the remaining systems, such as motor control and shift execution, intact. It is important to understand GM's control system architecture, as it informs the development of UVic's control system. Though specific details cannot be disclosed, the generalized flow of control system logic for the example of ICE speed and torque control is shown in Figure 5-1.

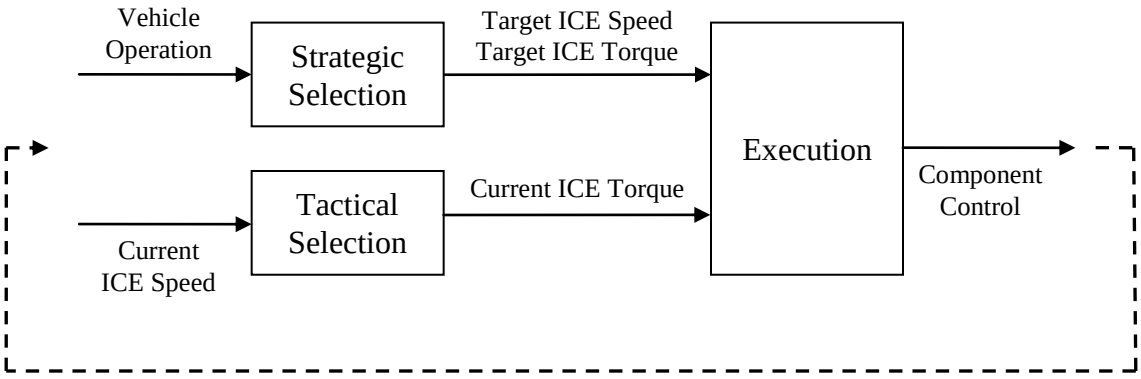

Figure 5-1: Control System Command Logic Flow

As shown, a distinction between strategic and tactical selection is made within the control system. Strategic selection determines the desired or optimal operating state for the vehicle; however, this state may not be immediately attainable. Hence, tactical selection manages instantaneous component operation and while the transition towards optimal operating states determined through strategic selection is being executed. At steady state, the outputs of strategic and tactical selection are theoretically equivalent.

For example, consider a hard acceleration event from a standstill while in an ECVT mode. As the driver depresses the pedal quickly, demanding high amounts of power, strategic selection may request high ICE output power, say an optimal operating point of 3500 rpm and 180 Nm, to accelerate the vehicle. As the ICE was presumably at idle, though, it takes some time before this optimal target is reached. During this transition to the target ICE speed, tactical selection manages ICE torque at the current ICE speed to deliver the required power and ensure attainment of optimal ICE operation. Torque commands from tactical selection are relayed to the ICE controller, where they are executed in the form of fuel injection/throttle commands. Similar decision making is applied for other control variables such as gear.

In terms of implementing a real-time control system with the intent of optimal control of ICE torque, speed, and traction split, the previous example is enlightening. Considering the ECVT modes, it first demonstrates that optimal ICE speed and torque determination must be decoupled; strategic selection should determine an optimal ICE speed/torque operating point while tactical selection determines the optimal torque path to reach the desired operating point. However, the additional requirement of determining the optimal traction split adds complexity to the problem: shifting torque between axles not only alters the operating point of the transmission, but may also take time to implement due to safety and traction considerations. While it would be possible to include traction split determination in the same logical ‘layer’ as ICE speed determination, it is theoretically optimal to separate these two variables so that an efficient speed path can be traced between different optimal traction split operating points. Practically, this means that three separate layers of decision-making should exist

for the ECVT modes, as shown in Figure 5-2. In the fixed gears, ICE speed is defined, and there are only two layers of HOS: traction split and ICE torque determination.

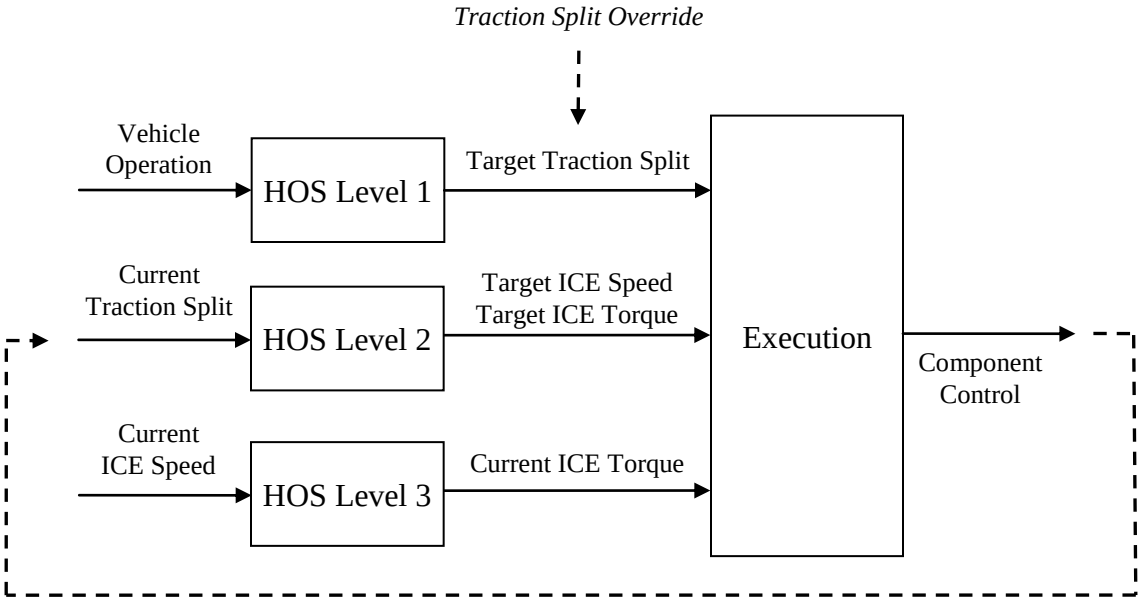

Figure 5-2: Hybrid Operation Selection Logic Flow

The first two levels of HOS represent strategic selection, while HOS level 3 represents tactical selection. In addition to the theoretical increase in efficiency which can only be achieved by separating traction split and ICE speed determination, this separation also makes sense from a logistical standpoint. It is quite possible that the system may be required to operate at a non-optimal traction split, for reasons related to safety or vehicle dynamics for example. Should traction split and ICE speed determination be combined into a single stage while a non-optimal traction split is enforced, the ICE would also be operating in a non-optimal region. The current system ensures that the ICE operates in an optimal region at any given traction split, whether or not this traction split has been implemented through HOS or by some other method.

An in-depth discussion of HOS as described above will follow a review of the ECMS as applied to the UVic architecture.

5.3. Equivalent Consumption Minimization Strategy

The overarching goal of a charge sustaining control strategy is to minimize fuel usage while ensuring a negligible SOC change over the course of any given drive cycle. These two requirements can be represented by Equations 5-1and 5-2.

$$min\left(\sum \dot{m}_{fuel}(t)\right) \quad 5\text{-}1$$

$$\sum P_{ESS}(t) \approx 0 \quad 5\text{-}2$$

Where $\dot{m}_{fuel}$ and P_{ESS} represent fuel mass flow rate and ESS or electric power. As previously discussed, the ECMS equates electricity and fuel usage through the application of an EF to electric power usage, as per Equations 5-3 and 5-4. For the sake of intuition, the unit of measure in this work has been chosen as equivalent power in kilowatts, as opposed to mass fuel flow rate; this choice has no effect on the net result.

$$P_{total} = P_{fuel} + P'_{ESS} \quad 5\text{-}3$$

$$P'_{ESS} = P_{ESS} \cdot {}^{1}/_{EF} \quad 5\text{-}4$$

Placing both energy sources on common ground allows for the formulation of a cost or objective function to be minimized, whereby minimizing the total power of Equation 5-3 over each time interval is assumed to approach the requirements of Equation 5-1, as shown in Equation 5-5.

$$\sum min(P_{total}(t)) \approx min\left(\sum \dot{m}_{fuel}(t)\right) \quad 5\text{-}5$$

Recall, though, that as mentioned in §2.3, Equation 5-5 does not equal Equation 5-1 because no prior knowledge of the drive cycle is available. This means that the real-time optimization-based control that results from the use of the ECMS is sub-optimal by nature, with the goal that the sum of the instantaneous ECMS solutions approaches the true optimal solution over the whole drive cycle. In practice, it is not possible to achieve the true optimal solution, because the operation of the vehicle over a given trip is not known in advance. In general then, the optimal solution can be found using offline methods to set a benchmark for vehicle performance on a known cycle.

Equation 5-3 (the objective function) can be solved using the governing speed and torque equations presented in §3.3 and component data for the ICE and three MGs provided by manufacturers. Using Mode 1 as an example, the following points illustrate the general flow of logic for the calculation of one operating point at the highest level of HOS:

1. Speeds of the transmission output and RTM, and the total axle torque request from the driver are known;
2. Select a desired traction split to determine front and rear axle torques;
3. Calculate the speed of MGB based on transmission output speed;
4. Select an ICE speed;
5. Calculate MGA speed using ICE and MGB speeds;
6. Select an ICE torque;
7. Calculate torques required at MGA and MGB to meet front axle torque request based on ICE torque;
8. Calculate required RTM torque to meet rear axle torque;

9. Check to see that ICE and MG torques and speeds to do not exceed component limits; if so, terminate calculations and prohibit selection of this operating point;
10. Calculate total electrical power consumption of MGA, MGB, and RTM at calculated operating points using component data;
11. Calculate ICE fuel power at selected operating point using component data; and finally,
12. Calculate total equivalent power as per Equation 5-3.

This list represents the calculation of only one operating point. In order to determine the most appropriate combination of traction split, ICE torque and ICE speed, optimization techniques must be used to systematically evaluate the objective function in order to locate the minimum or maximum value within a given region. The optimization technique used in this work is discussed in Chapter 5.

5.3.1. SOC Management and the Equivalency Factor

Maintaining SOC is one of the primary requirements of a CS strategy, and though SOC is not explicitly used in the objective function, it is through the EF that SOC is maintained.

The EF essentially represents the ‘cost’ of electricity as compared to fuel at any given time. Theoretically, over the course of a drive cycle, one could specify a single, static EF such that the final SOC would be equivalent to the initial SOC; this EF represents the average EF over the drive cycle, though during the drive cycle the actual SOC would fluctuate about the initial/final value. Practically, the use of a static EF is not feasible, since every drive cycle has a unique average EF, and without prior knowledge of the

exact drive cycle – and in fact, exact driver behavior, traffic patterns, and road/weather conditions, which can all affect the EF – a unique EF cannot be formulated.

To ensure charge sustaining behavior under all driving conditions the EF must be dynamic, changing the balance between fuel and electric power consumption in order to move the system operating point towards areas that meet the charge sustaining objective. There are several methods by which to dynamically alter the EF, and while some groups have used predictive and optimization algorithms to estimate the EF over drive cycle in real time [38], the most simple and least computationally expensive methods alter the EF based on the difference between the desired and actual SOC, as per Equation 5-6.

$$EF = f(\Delta SOC) = f\left(SOC_{target}, SOC_{actual}\right) \quad 5\text{-}6$$

Equation 5-6 should be formulated such that a SOC higher than the target results in an increase of the EF, thus reducing the cost of electric power, P'_{ESS}, in Equation 5-4, and biasing the objective function towards regions in vehicle operating space that favor higher electric power consumption. Conversely, a SOC lower than the target should result in a decrease in the EF, such that the objective function is biased towards regions of operating space that result in higher ICE power.

For example, the EF was initially implemented in this work as a linear factor proportional to the difference between the current and target SOC, as shown in Equation 5-7.

$$EF = EF_{const} + \beta\left(SOC_{actual} - SOC_{target}\right) \quad 5\text{-}7$$

Where β has been set to 0.1 based on results obtained by Wise [4], and EF_{const} as 0.38. Several alternative implementations and their results on the system are discussed in §6.4.

5.4. Hybrid Operating Selection

To better demonstrate the methodology of HOS using the process described above, an example based on one ECVT mode and one fixed gear is given at an output torque request of 450 Nm at a vehicle speed of about 65 km/h and with an EF of 0.35. This represents mild acceleration with an EF biased towards using ICE power (ie: the SOC is lower than the target SOC).

5.4.1. HOS in ECVT Modes

As previously discussed and shown in Figure 5-2, the first layer of HOS is traction split selection. Throughout this work, traction split is expressed as a decimal value between 0 and 1, representing the proportion of total axle torque applied to the front axle.

Figure 5-3 shows a slice plot of Mode 1 operating space. The marker shown in the figure represents the optimum target of the system in Mode 1. In this case, the optimal traction split is 1.0.

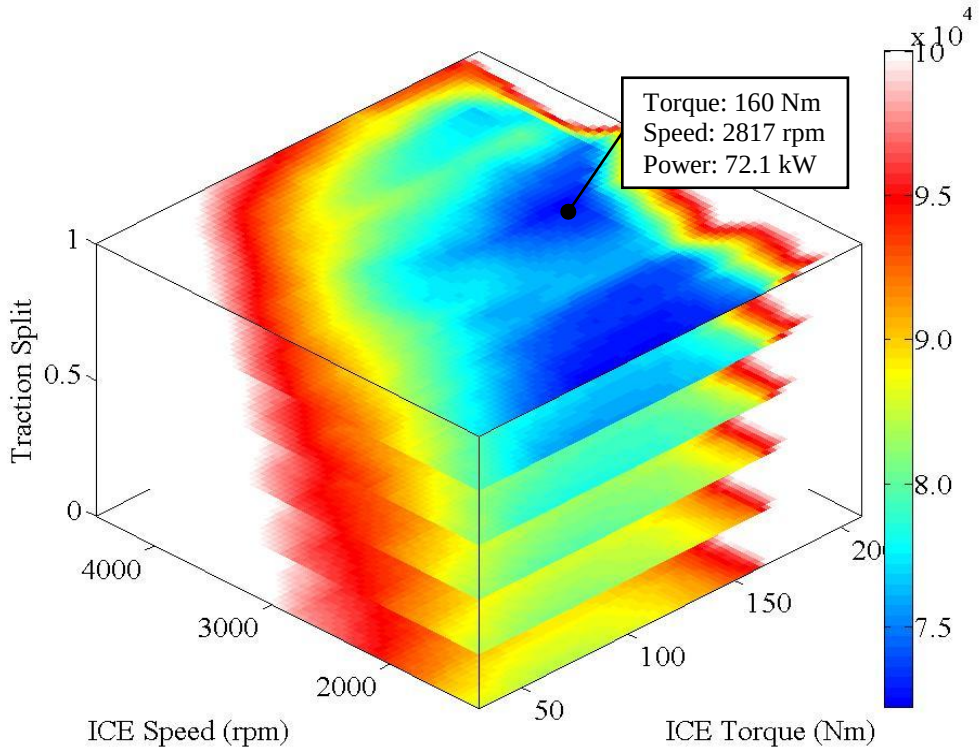

Figure 5-3: Total Power (kW) in ECVT HOS Level 1

As stated in §5.2, the traction split determined above may not be implemented immediately, and the point shown in the figure represents merely the target operating region for the system at the given point in time. The control system must still ensure that the vehicle is operating at peak efficiency during the transition to this operating point.

For the sake of this demonstration, let us assume that the system is currently operating at a traction split of 0.8. Figure 5-4 illustrates the next level of HOS, which is ICE speed selection.

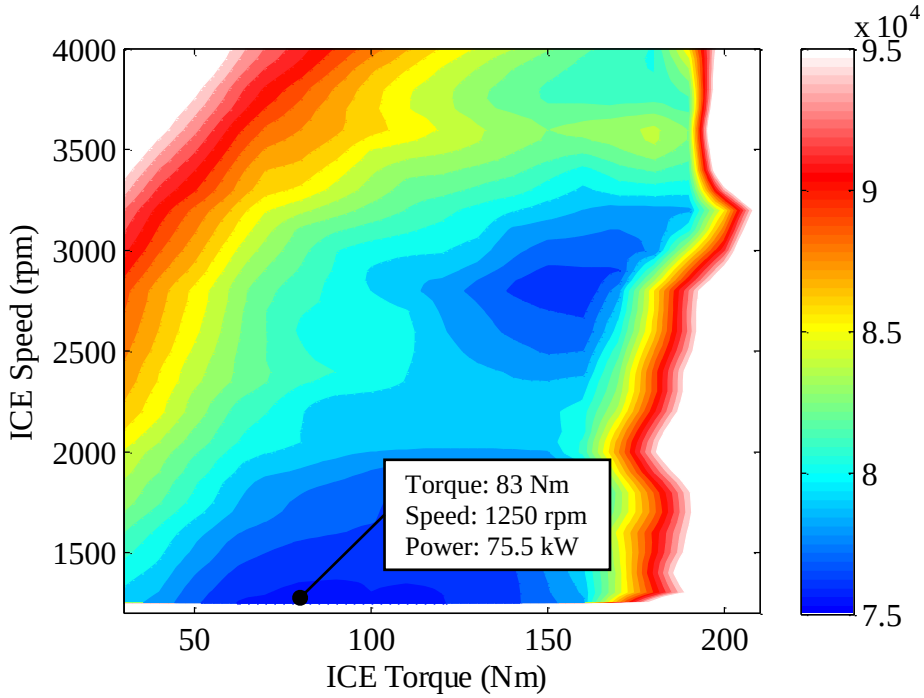

Figure 5-4: Total Power (kW) in ECVT HOS Level 2

The ideal ICE operating point at the current traction split of 0.8 is very different from the first layer of HOS. Though the first and second layer of HOS will produce the same result during steady state operation, the system is dynamic and this is not always the case. Here, the target ICE operating point is lower in power because at a traction split of 0.8 under the given driver torque request, higher levels of ICE power result in larger amounts of circulating electric power – with the 2-Mode MGs generating power for the RTM – and thus higher electrical losses (see §7.4 for a detailed explanation).

The final layer of HOS is ICE torque determination. This layer differs from the two layers above in that ICE torque can be modulated very quickly, and therefore, this level essentially determines the true operating point of the ICE at the given traction split and ICE speed. Let us assume that the ICE is operating at 1250 rpm, the current target

determined by HOS level 2. The objective function for ICE torque determination is shown in Figure 5-5.

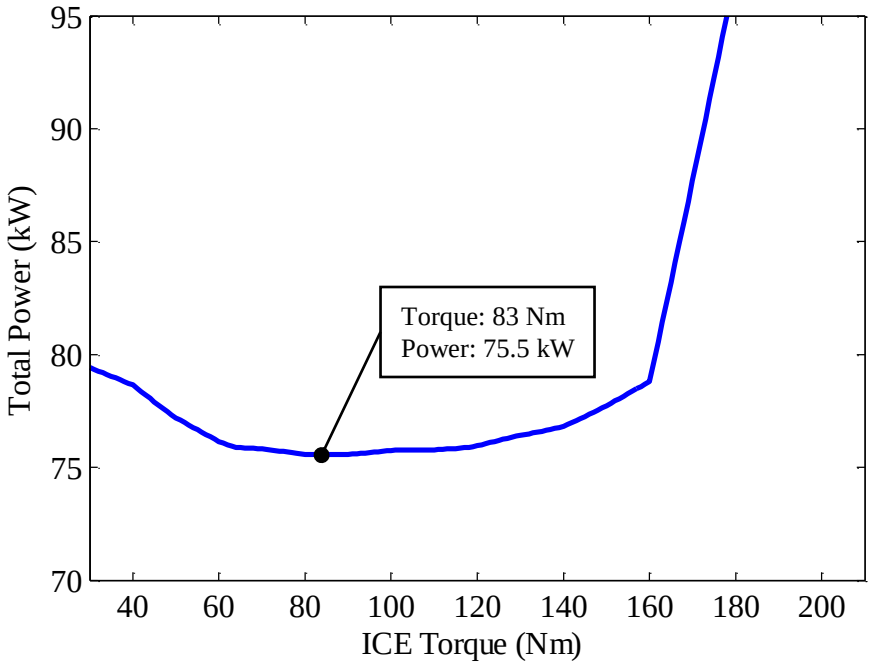

Figure 5-5: Total Power in ECVT HOS Level 3

Here, because the ICE has achieved the speed target set forth by HOS level 2, the torque determined by HOS level 3 matches that of the target from HOS level 2.

5.4.2. HOS in Fixed Gears

The selection process is simpler in the fixed gears, as ICE speed is a function of vehicle speed and gear ratio. Therefore, only two operating parameters must be determined – traction split and ICE torque. Figure 5-6 shows the search space for FG3, where the ICE speed is 1500 rpm, due to the 1:1 gear ratio of FG3.

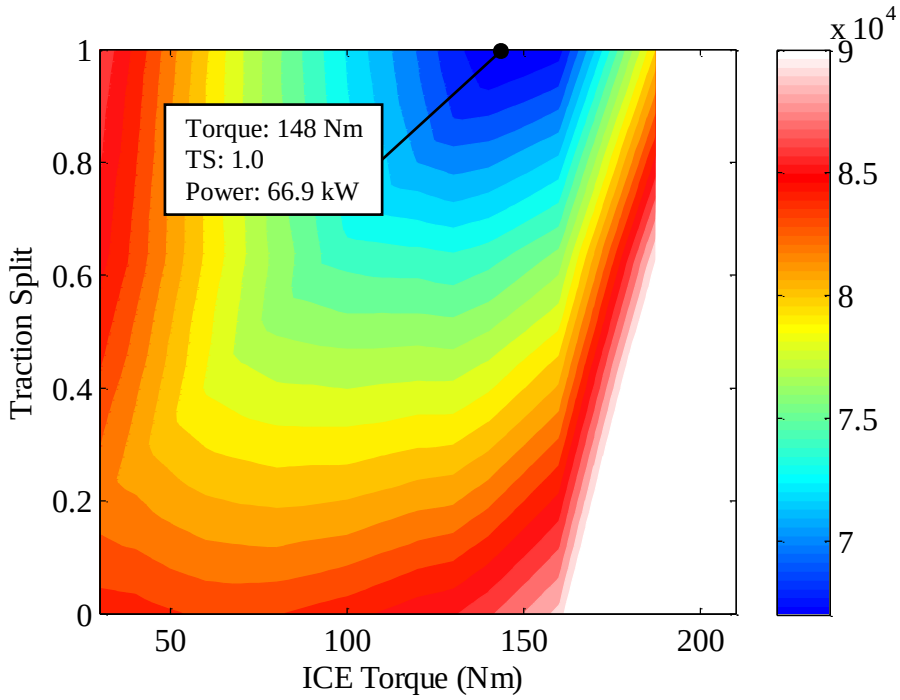

Figure 5-6: Total Power (kW) in FG HOS Level 1

Once again, the marker represents the optimal operating condition, and the determined traction split is a target towards which the system will trend. As in the ECVT example, ICE torque determination is also required, and it will be assumed again that the current traction split is 0.8. Figure 5-7 shows the objective function and selected optimal ICE torque.

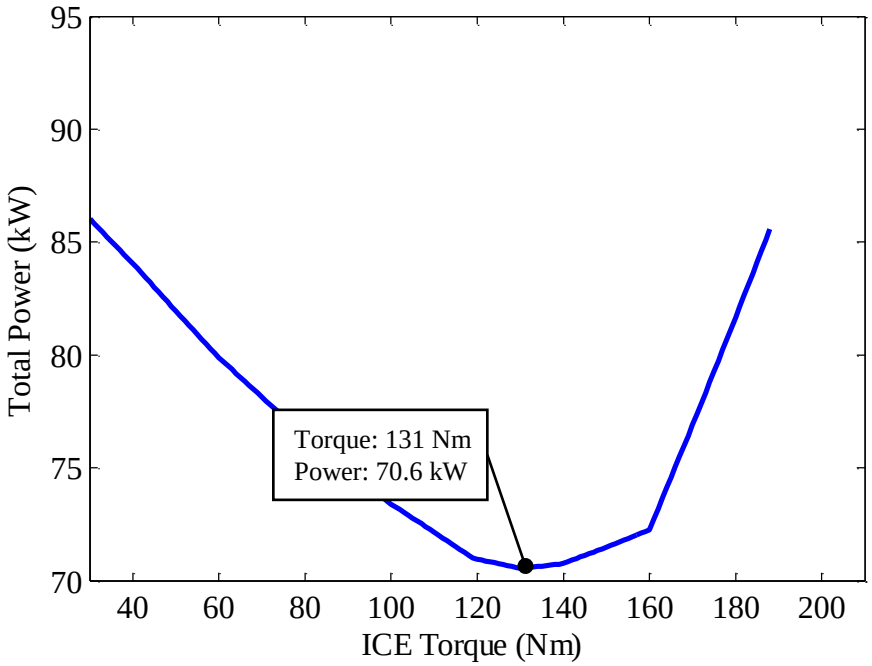

Figure 5-7: Total Power in FG HOS Level 3

Note again the difference in ICE torque values between the target operating point of HOS level 1 and HOS level 3. This is once again because higher ICE power production at the current traction split would result in higher electrical losses.

5.4.3. Gear Selection

Also evident from Figure 5-3 and Figure 5-6 is the fact that the optimal total power usage for Mode 1 and FG3 are substantially different. The gear with the lowest target total power consumption, as calculated in the first layer of HOS, is assumed to be the optimal gear for the system, and this is the basis of gear selection, as shown in Figure 5-8.

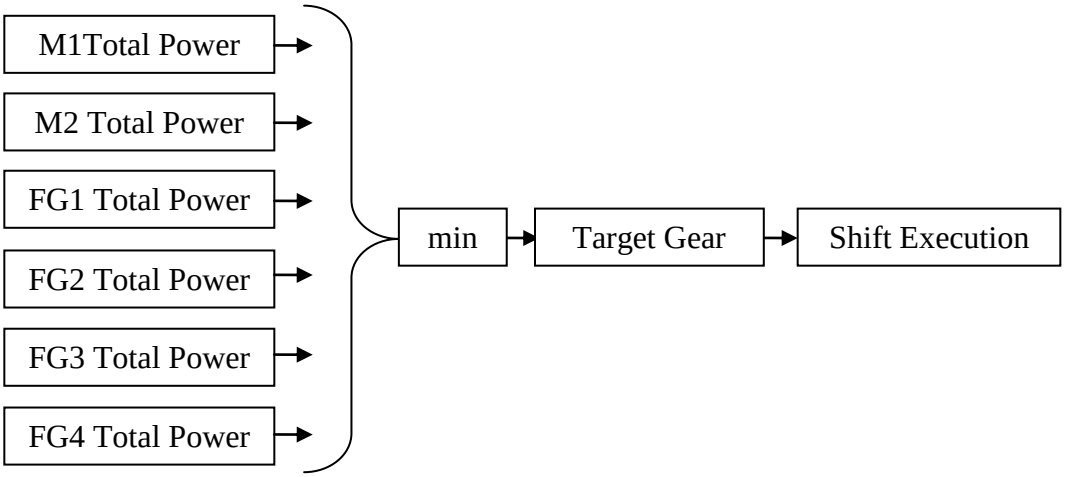

Figure 5-8: Gear Selection

Figure 5-9 illustrates the optimal mode/gear as a function of total axle torque and vehicle speed. While optimal mode is also a function of traction split, the three-dimensional operating space is difficult to show, and the results at a traction split of 1.0 have been selected for clarity.

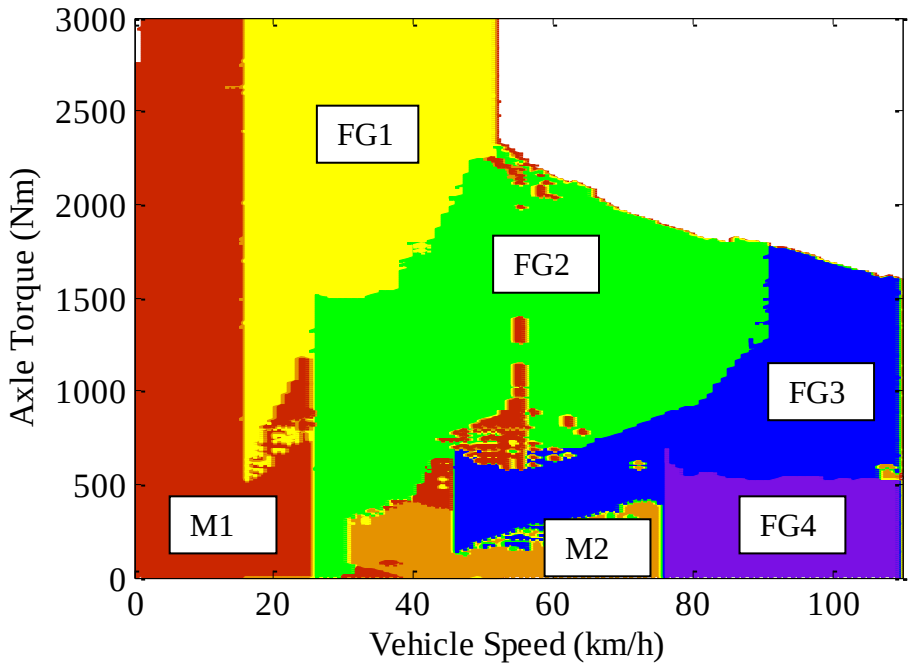

Figure 5-9: Gear Selection Map

The figure demonstrates that there are indeed several contiguous regions of operating space in which a single mode or gear is desired, which lends weight to the aforementioned method of gear selection. However, there are small regions where choice of operating mode is not clear-cut and the potential for shifting oscillations exists. This is an indication that simply selecting the most efficient gear as a target may produce optimal results. This is examined in §6.1.

5.5. Implementation of Optimization Search

Throughout the previous section, the difficult task of actually finding the optimal operating point within the search space, especially for the three- and two-dimensional layers of HOS, was not addressed; the following sections will do so.

5.5.1. Multi-Dimensional Optimization

In the examples of HOS above, only the global minimum is shown, but there are a number of local minimums as well, three of which are highlighted in Figure 5-10 for the ICE speed determination example given above.

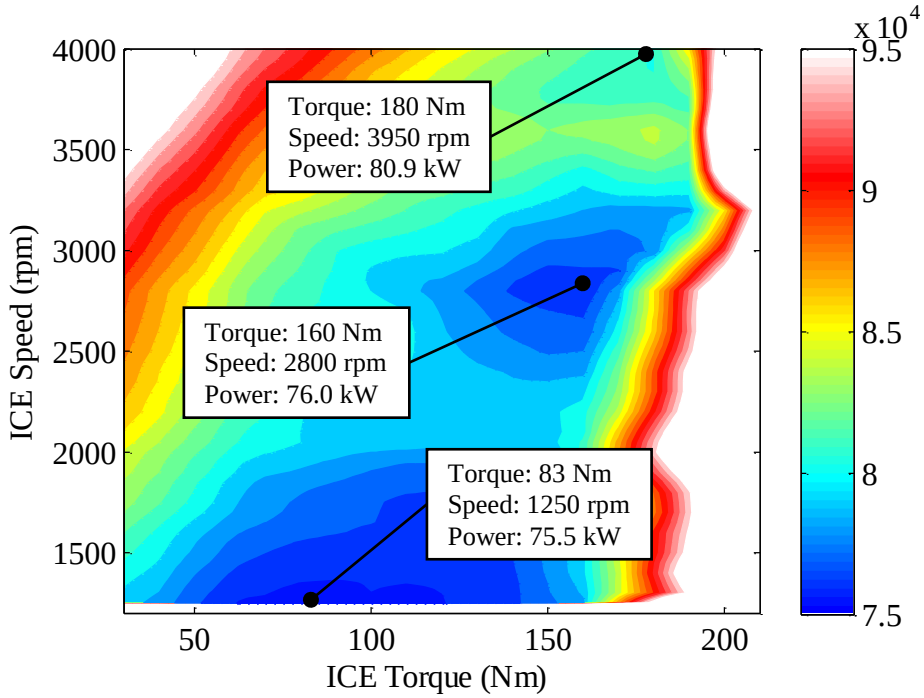

Figure 5-10: Example of Local Minima in Search Space

Three local minima of the objective function are shown, though more exist which are less defined and are thus exceeded by the resolution used for the figure. The existence of complex objective functions combined with the requirement that the optimization algorithm run in real-time on an automotive-grade controller make finding the global minimum of a given objective function difficult. Typically, the solutions provided by simple optimization algorithms – those that require the least computing time – are more likely to be local minima as opposed to the global minimum, and are heavily dependent on the starting points of the algorithm. More complex algorithms more frequently return the global minimum, but are also more computationally expensive. Therefore, a fine balance must be found between the efficacy and the computing time of the optimization algorithm.

Wise [4] previously examined several potential optimization methods – including simple pattern searches, the scan and zoom method, and the simulated annealing and genetic algorithms – for this real-time application, and encountered the aforementioned challenges. In addition, the author found that many complex optimization algorithms rely on random number generation, and have the potential to return different results across several solutions to an identical problem. As a result, Wise developed a two stage optimization method that resulted in high accuracy, acceptable computing time, and deterministic behavior. Wise's methodology has been adopted in this work, and though the method was originally developed for a two DOF problem, it has been expanded in order to solve the three DOF objective function of traction split selection in Mode 1 and Mode 2. The two DOF method is used to solve the ICE speed determination objective function in the ECVT modes and the traction split determination objective function in the fixed gears.

The first stage of Wise's method involves a low resolution, grid-based scan of the search space in order to find approximate local minima for the system. This is illustrated in Figure 5-11, in which an exemplary search grid depicted using blue markers has been placed over the objective function of Figure 5-10 for demonstration.

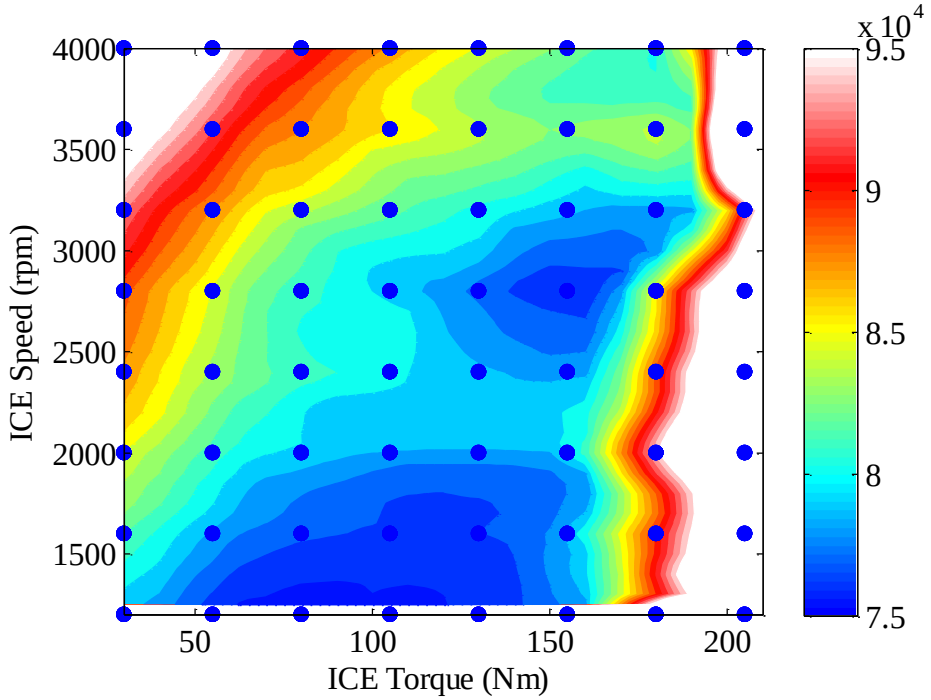

Figure 5-11: First Stage of Optimization – Initial Search

From this initial scan, several approximate local minima can be found. With these approximate local minima presumably located within a close distance of each respective true local minima, dependent on the resolution of the initial scan, they serve as ideal starting points for the aforementioned simple optimization algorithms. Figure 5-12 shows three approximate local minima for this problem enclosed in black squares.

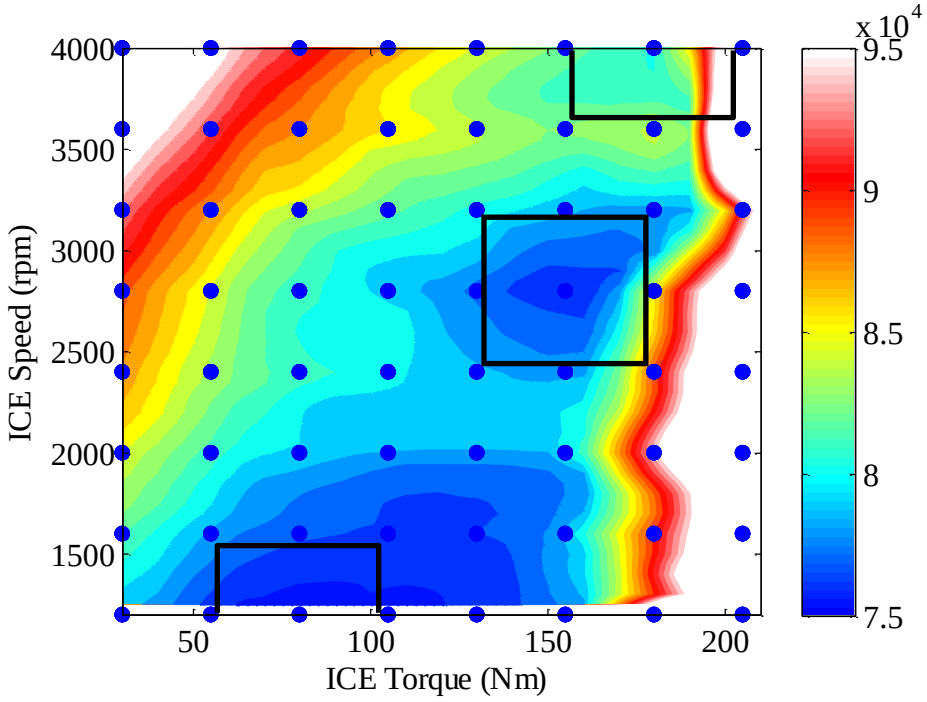

Figure 5-12: Second Stage of Optimization – Local Optimization

The area enclosed by each black boxe in Figure 5-12 represents the maximum area that could potentially be searched by an algorithm starting at the point enclosed within each box. By using this method, the effective area that must be searched using a high-resolution algorithm (to find the true local minima) is significantly reduced, and simpler algorithms can be used because of the advantageous start point. In this case, the simplest algorithm, a pattern search, is used at each start point. By comparing the minimum result of each separate optimization, the global minimum of the system can be found.

The example above was given in two dimensions for ease of viewing; however, the same process has been implemented in three dimensions, whereby an initial scan reveals cubic regions of operating space to be explored, as opposed to square regions. In this case, a three-dimensional pattern search algorithm was also used. The addition of this

extra degree of freedom increases the processing time for the algorithm, an issue which will be examined in §6.6.

5.5.2. Uni-Dimensional Optimization

Selection of ICE torque in the final level of HOS is a single DOF problem, making it simpler to solve than the two- and three-dimensional cases. Here, and again informed by Wise [4], the scan and zoom method was used. This method scans the search space at a low resolution, locates minimums in the search space, performs a higher resolution scan about the minimum, and repeats this process at ever increasing resolutions until satisfactory precision is achieved. An example of three levels of search points for a solution using this algorithm is shown in Figure 5-13.

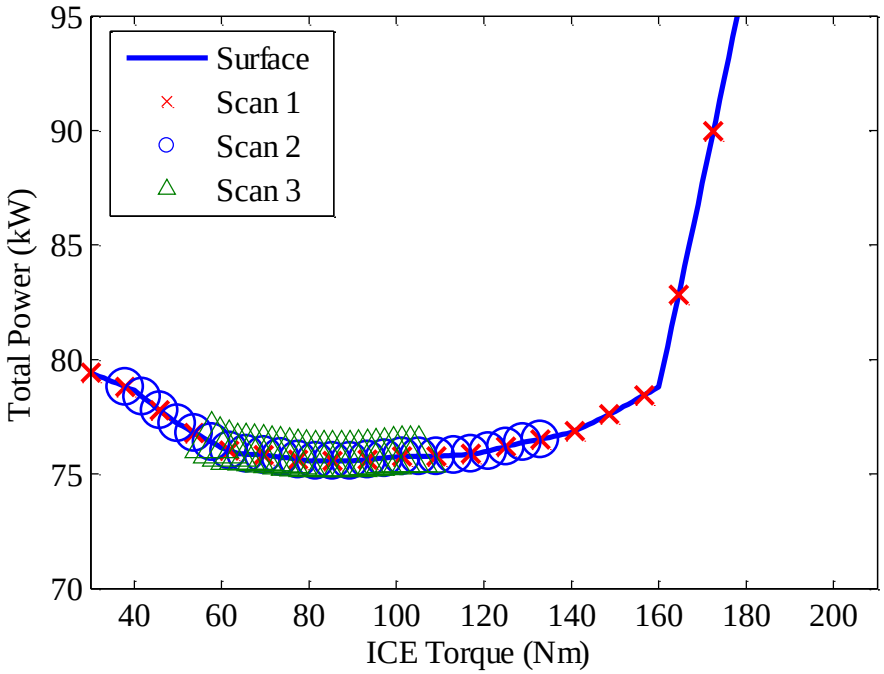

Figure 5-13: Single DOF Optimization – Scan and Zoom

The objective functions of HOS level 3 are the simplest to solve, and even with much finer point spacing during scans, solving these one-dimensional problems typically

requires significantly fewer evaluations of the objective function as compared to HOS level 2 and level 3.

Having developed the algorithms for HOS, the next step in the process is to validate the results.

5.5.3. Validation of Optimization Results

In order to validate the results of this algorithm, the MATLAB Optimization Toolbox was used to find the minimum of each objective function under various vehicle operating conditions and for each mode and gear. Optimization parameters, such as the resolution of the initial scan and the desired tolerance of the solution, were also varied to determine the most optimal combination. Ultimately, the parameters outlined in Table 5-1 were selected for each level of HOS.

Table 5-1: HOS Optimization Search Parameters

Level	# of Scanning Points	Solution Tolerance
1	11 – 30 – 30 (Trac Split - ICE Spd - ICE Trq)	0.01 – 0.1 – 0.1 (% - rpm - Nm)
2	30 – 30 (ICE Spd – ICE Trq)	0.1 – 0.1 (rpm – Nm)
3	50 / scanning level	0.1 Nm

As a summary of the validation process, results for HOS level 1 (which has the most complex objective function) are compared across a sweep of vehicle speed values at a constant torque level. A total axle torque of 1000 Nm was chosen in this case because it results in a non-unity traction split for some portions of the sweep, thus demonstrating the efficacy of the algorithm in three dimensions. The minimum total power at the evaluated points for both algorithms is shown in Figure 5-14.

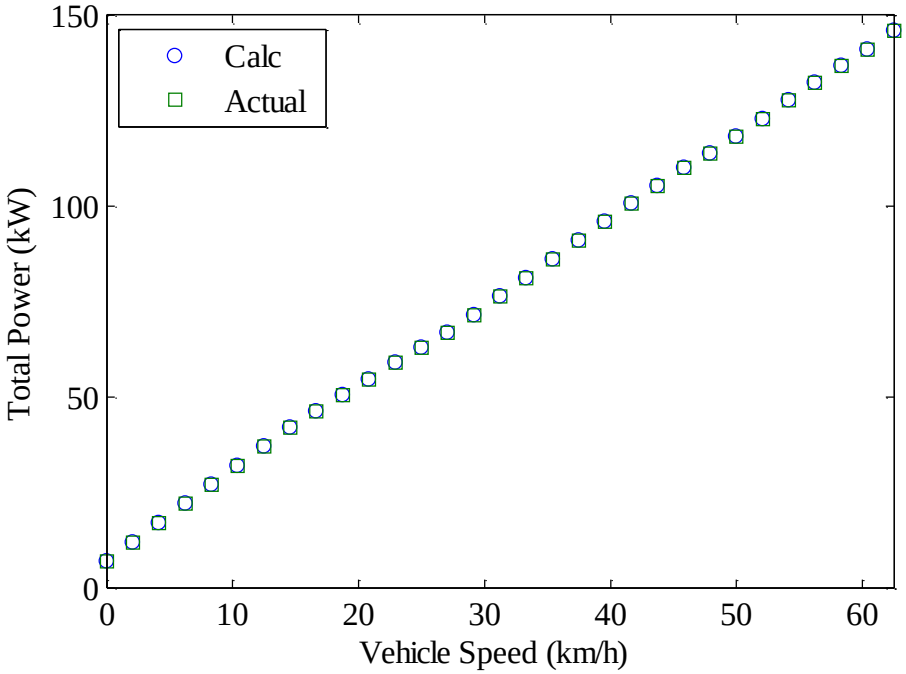

Figure 5-14: Algorithm Result Validation – HOS Levels 1 and 2

Both algorithms return near-identical results throughout the scan, with the average difference between results being less than 8 W of total power, with a maximum of 52 W. Consider though, that at such high torque levels a minute difference in determined ICE speed – and thus MGA and MGB speed – can have a significant effect on the solution. Because algorithm speed is extremely important in a real-time application, such error is deemed very acceptable, and in nearly all cases is within the error allowed by the selected tolerance. Consider also that the desired traction split and ICE speed are *targets* and that the system is very dynamic. This means that, while the system is always trending towards the targets, it doesn't necessarily operate at the target. Therefore, a target very close to the optimal solution may for all intents and purposes be just as good as the optimal solution. Increasing the tolerance of the algorithm or the number of initial scanning points has a large effect on computational requirements, and in this case, is deemed unnecessary.

The algorithm for HOS level 2 is identical to that for HOS level 1, save the complexity of the traction split dimension, so a summary of validation is not warranted here.

Figure 5-15 shows the results for HOS level 3 in FG2 at an axle torque of 1000 Nm and a constant traction split of 1. Choosing a traction split is necessary for validation of this algorithm, since HOS level 3 always relies on the current traction split and ICE speed, and only selects ICE torque.

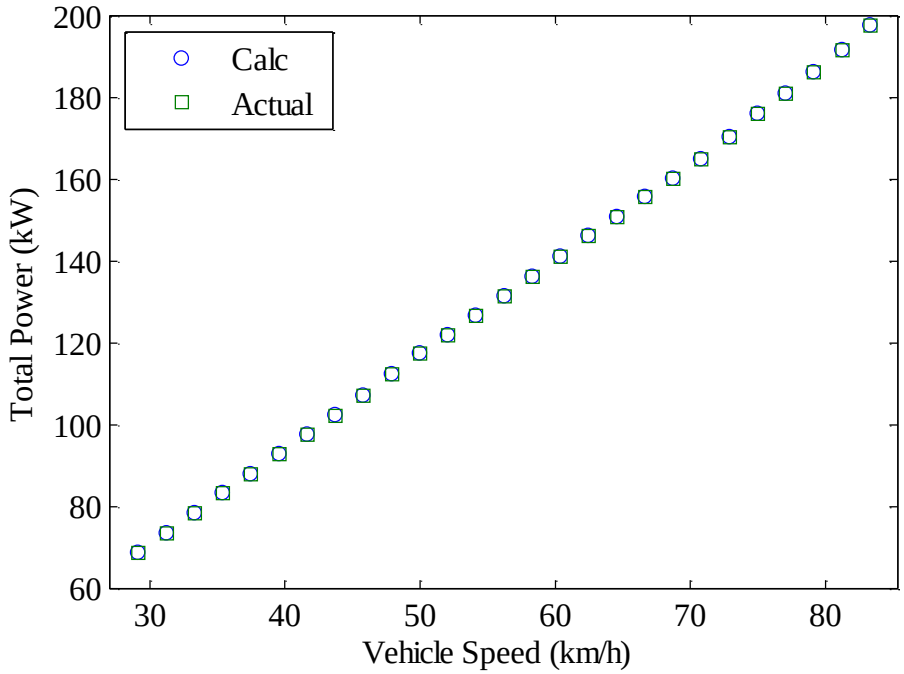

Figure 5-15: Algorithm Result Validation – HOS Level 3

The average difference in total output power for this case was 4 W, with a maximum of 25 W. The average difference in the selected ICE torque was 0.008 Nm, a very reasonable result.

CHAPTER 6 AWD 2-Mode Control Implementation

Thus far, the fundamental operation of HOS has been reviewed in detail. This section examines the application of HOS in practice, which presents challenges in terms of drivability, component longevity, and consumption of computational resources, among other factors. The goals of initial testing are to:

- Assess ICE operation from an efficiency standpoint, and also to ensure that it is operating within system constraints;
- Quantify use of the rear traction motor;
- Examine aspects of drivability and consumer acceptability, including ICE operation and shift execution/stability;
- Assess factors relating to component life and degradation, focusing mainly on the ESS;
- Examine the effects of a dynamic torque split on vehicle traction; and
- Quantify the computational demands of the HOS algorithms.

Algorithm development was completed using the plant model discussed in §4.3, and takes into account the limitations of the UVic architecture outlined in §4.4 apart from the constraint of operation in ECVT modes only. Algorithms for the fixed gears as well as the ECVT modes were developed and implemented in algorithm testing such that if issues with the vehicle related to operation in fixed gears were resolved at a later date, a full control strategy could be applied. The final section of this chapter will examine the effects of operation using only the ECVT modes.

Initial testing was based on a single drive cycle consisting of one UDDS and one HWFET cycle to capture elements of city and highway driving; the trace is plotted in Figure 6-1.

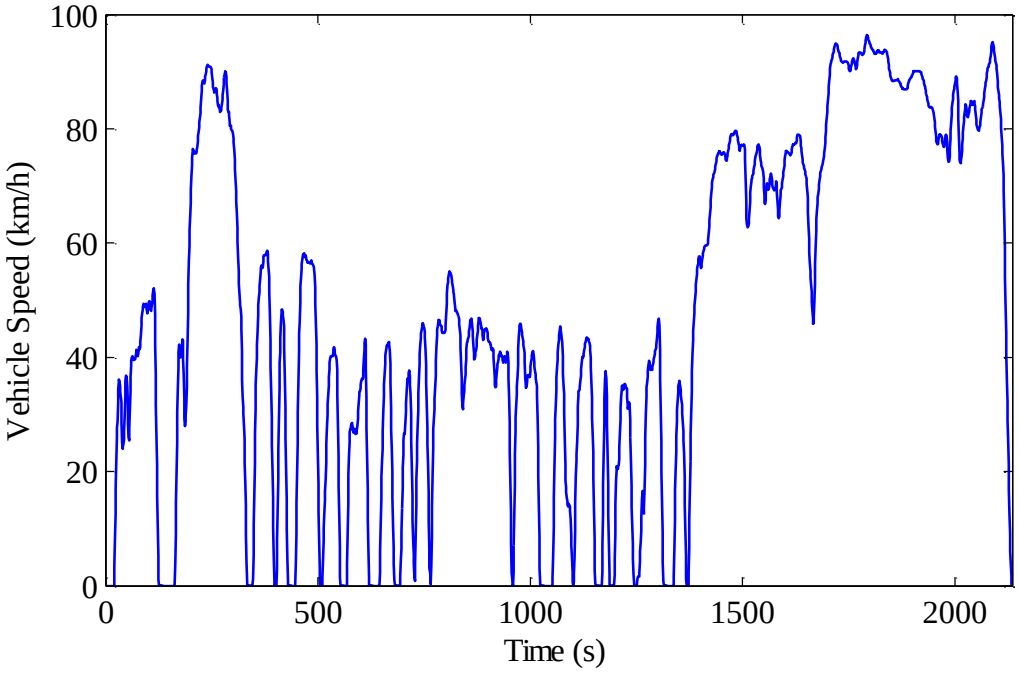

Figure 6-1: Concatenated UDDS and HWFET Cycles

Note that the metric for fuel consumption in coming sections is SOC-corrected liters of gasoline-equivalent per 100 km, or Lge/100 km, which takes into account the difference in initial and final SOC, as well as the energy density of the fuel being used, as shown in Equations 6-1 and 6-2.

$$FC_{SOCcorrected}\left[\frac{L}{100km}\right] = \frac{\left(V_{fuel}[L] + \frac{\frac{\Delta E_{ESS}}{0.25}[kWh]}{LHV_{fuel}\left[\frac{kWh}{L}\right]}\right)}{\frac{Distance\ Driven}{100}\ [100km]} \qquad 6\text{-}1$$

$$FC_{ge}\left[\frac{Lge}{100km}\right] = FC_{SOCcorrected}\left[\frac{L}{100km}\right] \cdot \frac{FED_{fuel}\left[\frac{kWh}{L}\right]}{FED_{gasoline}\left[\frac{kWh}{L}\right]} \qquad 6\text{-}2$$

With the following representations:

V_{fuel} = volume of fuel used over the course of the drive cycle

ΔE_{ESS} = change in stored energy of the ESS over the course of the drive cycle

FED_x = fuel energy density of fuel x

This differs from the UF weighted FC calculation outlined in §2.2.2, but is necessary because the simulations that follow concern only CS operation, and don't include an AER; as such, a method for correcting fuel consumption based on differences in SOC between the beginning and end of a cycle is necessary.

In the case of E85, the fuel energy density ratio in Equation 6-2 is approximately 0.746, meaning that fuel consumption values will appear relatively low: for example, a gasoline-equivalent fuel consumption of 7.0 L/100km actually uses 9.38 L of E85 per 100 km.

6.1. Baseline Testing

In initial testing, vehicle operation was controlled using the raw output of HOS, without any modifications. While theoretically this means that the vehicle should operate throughout the cycle at optimal efficiency, in practice this is not the case, primarily because driving conditions are always changing. The examples provided in Chapter 5 were based solely on a single snapshot of the system, but the system is constantly changing with the torque requested by the driver, the vehicle speed, and the SOC of the battery. The torque request from the driver is the most transient variable with the quickest response time, and is plotted in Figure 6-2.

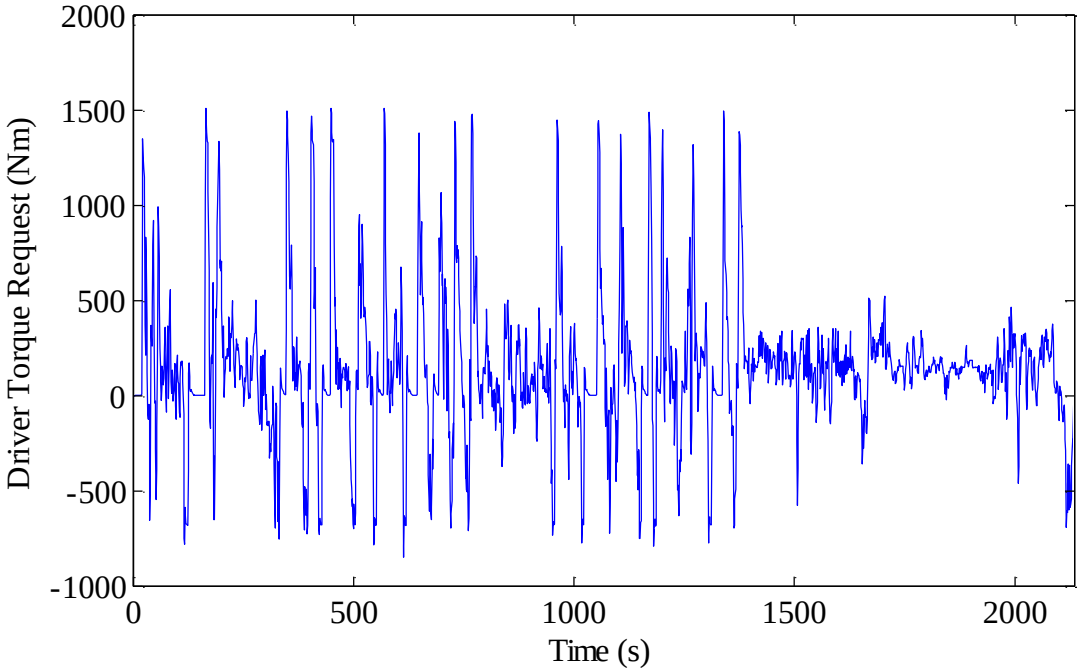

Figure 6-2: Baseline Testing – Driver Axle Torque Request

It is evident from Figure 6-2 that the torque request fluctuates very quickly, with much higher torque requests present during the city cycle, and on a much smaller timescale than the vehicle speed shown in Figure 6-1. As will be demonstrated, this dynamic input has the potential to seriously affect the performance and drivability of the system without intuitive checks and bounds provided by a human designer.

6.1.1. ICE Operation

Figure 6-3 displays 1 Hz ICE operating points throughout the cycle.

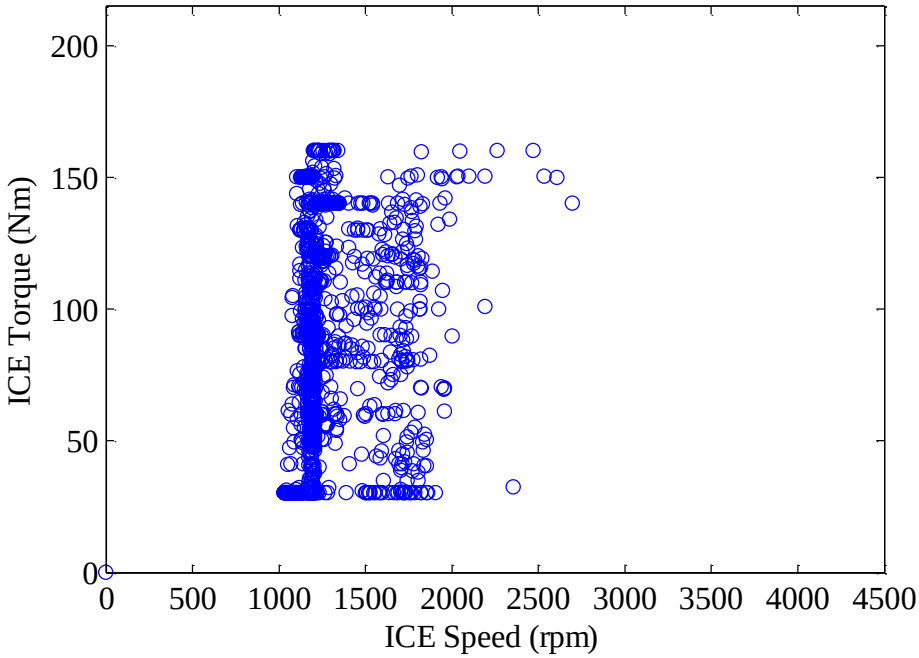

Figure 6-3: Baseline Testing – 1 Hz ICE Operating Points

The ICE operates primarily around its minimum speed of 1200 rpm, even at torque levels up to 160 Nm, as this represents a high-efficiency operating region. Additionally though, the ICE operates in some very low-efficiency regions, such as above 1500 rpm with torque values of less than 60 Nm. With no immediately visible trends, even with the availability of an ICE operating efficiency map (which is proprietary), this plot provides little quality information about ICE operation.

A time-based plot of ICE operation over the course of the cycle, shown in Figure 6-4, is more enlightening.

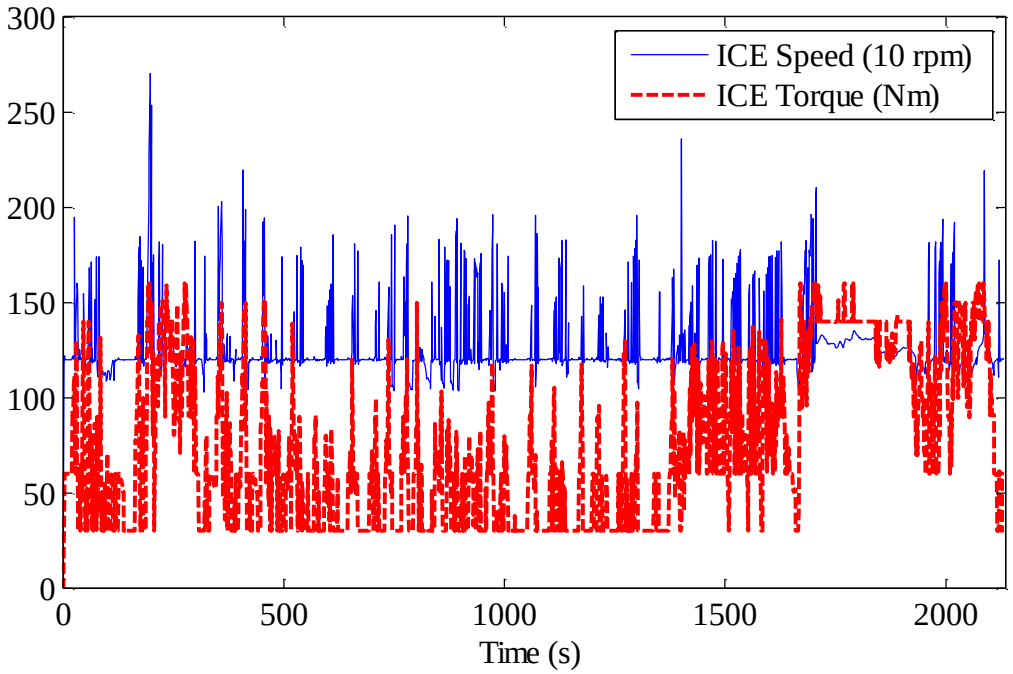

Figure 6-4: Baseline Testing – ICE Operation

There are many 'spikes' in ICE speed, which would not be expected based on the speed profile of the cycle. Rather than a direct result of the ICE speed optimization commands, these spikes are in fact due to gear shifting. In these cases, the transmission controller is bypassing HOS commands in order to execute the synchronous shifts required by the transmission. ICE speed changes to match the gear ratio of the target fixed gear, and recall that even when shifting between Mode 1 and Mode 2, the transmission must pass through FG2 in order to maintain the desired output power.

6.1.2. Gear Selection

Figure 6-5 shows a plot of desired ranges during the cycle.

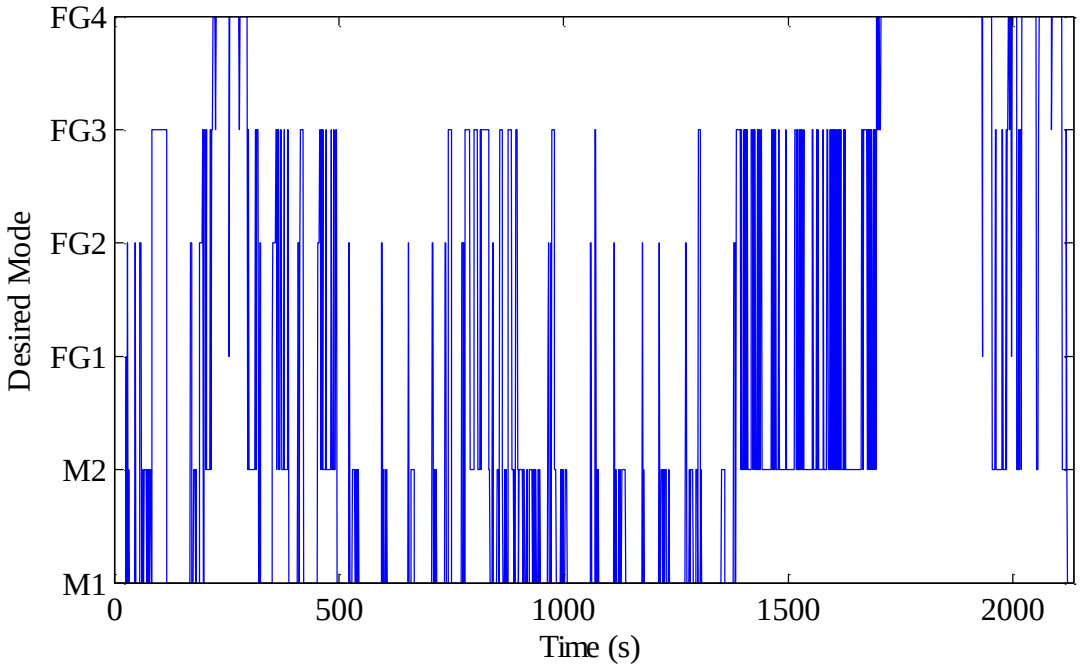

Figure 6-5: Baseline Testing – Range Requests

In total, there are 364 shifts throughout the course of the cycle, and many of the commands oscillate quickly between various desired ranges. This behavior – a result of the direct selection of desired gear as shown in Figure 5-8 – undoubtedly adversely impacts not only the performance, efficiency, and drivability of the vehicle, but also the life of transmission. This issue is addressed in §6.2, but first several additional baseline performance factors will be investigated.

6.1.3. ESS Power

Rapid fluctuations in ESS power and/or repeated high levels of charge or discharge power affect the rate of degradation of an HEV ESS, and also decrease overall system efficiency due to ESS charge and discharge losses, which increase with increasing power draw. When using the ECMS these circumstances may be created due to the fast response time of the algorithm to changes in system operating conditions and its sensitivity to changes in SOC, combined with the resulting dynamic weighting of electric versus fuel

power (via the EF). For example, at times when the SOC exceeds the target and electricity becomes ‘cheap’, a high torque request will most likely draw large amounts of electrical energy to meet the driver’s power demand. The system will naturally correct as SOC drops, but in some cases this may not be desired behavior. Conversely, limiting the charge or discharge power of the ESS can also have detrimental effects on fuel consumption.

Figure 6-6 shows a plot of ESS power over the course of the drive cycle, with a representative 60 second portion shown in the inset.

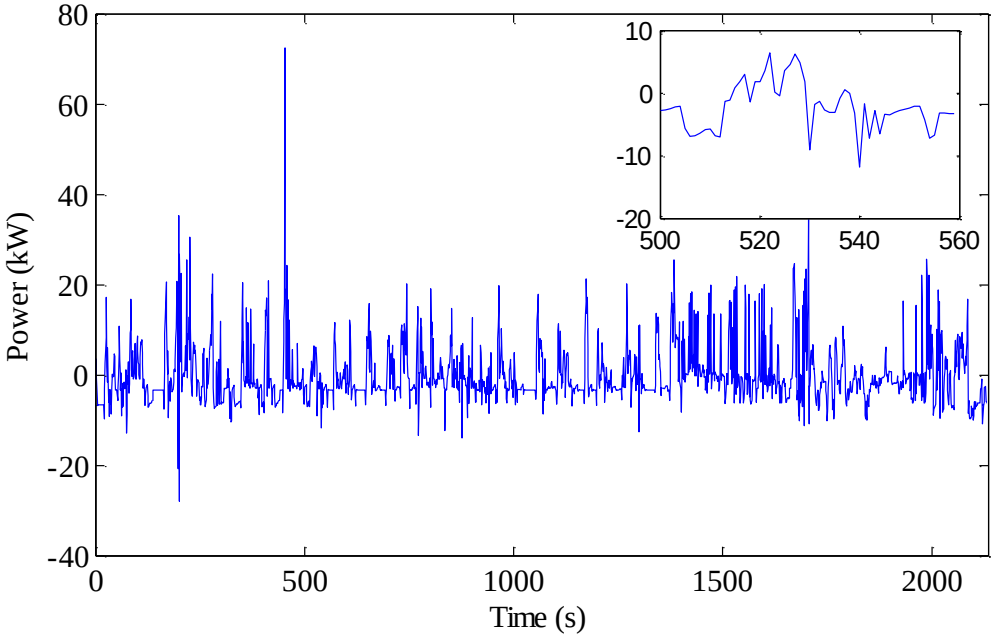

Figure 6-6: Baseline Testing – ESS Power

There appear to be many sharp fluctuations in ESS power, though based on the large fluctuations of ICE torque shown in Figure 6-4, this is to be expected. Figure 6-7 illustrates the effects of this power flow on SOC; an arbitrary SOC target of 50% was chosen for baseline testing.

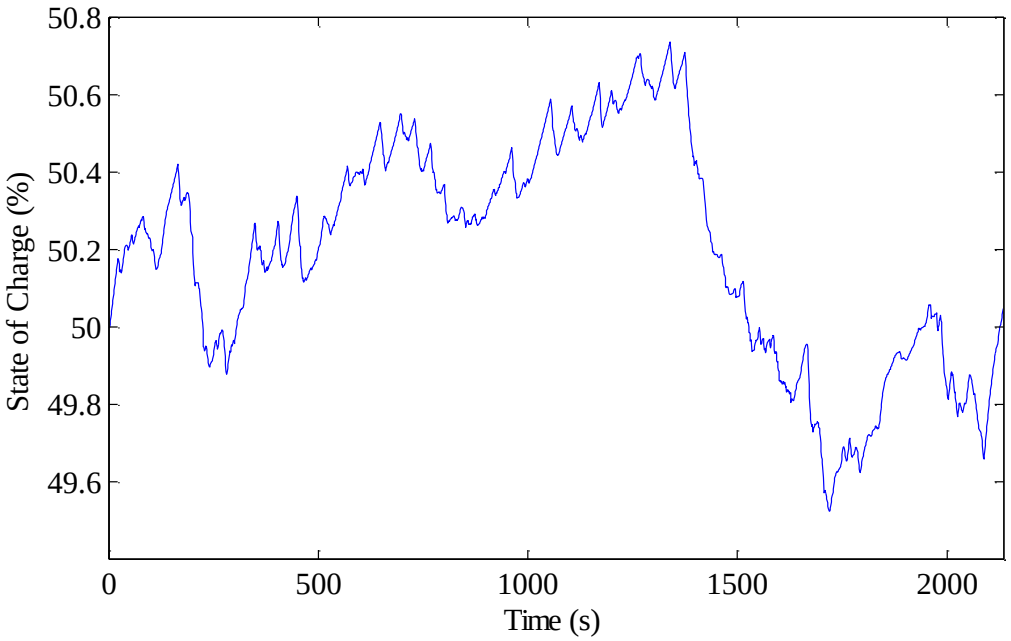

Figure 6-7: Baseline Testing – SOC Curve

Again, the results are as expected, and may be partially due to the rapid oscillations in ESS power. This behavior may have been exacerbated by the high number of requested shifts during the cycle. Additionally, many of the constant positive slopes in the SOC profile – especially noticeable during the UDDS cycle – are the result of ICE idle-stop being disabled and the minimum speed and torque limits imposed by the ICE/2-Mode system. Essentially, the vehicle is always charging while stopped.

The root-mean-square (RMS) of ESS current will be used to quantify ESS power draw. Though a full analysis of the long-term effects of current draw on the UVic EcoCAR ESS or similar ESSs will not be undertaken, the goal in introducing this metric is to provide a means to assess changes in ESS power draw. In baseline testing, the RMS ESS current was 17.5 amps. Section 6.3 examines the effects of manipulating ESS power draw at the level of the HOS optimization algorithms.

6.1.4. RTM Use

Figure 6-8 shows a plot of traction split over the course of the drive cycle, with a representative 10 second portion shown in the inset.

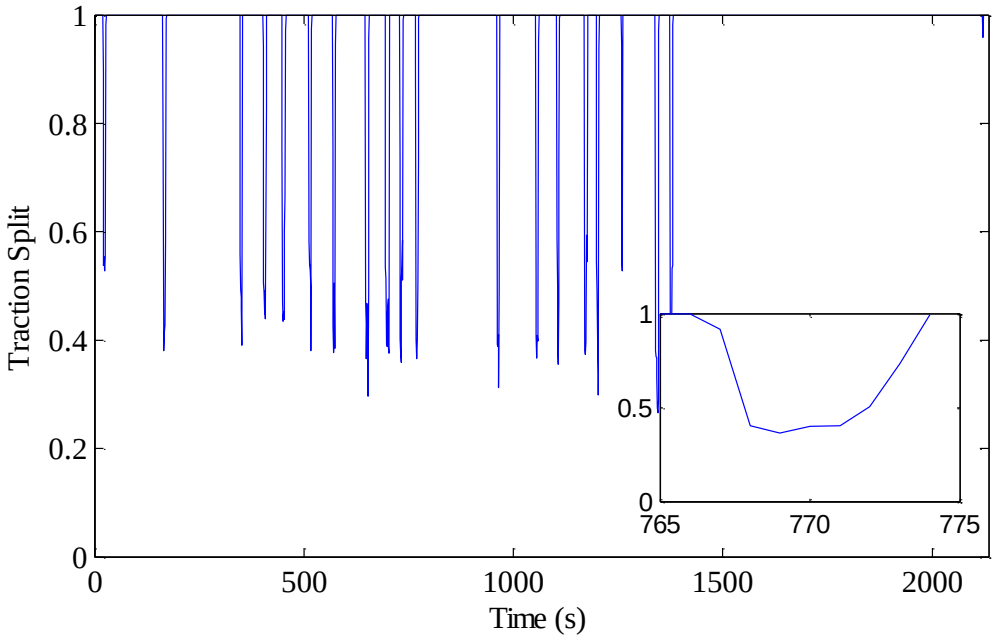

Figure 6-8: Baseline Testing – Traction Split

From the figure, it appears that the RTM is used only sparingly, or more specifically, to provide additional propulsive power during accelerations. When cruising at a steady speed, the RTM is not used at all. To quantify RTM use for comparison, metrics of average traction split and the percentage of total drive cycle power provided by the RTM will be used. Table 6-1 summarizes the results for baseline testing.

Table 6-1: Baseline Testing – RTM Use

Metric	Full Cycle	UDDS	HWFET
Average TS	0.968	0.954	0.994
RTM %	6.6%	12.4%	1.0%

These results confirm much higher use for city driving as opposed to highway driving, as observed in Figure 6-8. Figure 6-9 shows RTM operating points overlaying the UQM145 efficiency map.

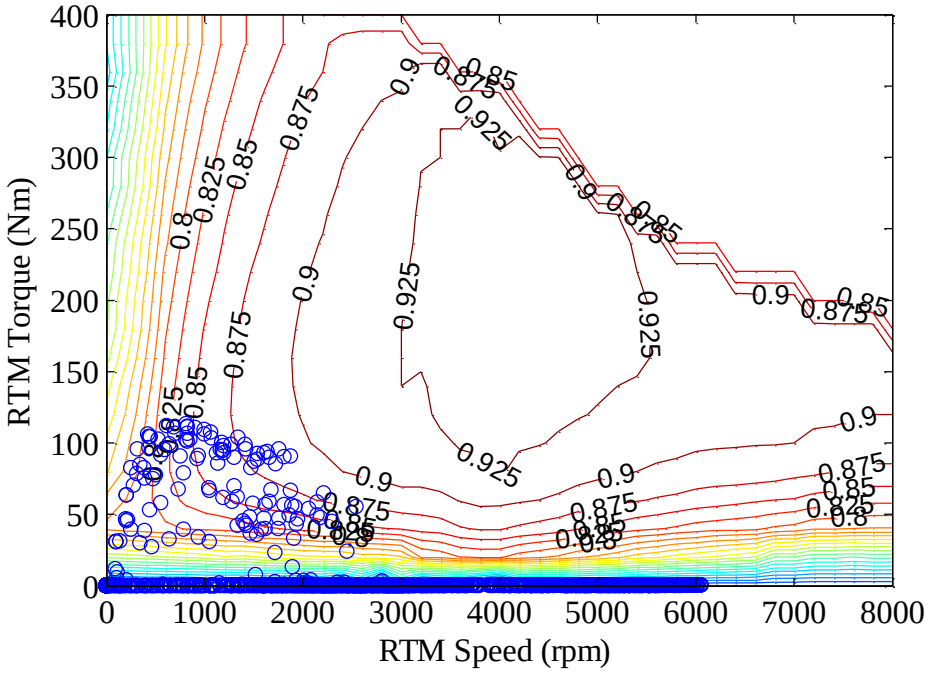

Figure 6-9: Baseline Testing – 1 Hz RTM Operating Points

As shown, essentially none of the RTM operating points are within regions of greater than 90% efficiency. The fact that the points at which the RTM does operate are clustered in regions of between 80% and 90% efficiency, and that virtually no operating points can be seen in very low efficiency regions, suggests that the traction split optimization is selecting regions of 'relatively' high efficiency. However, this begs the question of why operating points of maximum efficiency are not selected. Figure 6-10, which plots the total torque request assuming a traction split of 0 (*ie*: assuming all propulsive power is provided by the RTM), is enlightening.

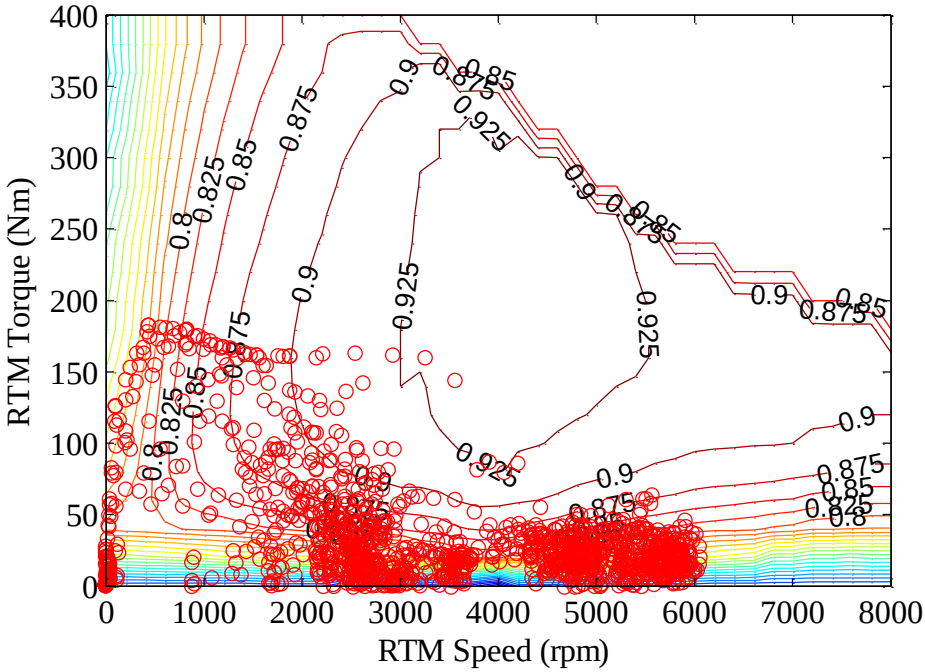

Figure 6-10: Baseline Testing – RTM Operating Points for a Traction Split of 0

The figure illustrates that even if providing the entirety of propulsive power for the vehicle, the RTM would rarely operate at above 90% efficiency on the selected drive cycles, and would frequently operate at efficiencies well below 90%. It is therefore not surprising that a traction split of 1.0 is maintained for a large majority of this drive cycle.

One factor to consider is that the selected drive cycles – UDDS and HWFET – are relatively mild in terms of total power demand. More demanding cycles, such as those involving higher accelerations, highway-speed passing maneuvers, or towing, would undoubtedly use the RTM to a greater extent. In general, though, for the majority of the average consumer's driving needs, the current configuration (UQM size combined with transaxle gear ratio) is not ideal; recall however, that at the time of component purchasing the desired gear ratio was not available for the BorgWarner transaxle. The effects of possible modifications to the RTM system will be examined in §7.5.

Having examined the baseline testing scenario in detail, the following chapter sections will examine possible improvements to the algorithm.

6.2. Gear Selection

The most glaring deficiency of the algorithm as implemented in baseline testing, which requires a solution before fuel consumption values can be reasonably compared, is gear selection. The proposed method to improve the gear selection strategy is the use of a shift buffer to add hysteresis to the system. Essentially, the buffer prevents the system from shifting unless the difference in total power between the current and potential target gear exceeds a given value. Figure 6-11 illustrates this change in logic.

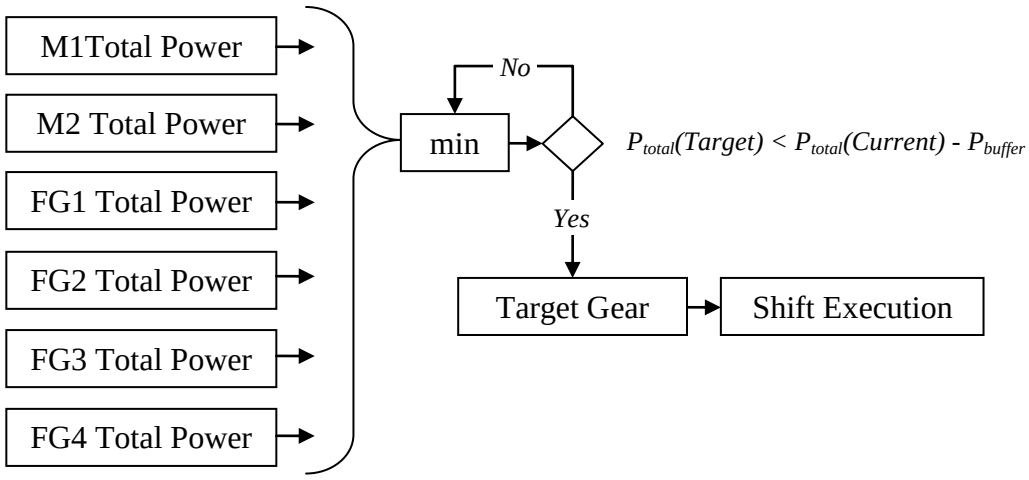

Figure 6-11: Gear Selection with Shift buffer

Fuel consumption and shifting results for a range of buffer values are given in Table 6-2.

Table 6-2: Gear Selection – Summary of Shift buffer Results

P_{buffer} (kW)	FC (Lge/100km)	# of Shifts (UDDS)	# of Shifts (HWFET)
0	6.86	232	132
1	6.75	114	100
2	6.72	84	68
3	6.72	59	54
4	6.77	54	26
5	6.85	36	22
6	6.82	31	13

As expected, reducing the number of shifts has a significant effect on fuel consumption. Intuitively, it seems reasonable to reduce the number of shifts by as much as possible without seriously affecting fuel consumption. In this case, a buffer value of 4 kW appears to be the best choice, as it significantly reduces the number of shifts while only increasing fuel consumption from the minimum result – those at buffer values of 2 and 3 kW – by a fraction of a percent. Figure 6-12 plots the result of this selection.

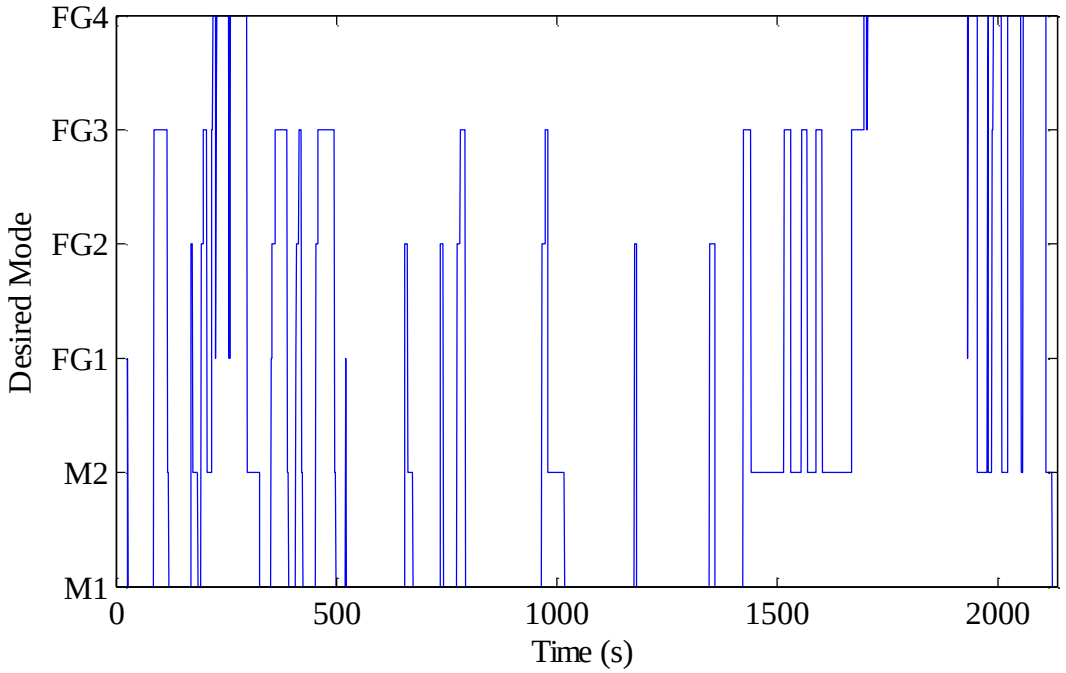

Figure 6-12: Gear Selection with a Shift buffer of 4 kW

Though the results have improved dramatically there are still 11 failed shifts throughout this cycle, which have been defined here as shifts that occur within 2 seconds of a previous shift. To improve these results, additional hysteresis based on time was added to the system to prevent failed shifts. Care was taken to ensure that this hysteresis did not impair shifts that were occurring as a result of the unavailability of a given range, as opposed to those based on efficiency. Implementing this solution had a negligible effect on fuel consumption, which remained at 6.77 Lge/100km, but reduced the number of shifts to 42 and 21 on the city and highway cycles, respectively.

ICE operating points were slightly more favorable, as shown in Figure 6-13

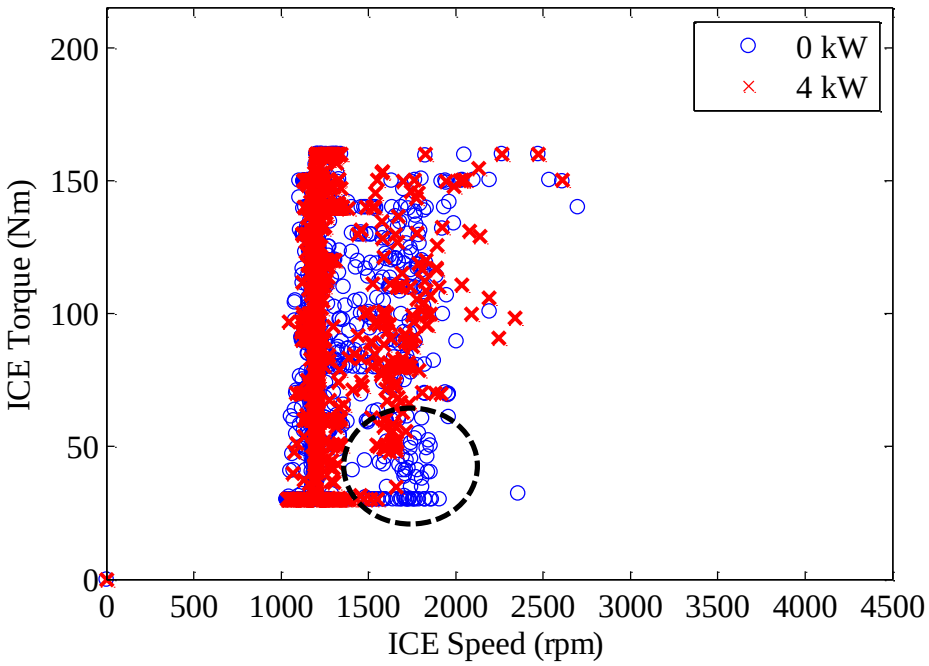

Figure 6-13: ICE Operating Points with Shift buffer

With the shift buffer implemented, significantly less time was spent in the inefficient region circled in the figure: 3.0% as compared to 7.5% without the shift buffer. Figure 6-13 also shows a marked decrease in the number of ICE speed spikes when compared to Figure 6-4.

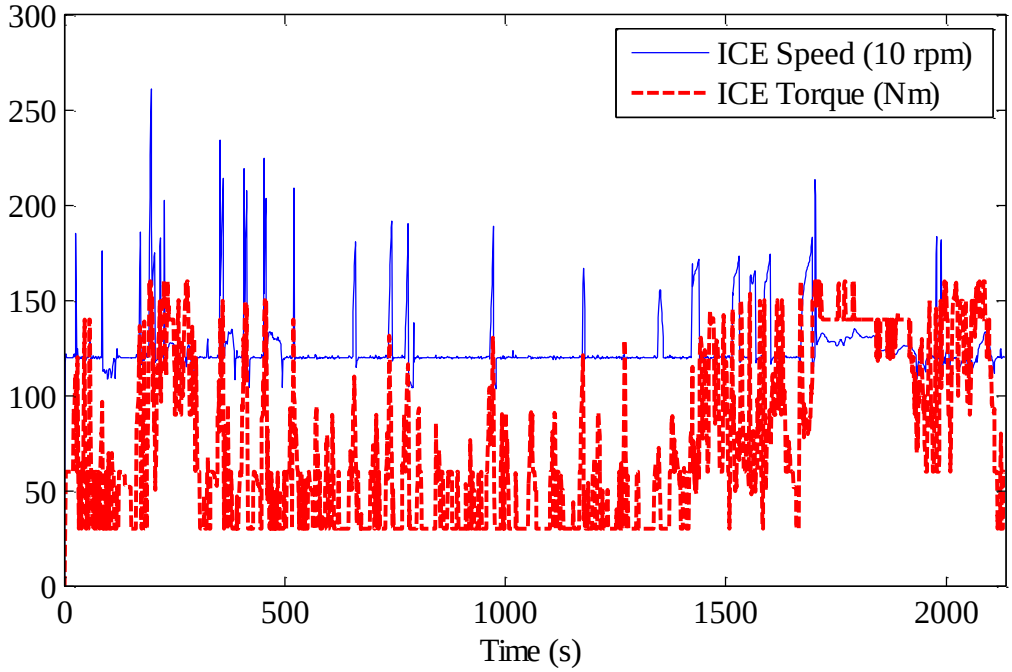

Figure 6-14: ICE Operation with Shift buffer

Changes in RTM use were negligible with the introduction of a shift buffer; results for a 4 kW shift buffer are summarized in Table 6-3.

Table 6-3: RTM Use with Shift buffer

Metric	Full Cycle	UDDS	HWFET
Average TS	0.969	0.955	0.993
RTM %	6.6%	12.5%	1.3%

Having developed a suitable method for gear selection, a method for controlling ESS power fluctuations is investigated in the next section.

6.3. Battery Power Limits

To manipulate the amount of electric power usage, a modification to the objective function of Equation 5-3 has been included, as shown in Equation 6-3.

$$P_{total} = P_{fuel} + P'_{ESS} + \propto \cdot P_{ESS}{}^{x} \qquad 6\text{-}3$$

Where:

α = ESS power correction factor (known henceforth as the power factor)

x = exponential factor applied to ESS power

Preliminary testing of this addition to the objective function suggested that a linear factor (*x* = 1) was not suitable. Figure 6-15 plots results for a squared relationship (*x* = 2).

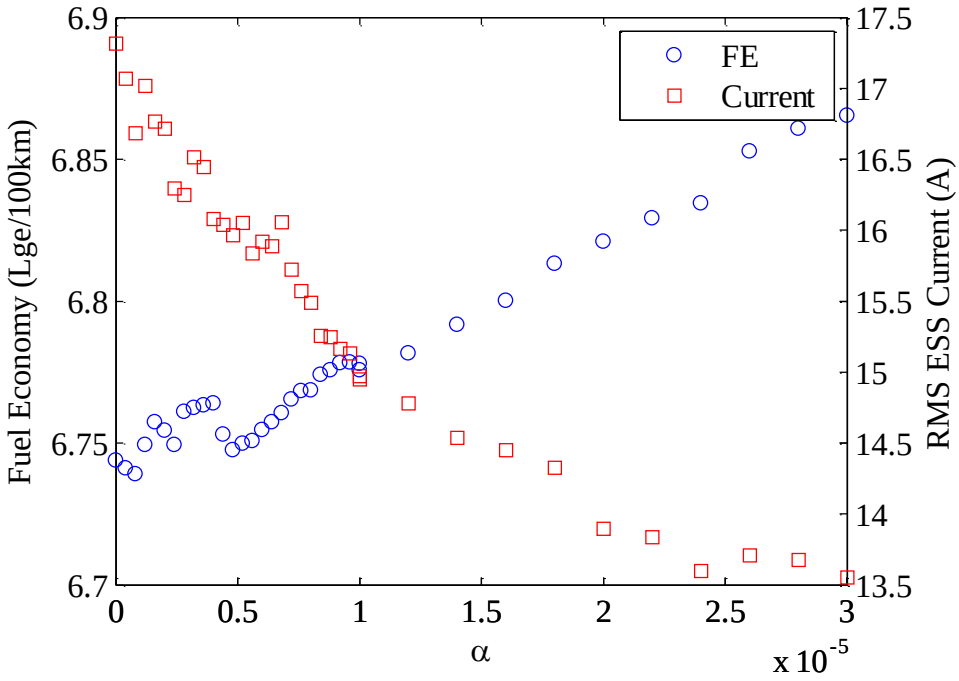

Figure 6-15: Fuel Consumption and RMS Current vs ESS Power Factor

As expected, fuel consumption increases and RMS current decreases with increasing power factor. The results for fuel consumption are interesting, in that they rise sharply with small values of power factor, only to briefly fall upon reaching a power factor of roughly $5x10^{-6}$. The following paragraphs will shed more light on this behavior.

Essentially, during events that require high total power, the power factor is biasing the objective function towards regions of operating space that use more ICE power and less ESS power. This is demonstrated in Figure 6-16 which plots ICE and propulsive power for two different power factors.

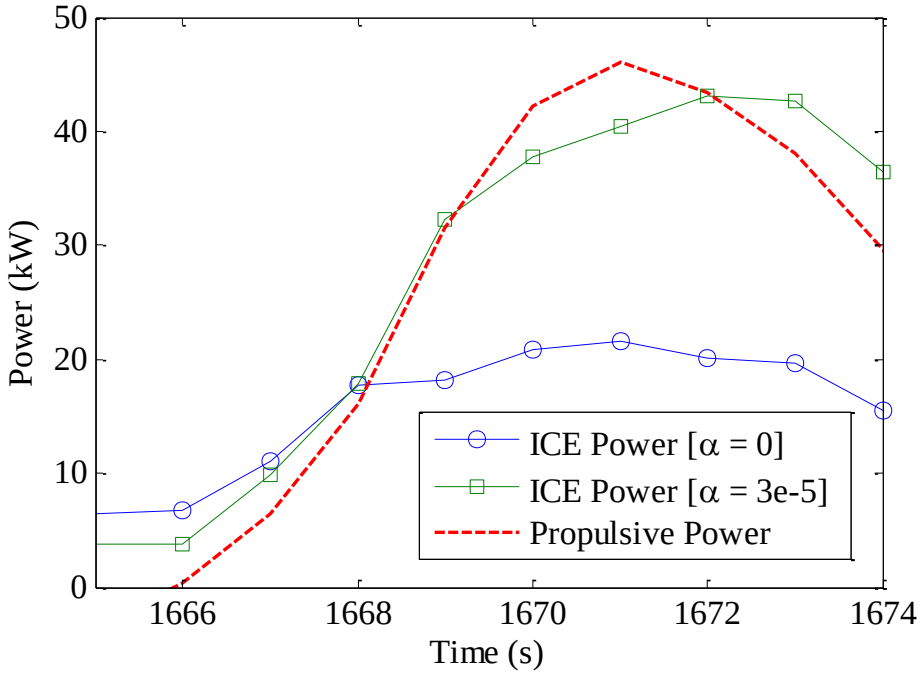

Figure 6-16: ICE Power Production with Power Factor

Figure 6-16 is a snapshot of the large acceleration event at the beginning of the HWFET cycle, and though ICE power differs greatly between these two simulations with different power factors, the vehicle still meets the speed trace. This means that without the power factor much more electrical energy is used to make up the difference between ICE power and propulsive power. With no power factor, after such acceleration event ICE power remains above the average road load for a time in order to replenish the ESS.

Indeed, the entire premise of a hybrid vehicle is that the availability of two on-board power sources allows one to select the appropriate combination of the power from each source to maximize efficiency. By contrast, providing all of the propulsive power on a second-to-second basis using the ICE defeats the purpose of a hybrid vehicle. Theoretically, as the power factor increases, the fuel consumption of the vehicle should asymptote to the fuel consumption of a similar, non-hybrid vehicle, in which all propulsive power is provided directly by the ICE. From a theoretical standpoint then, a

power factor of zero should result in minimum FC; however, while overall FC does increase with increasing power factors, efficiency may not be the only consideration. In the case of the E-REV architecture of the UVic EcoCAR, it is intended to operate as an all-electric vehicle for long period of time over the course of its life, during which the ESS will supply all propulsive power. Therefore, minimizing ESS usage as much as possible at the expense of FC while in CS mode is counter to the philosophy of the vehicle.

Returning to the results, it appears that power factors below 5×10^{-6}, referred to as α_1, induces ICE operation similar to that shown in the plot of Figure 6-16 without power factor correction, while power factors at or above α_1 induce behavior similar to the plot with power factor correction. This may be the reason for the odd distribution of fuel consumption points shown in Figure 6-15, which rise and then fall during the transition between power factors of 0 and α_1. At $\alpha_{1,}$ ICE power increases more frequently in order to order to meet propulsive power demands. Consequently, ICE speed also increases more frequently with larger values of α; an example of this difference in ICE speed is shown in Figure 6-17.

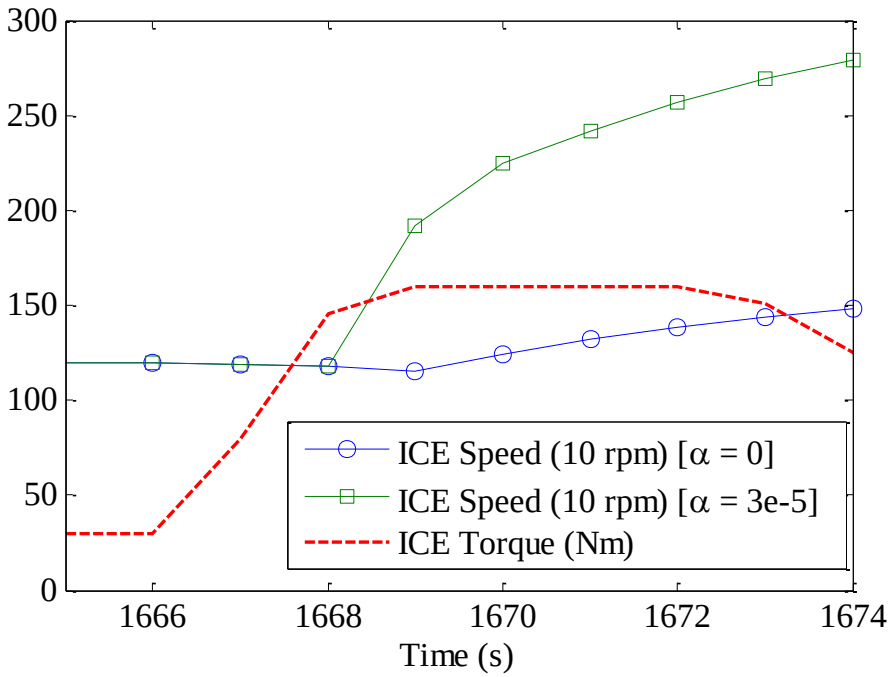

Figure 6-17: ICE Speed with Power Factor

As α increases beyond α_1, the proportion of ICE power used for propulsion increases and as does fuel consumption. An advantage of selecting a power factor at or above α_1 is an increase in consumer acceptability, as drivers are very accustomed to hearing increased ICE noise with increased power request. This distinction may seem counter-intuitive and against the philosophy of a hybrid vehicle, but consumer acceptability is a very important factor in the overall design of a vehicle.

Supplying the majority of propulsive power using the ICE undoubtedly also has an effect on use of the RTM since the results thus far suggest that the RTM is only used for high power events. As shown in Table 6-4, RTM use declines slowly with increasing power factors, as expected.

Table 6-4: RTM Use at Several Power Factors

Metric	$\alpha = 0$	$\alpha = \alpha_1$	$\alpha = 1.0 \times 10^{-5}$	$\alpha = 3.0 \times 10^{-5}$
Avg TS	0.969	0.968	0.971	0.975
RTM %	6.6%	6.5%	5.3%	4.0%

Based on the results of this section, α_1 will be chosen as the power factor; this results in a reduction of RMS current by roughly 1.5 amps with a negligible increase in fuel consumption and a negligible decrease in RTM use. This value also results in improved consumer acceptability, as ICE speed increases with increasing power demand.

Of note is that the development of a dynamic power factor may be a useful tool in the controller, as manipulating the proportion of power supplied by the ICE on the fly could have benefits. For example, such a tool could be used in a performance mode or a mountain mode to ensure that the electrical system is not taxed too heavily. Though not investigated here, this topic has potential to be included in future work.

6.4. Equivalency Factor Effects

As discussed in §5.3, a dynamic EF is necessary to maintain SOC over all drive cycles. Thus far implementation has been based on an EF correction that is linearly proportional to the difference between actual and target SOC, termed ΔSOC. This section examines alternative implementations of the power factor.

The term involving β in Equation 5-7 is referred to as the dynamic EF, or EF_{dyn}. While the initial value of EF_{const} is important, it is EF_{dyn} that controls the behavior of the EF over the course of the drive cycle.

A larger β results in larger changes in the EF at the same ΔSOC. The result of increasing β should therefore be smaller ΔSOC values over the course of the cycle. Here, three different types of EF correction will be investigated as shown in Equation 6-4.

$$Dyanmic\ EF\ Factor = EF_{dyn} = \beta\left(SOC_{actual} - SOC_{target}\right)^{x} \qquad 6\text{-}4$$

The effects of different values of β will be examined with various exponents, or *x* values. With a linear dynamic factor the EF always changes proportionally with changes

in SOC, whereas a squared or cubic factor would result in low EF correction at small values of ΔSOC, with an increasing rate of correction with increasing values of ΔSOC. This is demonstrated in Figure 6-18 which plots dynamic factors with x = 1, 2, and 3, and β = 0.1.

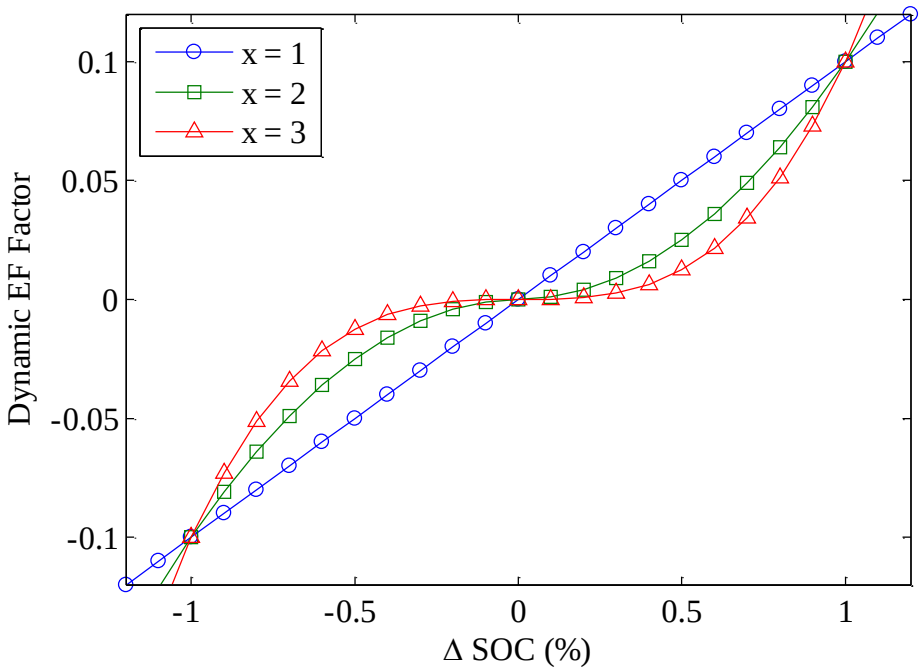

Figure 6-18: Dynamic EF Factors of Different Powers

The effects of different exponents on fuel consumption are summarized in Figure 6-19.

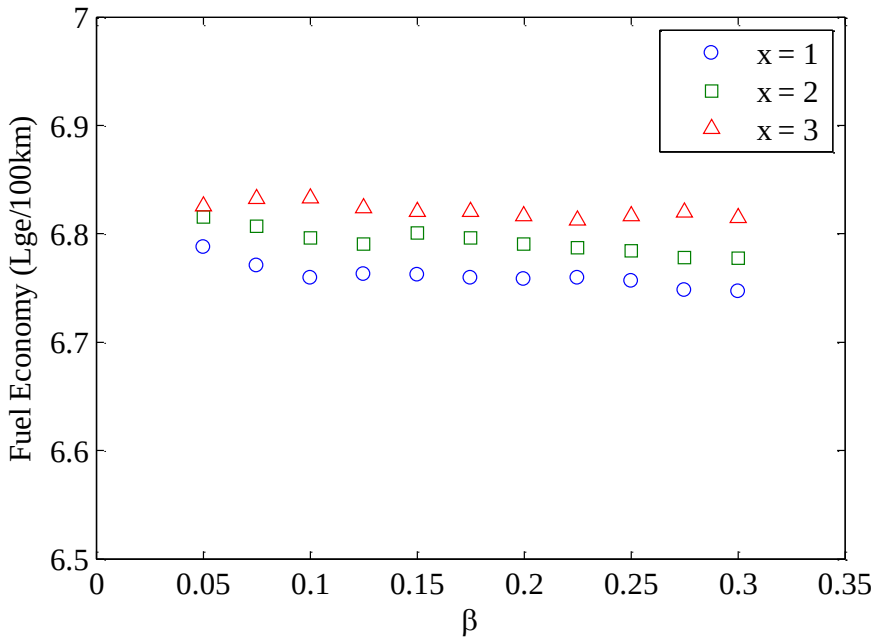

Figure 6-19: Fuel Consumption versus Dynamic EF

As shown squared and cubic EF_{dyn} terms result in overall higher fuel consumption than linear EF_{dyn} terms, and the effect of changing β has less of an effect than changing *x*. The increased fuel consumption for exponential terms of EF_{dyn} may be due to a combination of factors. First, the low rates of SOC correction at low values of ΔSOC mean that larger initial SOC changes can take place with only small amounts of SOC correction; this may be beneficial in some cases, but can lead to inefficiency if the ICE is used to charge the ESS frequently. Second, as ΔSOC increases, the *rate* of SOC correction increases, which may lead to more rapid changes in ICE operation. To illustrate, Figure 6-20 plots the SOC for the three implementations of EF_{dyn} for a β of 0.1.

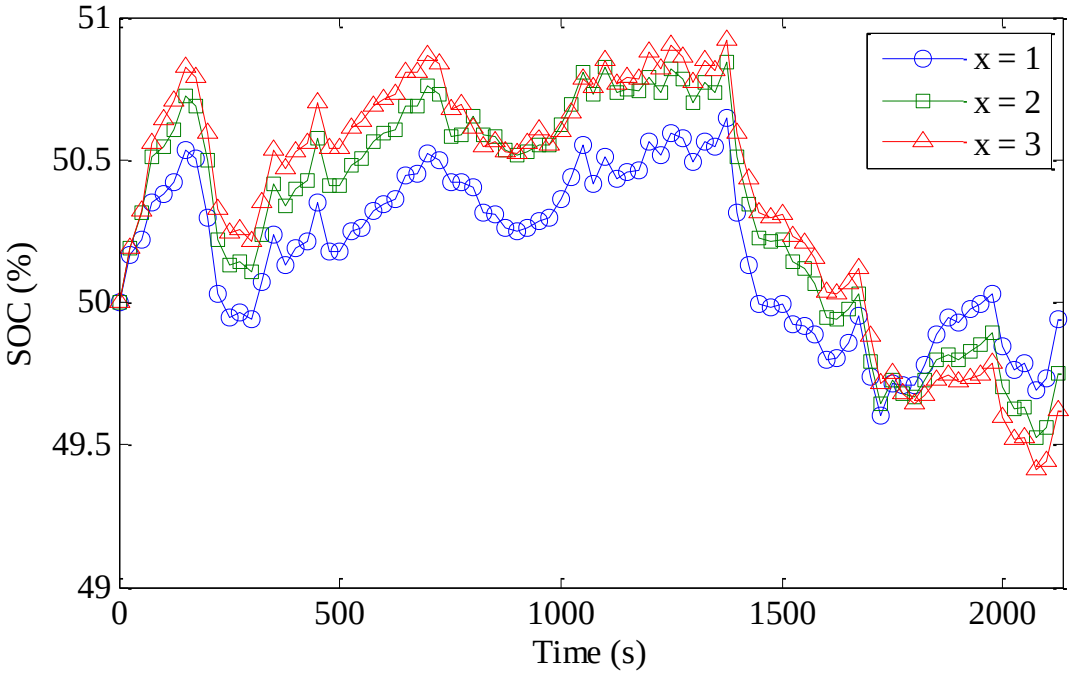

Figure 6-20: ESS SOC with Three Implementations of Dynamic EF Factor

Indeed, the exponential implementations allow the ICE to charge the ESS to a higher degree than the linear implementation at the same value of β. As shown in Figure 6-21, the EF does indeed respond slowly at low values of ΔSOC, only to rise more quickly as ΔSOC increases.

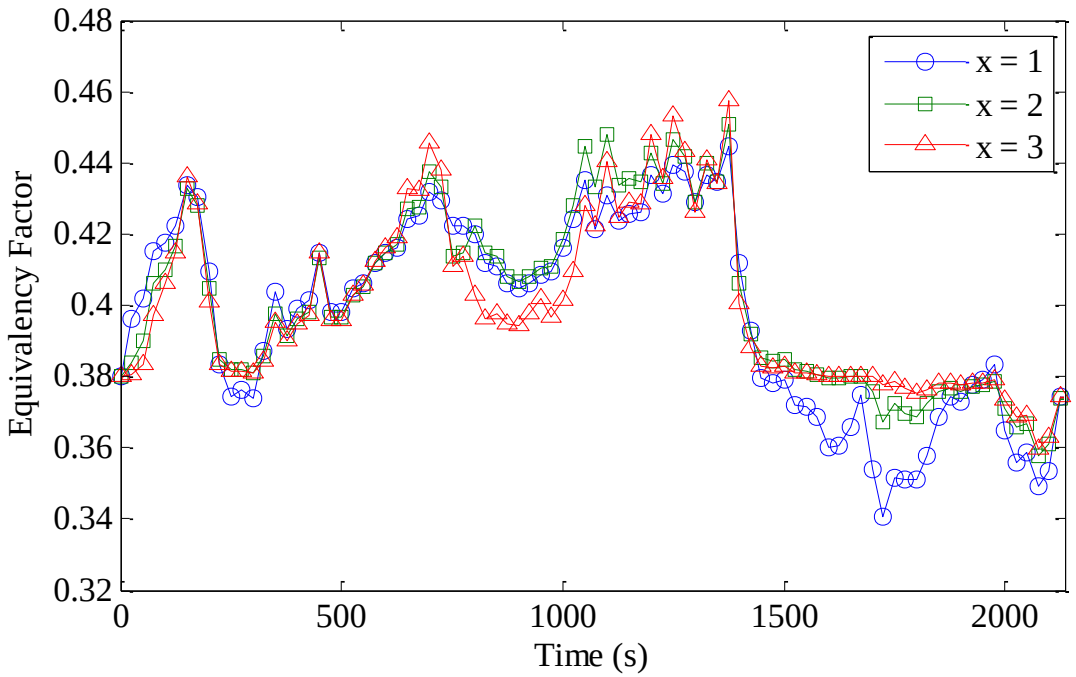

Figure 6-21: EF with Three Implementations of Dynamic EF Factor

As shown, at SOCs close to the target (see Figure 6-20 for reference), the EF with exponential EF_{dyn} values change more slowly than the linear implementation, but change more quickly with larger changes in ΔSOC.

Exponential factors at ΔSOC values below 1.0 result in smaller EF corrections than linear factors at the same value of β, which explains the large differential between SOC values in Figure 6-20. Figure 6-22 compares a linear EF_{dyn} term at a β of 0.1 to a squared EF_{dyn} term at a β of 0.3, which have fairly similar SOC profiles.

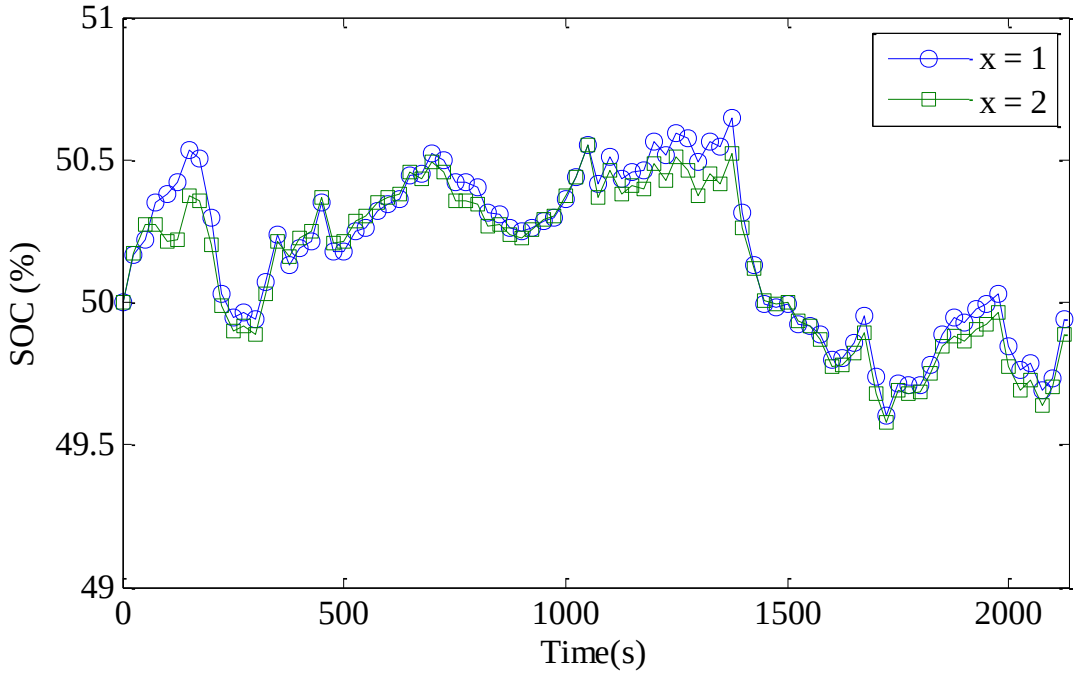

Figure 6-22: ESS SOC with (β, *x*) of (0.1, 1) and (0.3, 2)

As shown in Figure 6-23, the EF for the exponential implementation changes much more rapidly during the cycle.

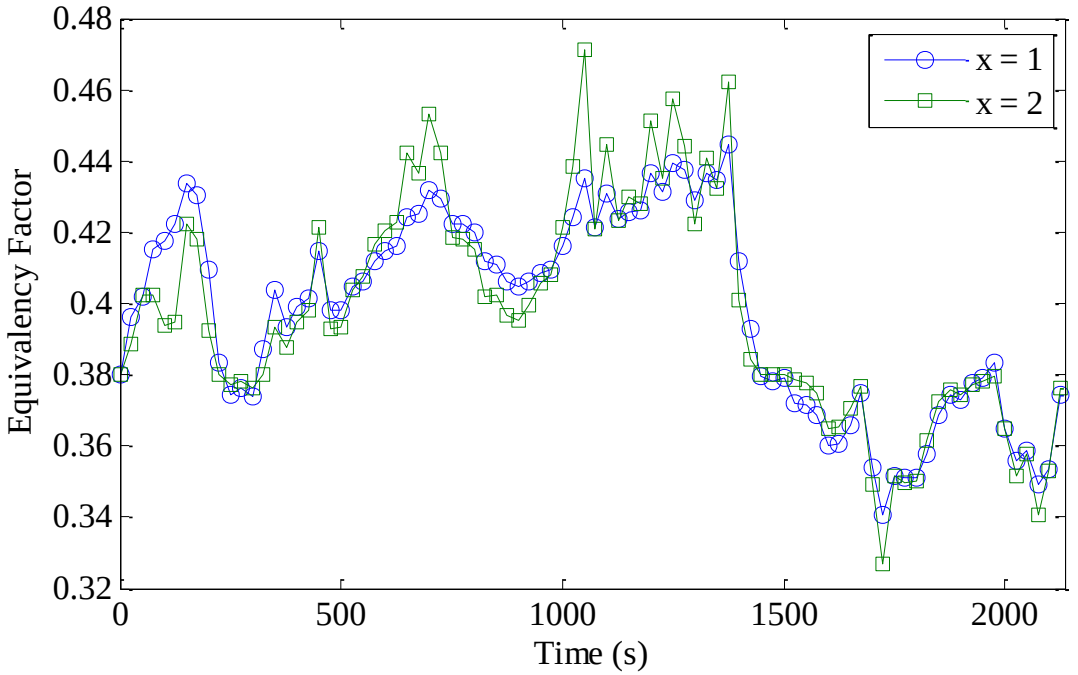

Figure 6-23: EF with (β, *x*) of (0.1, 1) and (0.3, 2)

From a drivability standpoint, because the optimization algorithm is so sensitive to changes in the EF, it is presumed that a rapidly changing EF such as illustrated in Figure 6-23 for $x = 2$ may be detrimental to drivability, and perhaps lead to inconsistent operation. Therefore, combined with the fuel consumption results, a linear EF_{dyn} term will be implemented: a value of 0.1 is appropriate given the comments above concerning drivability which also apply to linear dynamic EF factors with higher β values. Additionally, the difference in fuel consumption between β values of 0.1 and 0.3 is less than 0.2%, so an increase beyond 0.1 is not necessarily warranted.

Like the power factor considered in §6.3, the use of an adaptive EF_{dyn} may constitute another method to alter the performance of the vehicle under different circumstances. A mountain or towing mode, for example, where the vehicle is under heavy load may be a good application in order to prevent SOC from decreasing by a large margin.

6.5. Traction Considerations

One major advantage of vehicles with four-wheel drive capability is improved traction and handling. With an active traction split through which the amount of toque applied at either axle can change quickly – as compared to the constant traction split of conventional four-wheel drive vehicle – one might expect possible adverse effects on traction. For example, a rapid shift in traction from front to rear axle during a sharp turn may cause a loss of control. Fortunately, appropriate responses to such circumstances can easily be incorporated into the controller because of the multi-staged nature of HOS. Recall that the desired traction split from HOS can be modified and that subsequent levels of HOS will ensure optimal operation under the *current* operating conditions, not

the desired operating conditions. Therefore, a traction control system could override HOS level 3 commands to ensure stability under the given driving conditions.

The development of such a traction control system is beyond the scope of this work, but the dynamics of an active traction split are worth investigating further, especially considering the results thus far with regards to RTM use: that the RTM is used primarily to provide propulsive power during acceleration events.

Considering purely longitudinal acceleration events only – assuming that traction split may be altered by a traction control system during acceleration events that involve lateral acceleration (or turning) – an intermediary traction split (between 0 and 1, exclusive) will theoretically provide better traction than if the vehicle were propelled using only one axle, as the tractive force will be split across both front and rear axles. This is true regardless of how quickly the traction split changes during the acceleration event, as any intermediary traction split essentially represents some combination of pure front- and rear-wheel drive vehicles. Consider Equations 6-5 and 6-6 for the front wheels at an intermediary traction split.

$$s_F \propto F_N\,, F_T \tag{6-5}$$

$$F_T = \alpha \cdot F_{T,Total} \;\rightarrow\; \{\alpha \in (0,1)\} = pro \;\therefore\; F_T < F_{T,Total} \tag{6-6}$$

With the following representations:

S_F = slip of the front wheels,

F_N = normal force on the front wheels,

F_T = tractive force applied at the front axle, and

$F_{T,Total}$ = total tractive force at front and rear axles.

By Equations 6-5 and 6-6, the slip at the front wheels should be less during acceleration at an intermediary traction split than using purely the front-axle. The true interaction may be more complex due to body pitch during acceleration, thus leading to lower normal forces on the front tires, but assuming equal acceleration for both cases an intermediary traction split will result in less slip. This is well illustrated in Figure 6-24, which plots the total, front, and rear axle torques during a representative acceleration event during the UDDS cycle

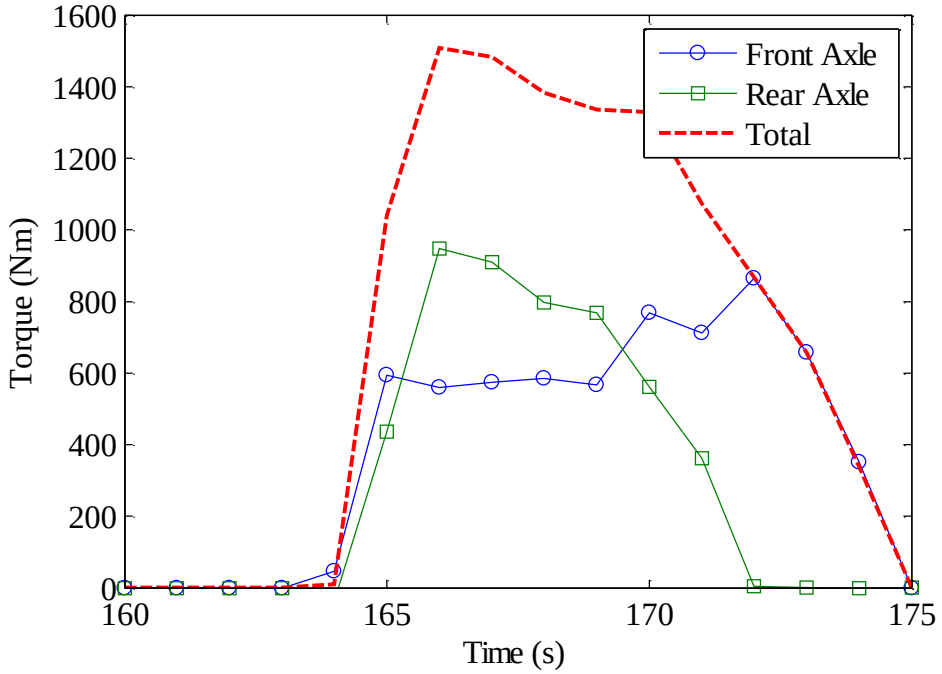

Figure 6-24: Representative Axle Torque Distribution during Acceleration

If the vehicle were powered by only one axle during this acceleration event, the likelihood of a loss of traction appears to be greater.

This same logic may not hold for rapid shifts in traction split from front to rear over short periods of time, though, and a number of other factors could play a role in the traction of the vehicle. A full analysis of the effects of a dynamic traction split on traction is difficult, as the vehicle model used possesses a ‘stiff’ driveline that is not suitable for

assessing traction or wheel slip. However, given the results thus far, two observations can be made regarding the tractive performance of the system in practice. First, the system as applied here appears to be ‘stable’ in that the equilibrium at essentially all cruising road loads is a traction split of one, so rapid oscillations in traction split under normal driving conditions seem unlikely. This may not be the case if the RTM were sized so as to operate primarily in a high-efficiency region; under these circumstances, rapid oscillations in traction split seem more likely. Second, a loss of traction is usually less likely to occur when the vehicle is moving as opposed to when at a stop, so rapid changes in traction split at cruising speeds may not be very detrimental to traction.

Further analysis beyond the scope of this work is necessary to evaluate the assumptions made above and could be included in future work. Once again, it is also assumed that a traction control system would manage and apply an appropriate traction split based on input from HOS and current operating conditions. This is essentially the same strategic/tactical relationship as discussed in §5.2 with regards to the different levels of HOS.

6.6. Optimization Sample Time

A final factor to be considered is the rate at which each stage of HOS optimization should be evaluated. Unfortunately, performing such an evaluation with the goal of application to a broad range of controllers is difficult due to differences in controller processing power, architecture, and task timing capability, and would most likely stray out of the context of this work. Therefore, specific focus will be placed on application of the algorithms to the UVic EcoCAR controller, not only because this is the platform intended for testing, but also because the controller hardware is available for direct

testing. The MABX is a 900 MHz high-performance rapid-prototyping controller that serves as the supervisory controller for the UVic EcoCAR, performing the high level functions outlined in §4.1, acting as a communication hub for the vehicle's four communication networks, and running on-board diagnostics for vehicle components.

To evaluate the speed at which a program runs on the MABX, it is first important to distinguish between single and multiple task timing operation. In single task timing operation, a control unit attempts to complete all computational tasks at each fundamental system time step. In the case of real-time applications such as the one being developed here, this method is unsuitable. Such applications simply require too much processing power to be completed in such a short period of time, and the results of the calculations are often not required at each fundamental time step (1 millisecond, for example). In multiple task timing operation, different sample times are assigned to different tasks and those tasks with larger sample times – tasks that require more than one fundamental time step to evaluate – are evaluated in small chunks over many consecutive fundamental time steps.

Next, a brief overview of turnaround time is necessary. At a given processor speed, the time to complete a given task is known as the turnaround time, and is independent of sample time. A sample time greater than the turnaround time for a given task means that all necessary computations will be completed, and the task will proceed as expected. If the turnaround time is greater than the sample time, a task overrun occurs and the computations for the task during one sample time interfere with the computations required for that same task or other tasks during the next sample time. For example, assuming a maximum turnaround time of 0.05 seconds for an algorithm, a sample time of

0.1 seconds would mean that roughly 50% of the calculations per fundamental time step would be devoted to calculations for this algorithm. A sample time smaller than 0.05 seconds would cause a task overrun. Task overruns, which result in an application that does not run in real-time, must absolutely be avoided.

The multi-staged nature of HOS, along with the fact that the output of the HOS algorithms are not needed at each fundamental time step, means that different layers of HOS can operate at different sample times. The control system has three separate layers of optimization for each ECVT mode and two layers for each of the four fixed gears. Because gear selection is based on the total power calculations of the first level of HOS (traction split determination) the entire first layer – six optimization algorithms – must be evaluated at all times. Subsequent layers must only be evaluated for the current gear. So, in each ECVT mode, eight algorithms are evaluated: all of HOS level 1, and both ICE speed and torque determination for the respective ECVT mode. In each fixed gear, seven algorithms are evaluated consecutively, since ICE speed is already determined by the gear ratio. While this is helpful in terms of conserving computational resources, the first level of HOS is unfortunately the most time consuming on a per-gear basis, since the first level has the highest DOF.

First, each stage of HOS was implemented independently on the MABX, which in the case of the UVic EcoCAR has a sample time of 1 millisecond, in order to determine turnaround time. Turnaround time for these algorithms is not constant, and depends on the number of required evaluations of the objective function which is in turn related to the complexity of the search space. Figure 6-25 plots the turnaround time of the three levels of HOS during the drive cycle used throughout this chapter.

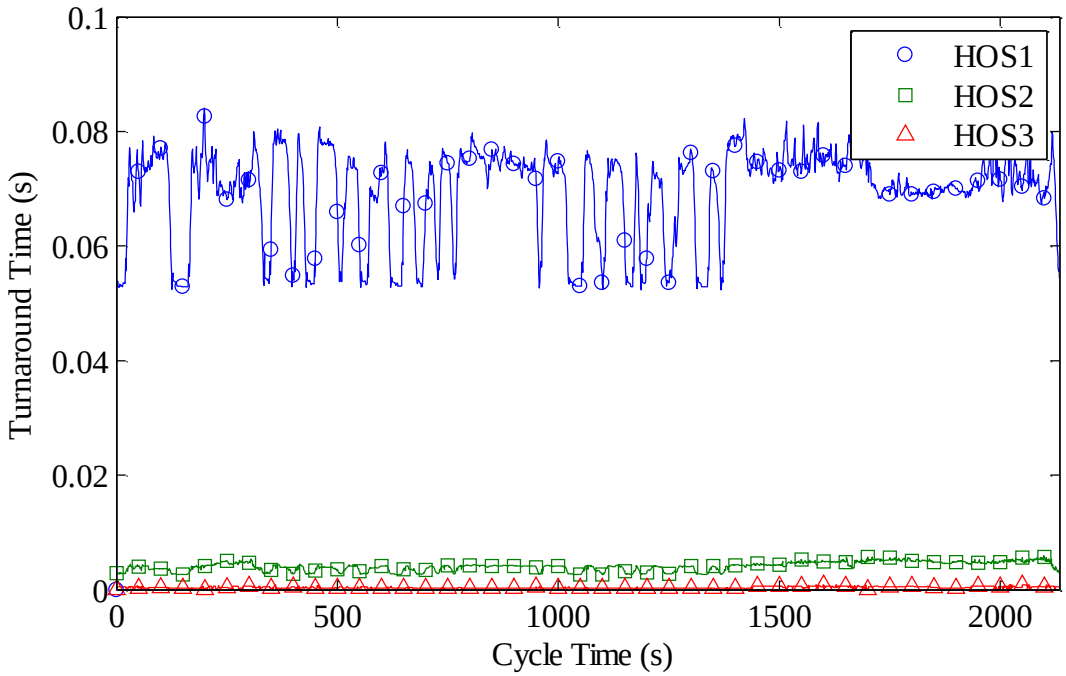

Figure 6-25: HOS Turnaround Times on MicroAutoBox

As expected, turnaround time varies throughout the drive cycle and the turnaround time for HOS level 1 dwarfs that of the other algorithms. The effects of implementing all three algorithms at the same time with three different sample times becomes difficult to analyze, as computations for a single level of HOS can be shared between processes running at different sample times. Basically, though, these turnaround times represent the absolute minimum sample time at which each individual algorithm could operate at in real-time. Therefore, based on the definition of turnaround time, a sample time should be chosen for each level of HOS so as to leave enough time for the execution of all other calculations during each fundamental time step.

Rather than arbitrarily assigning a suitable sample time based on the information above, it is important to understand the effects of sample time on the performance of the system. Throughout testing thus far, all layers of HOS were evaluated using small sample times in simulation, where real-time operation is not required. To determine the effects of

sample time on vehicle performance, the sample time for HOS level 1 was increased while keeping speed and torque determination sample times small (0.05 and 0.01 seconds for speed and torque determination, respectively). The results, plotted against fuel consumption, are shown in Figure 6-26.

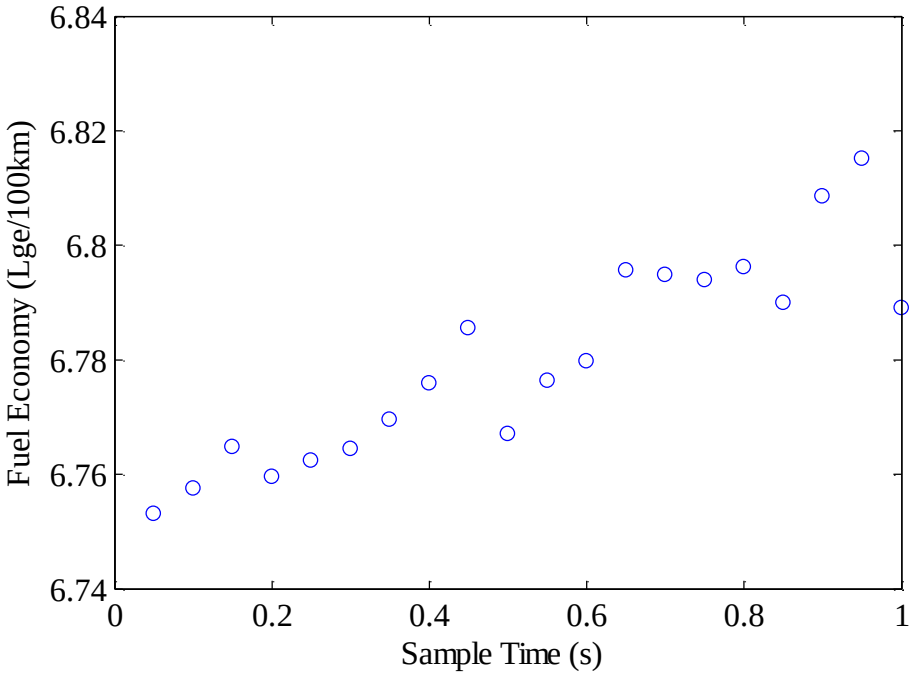

Figure 6-26: Fuel Consumption versus Sample Time of HOS Level 1

Basically, a sample time of 1 second means that the target traction split and the gear will remain constant through each second of operation, so increasing fuel consumption with increasing sample time is expected.

Effects on ESS RMS current are negligible, which is reasonable considering that ICE torque, the final level of HOS, would have the most impact on ESS current. RTM use does increase slightly with increasing sample times, as shown in Figure 6-27.

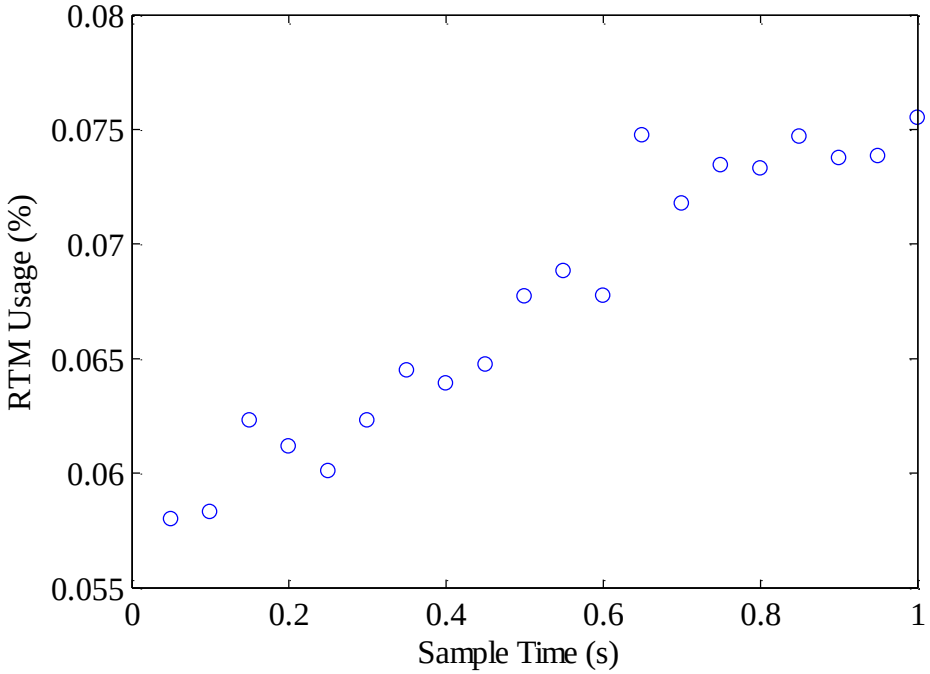

Figure 6-27: RTM Usage versus Sample Time of HOS Level 1

Again, this increase in RTM use is expected, as the system will trend towards or remain at the target traction split for the duration of the sample time; thus, increasing sample time has the potential to increase the amount of time spent at a traction split less than 1.0.

For the current application, where the MABX is performing only high-level supervisory functions, all processes aside from HOS consume roughly 20% of controller resources. Based on this, the results of this section and intuition, a sample time of 0.3 seconds for HOS level 1 seems reasonable. At this rate, traction split and gear targets update faster than 3 times per second, and HOS level 1 consumes less than 33% of system resources. This leaves 50% of system resources for the two layers additional levels of HOS and further system expansion if necessary.

This same exercise can now be repeated for the subsequent layers of HOS. HOS level 2 must operate faster than HOS level 1 to ensure optimal system operation as the system

transitions between optimal points determined by HOS level 1. Results are shown in Figure 6-28.

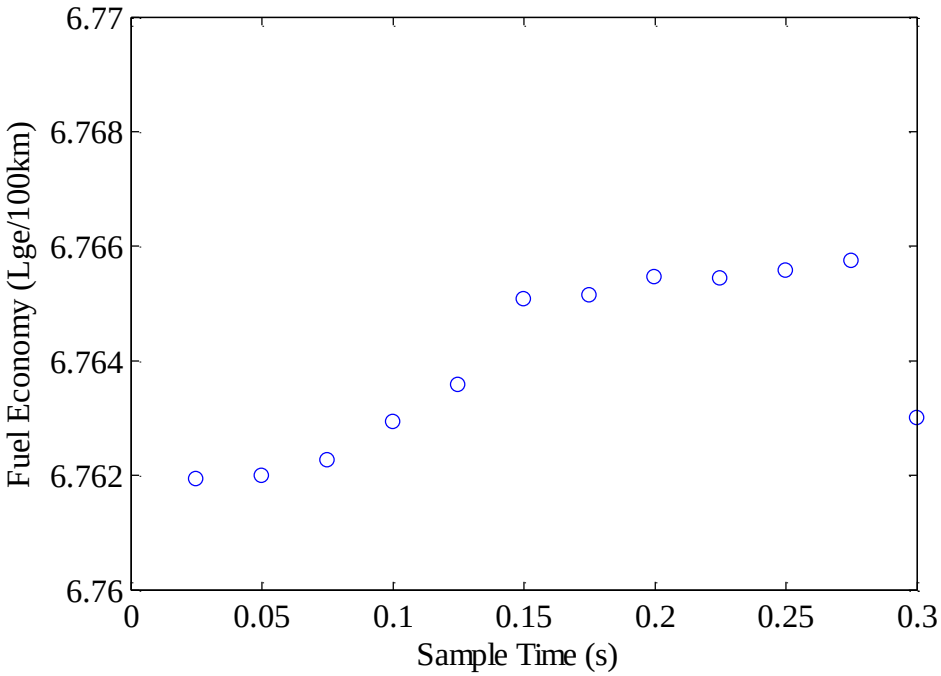

Figure 6-28: Fuel Consumption versus Sample Time of HOS Level 1

Fuel consumption increases once again, as expected. However, all fuel consumption values are within a tenth of a percent of the minimum value, so basically any value would be suitable. In this case, one must also consider the maximum rate of change of ICE speed: updating the ICE speed target too quickly may be a waste of resources as the response time of the ICE to speed requests is slow compared to the absolute minimum sample time outlined in Figure 6-25. Considering this, a sample time of 0.1 seconds seems reasonable, as it consumes a maximum of only 6% of controller resources and updates the desired speed target three times over the span of a given traction split target set forth by HOS level 1.

The final step is to examine the effects of sample time on HOS level 3. Figure 6-29 shows the results, again assuming that the sample time of HOS level 3 should be smaller than HOS level 2.

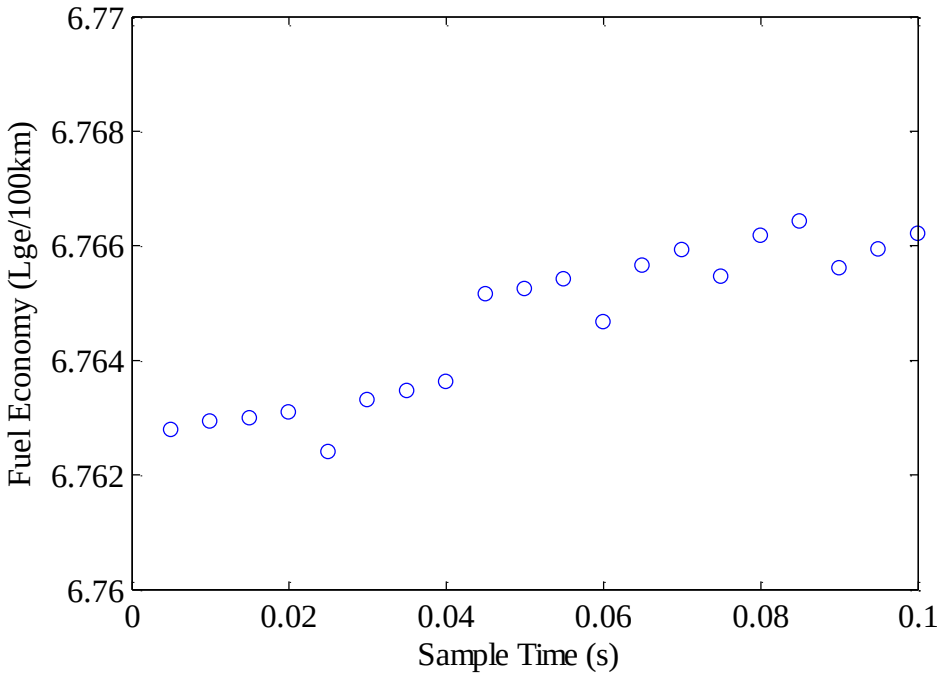

Figure 6-29: Fuel Consumption versus Sample Time of HOS Level 3

Again, all results are within a tenth of a percent of the minimum. Additionally, the effects of changing the sample time of HOS level 3 have negligible effects on ESS RMS current and RTM use. ICE torque can be modulated much more quickly than ICE speed, and even at the minimum sample time shown, 0.005 seconds, only 18% percent of controller resources are consumed. However, such a sample time seems unnecessary; a value of 0.025 will be selected here, as this updates ICE torque 40 times per second and four times between each update of ICE speed from HOS 2 (in the ECVT modes), and uses less than 4% of controller processing power.

6.7. ECVT-Only Operation

As mentioned in the opening section of this chapter, algorithm development has included the use of fixed gears for completeness, despite the fact that the vehicle currently does not use them (aside from FG2, which is used for short instances during the transition between Mode 1 and Mode 2). This section will now analyze the performance of the system using only the ECVT modes, as this scenario reflects the true operation of the vehicle.

Removing fixed gears from vehicle operation requires re-tuning the magnitude of the shift buffer, as the number of available gears has been reduced. Aside from the numbers of gears available, ECVT operation is not fundamentally different than operation in fixed gears, and an analysis of the remainder of the control variables during ECVT-only operation yielded essentially identical trends. Additionally, while the removal of fixed gears from HOS does reduce the turnaround time for level 1 significantly, the sample time was not changed so as to allow for future expansion to fixed gears, and because the effects on fuel consumption are negligible.

Operating in the ECVT modes with a shift buffer of 4 kW as implemented with the availability of fixed gears results in only six shifts. Further analysis revealed that a shift buffer of 2.5 kW was most suitable, yielding 14 shifts, as shown in Figure 6-30.

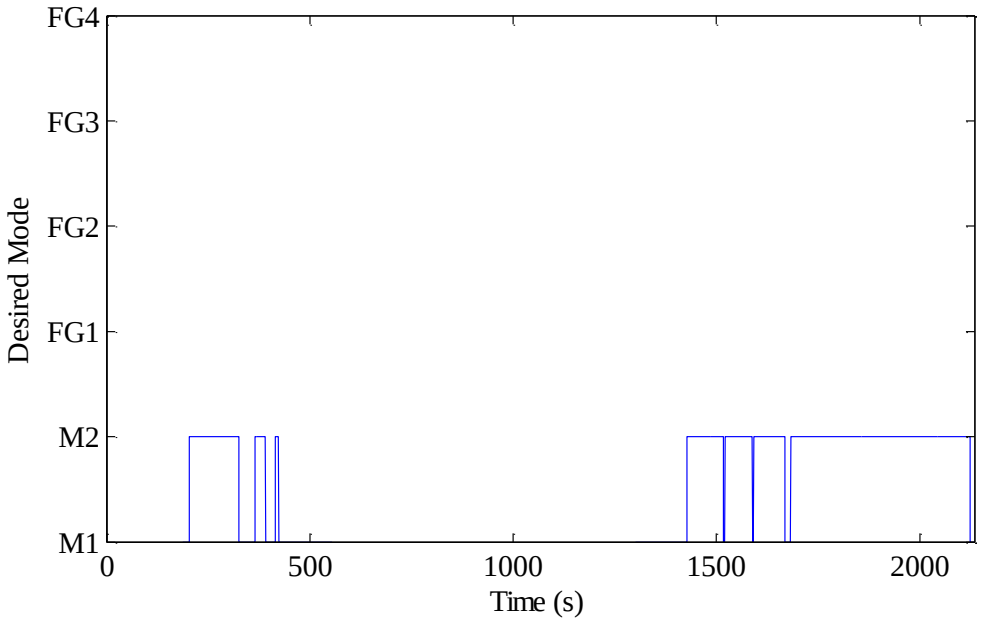

Figure 6-30: ECVT-Only Gear Selection

This significant reduction in the number of shifts also has an impact on ICE operation, which is concentrated a lower speed values since ICE speed is never coupled to wheel speed; this is illustrated in Figure 6-31.

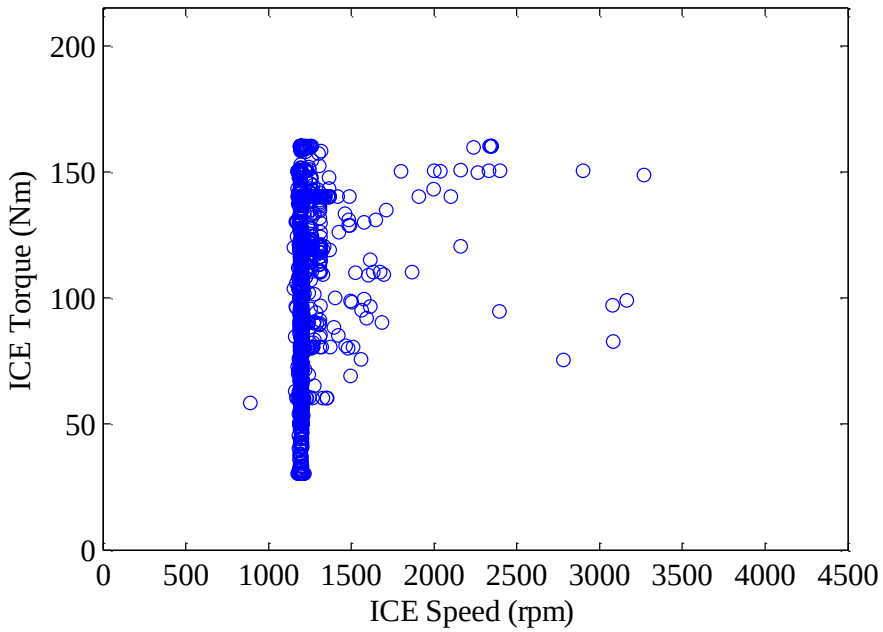

Figure 6-31: ECVT-Only ICE Operating Points

As was the case in the original tuning of the shift buffer in§ 6.2, much of this change in ICE operation may be attributed to a reduction in the number of shifts throughout the cycle, which thus requires less ICE speed matching for synchronous shifting.

There was essentially no change in RTM use, as illustrated in Figure 6-32, with the cycle showing an average traction split of 0.968 and a propulsive power percentage of 6.6%.

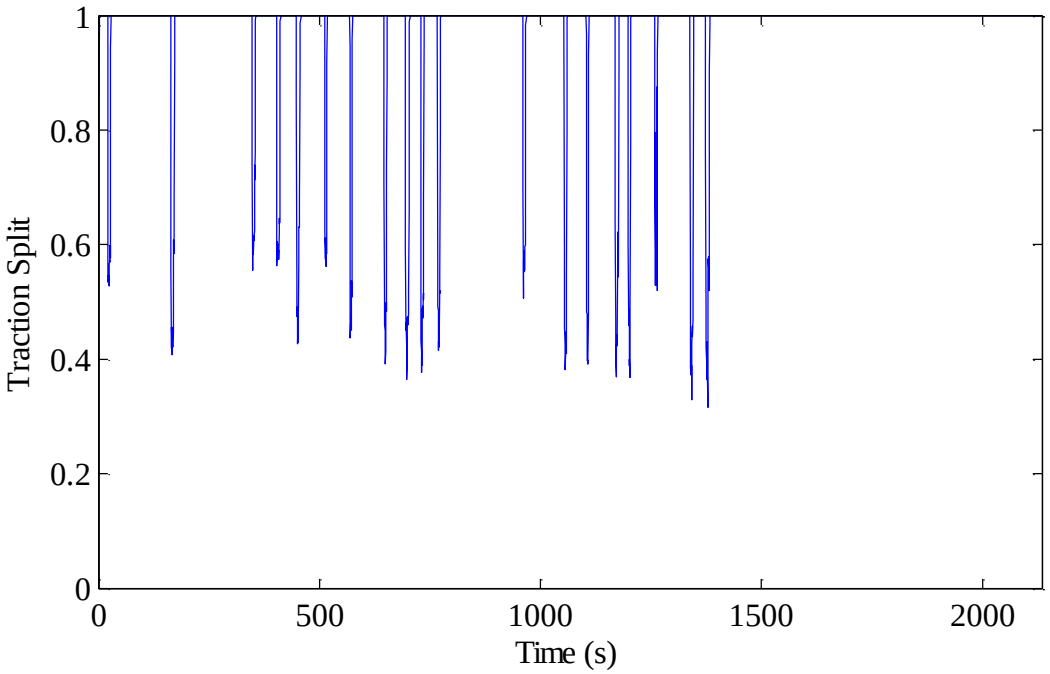

Figure 6-32: ECVT-Only Traction Split

CHAPTER 7 Results and Discussion

Having developed the basis of the HOS strategy, this section focuses the results of HOS in terms of its effects on vehicle fuel consumption and performance. Additional driving scenarios are introduced to test the robustness of the algorithm in meeting the control system requirements outlined at the beginning of Chapter 5 under various driving conditions.

Ultimately, while simulation is an important tool in the vehicle design process, significant amounts of real-world driving are needed to assess and tune any control strategy; drivability, smoothness, and 'feel' are difficult to assess in simulation, but are very important in the end product. As such, the goal of this section – and indeed this thesis – is to validate the operation of the algorithm as a fundamental step in the vehicle development process through simulation and initial in-vehicle testing. The goal is *not* to develop a complete solution for immediate and final implementation in the vehicle. Additionally, several possible changes to the vehicle that may impact algorithm performance are investigated.

7.1. Model Variants

The results of Chapter 6 reveal that with the current configuration, the RTM is only seldom used, and only at high levels of torque; though reasons for this were touched on in §6.1.4, they will be further discussed in 7.4. Achieving optimal RTM usage requires a large amount of processing power, and the limited use of the RTM as implemented on the current architecture suggests that dedication of such resources may not be worth the return. It is presumed based on the results that a rule-based traction split implementation may be a sufficient alternative. As this work has focused directly on the UVic

architecture, it makes sense that a comparison of the developed algorithm should be made against a vehicle that has RTM capabilities as well, as opposed to against a vehicle without an RTM. Therefore, a simple rule-based traction split strategy has been developed, whereby axle torque above a given threshold is applied by the RTM, up to a minimum traction split of 0.5. This strategy is illustrated for a threshold, T_{thresh}, of 1000 Nm in Figure 7-1.

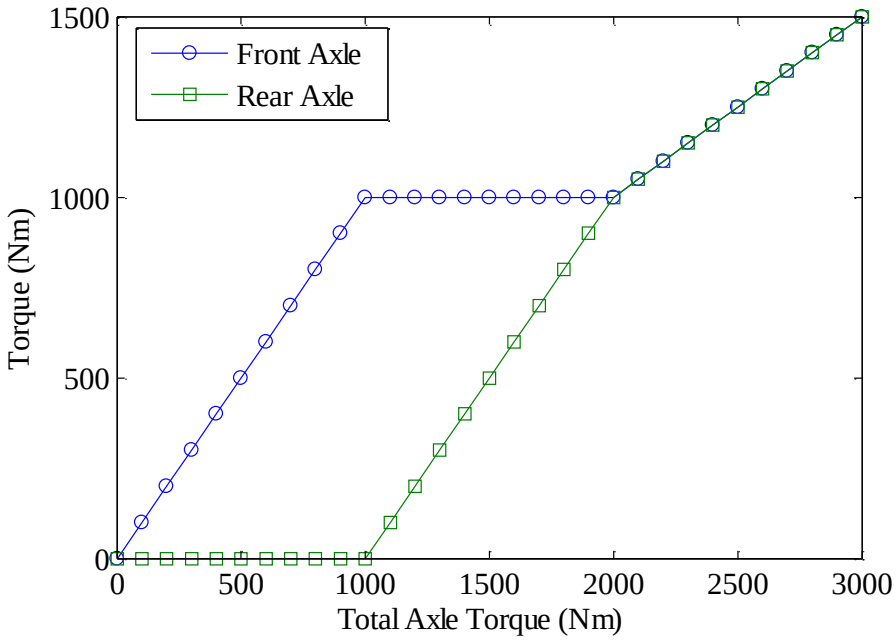

Figure 7-1: Rule-Based Traction Split

This simple rule is based on the results of the previous chapter, which show that the front powertrain is more efficient for the majority of vehicle operation, and that the rear powertrain is used only to meet high axle torque requests. Further experimentation with this rule suggested that a T_{thresh} of 750 Nm generated satisfactory results.

For reference against both of these architectures, an identical vehicle without a RTM (*ie:* FWD only) has also been included in testing. The weight of this vehicle has been reduced by 100 kg to represent the removal of the RTM, transaxle, and rear half-shafts.

7.2. Simulation Test Results

Simulation tests were completed using four separate drive cycles: UDDS and HWFET, as well as towing and acceleration cycles based on the requirements of the EcoCAR Challenge.

During the towing cycle, the vehicle is required to tow a 680 kg load at a constant speed of 72 km/h up a 3.5% grade for 20 minutes; the cycle is shown in Figure 7-2.

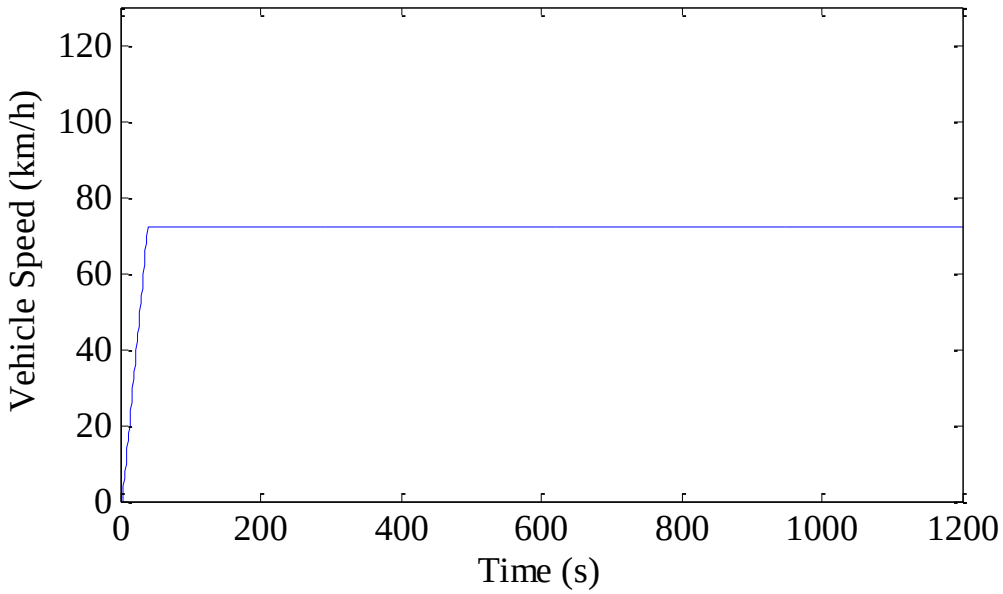

Figure 7-2: EcoCAR Challenge Towing Drive Cycle (3.5% Grade)

The acceleration cycle, shown in Figure 7-3, involves accelerations from both 0 to 100 km/h, and from 80 to 112 km/h which represents a high-speed passing maneuver.

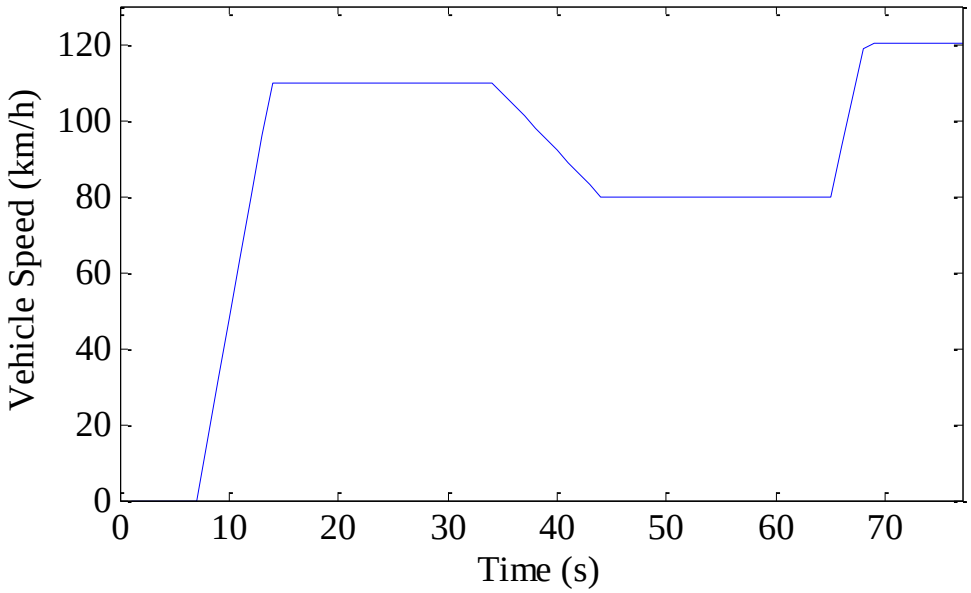

Figure 7-3: EcoCAR Challenge Acceleration Cycle

UDDS and HWFET drive cycles were run two and three times consecutively to ensure results were averaged over longer periods of time and distances. Memory usage limits during simulations prevented the use of longer cycles.

7.2.1. Fuel Consumption

For the sake of comparison, fuel consumption values for the standard, ICE-powered (stock) and 2-Mode Saturn VUE are presented in Table 7-1.

Table 7-1: Saturn VUE Fuel Consumption

Vehicle	Powertrain	Fuel Consumption (L/100 km) [City/Highway]
Stock VUE	4 cyl 2.4L ICE, 4 speed auto trans	11.25/7.92
2-Mode VUE	6 cyl 3.6L ICE, 2-Mode trans	7.92/6.43

These values are based on US Environmental Protection Agency dynamometer testing values found here [50], and have been scaled according to the information found here [51]. Essentially, raw dynamometer results are scaled before release to account for the differences between real-world driving and the test cycles typically used for testing. As

the results shown in this thesis are not scaled, we wish to compare against raw dynamometer results.

Table 7-2 summarizes fuel consumption results for the optimization-based, rule-based, and FWD variants over the selected cycles.

Table 7-2: Fuel Consumption Results (Lge/100km)

Variant	UDDS	HWFET	Towing	Acceleration
Opt	7.84	5.88	13.21	21.00
Rule	7.71	5.83	12.98	19.95
FWD	7.69	5.82	13.23	20.93

First, the results here are comparable to those of the original 2-Mode transmission, especially considering the number for the city (UDDS) cycle, which is promising. The discrepancy in highway values, however, may point to poor model performance at high speeds; this confirms that further model validation is necessary. Also worth noting is these values represent the CS fuel economy of the UVic EcoCAR; in reality, when the all-electric CD range is taken into account, the UVic EcoCAR will achieve much lower average fuel consumption.

From the perspective of fuel consumption on the standard drive cycles, it appears that the benefit of 100 kg of weight savings has a larger impact than operating at an optimal traction split. The results of the rule-based and optimization-based traction split variants offer further insight, as the use of the simple rule actually produces better fuel consumption. Considering these results, it appears that a constantly changing optimal target – which was the rationale for using three HOS levels – and the theoretically non-optimal operation en-route to these targets may result in overall higher fuel consumption. In other words, a changing traction split target every third of a second may cause ICE operating targets to change more frequently than at a comparable constant traction split

target, thus resulting in higher losses due to changes in ICE speed. To aid in the discussion of these results, Table 7-3 summarizes RTM use over the four cycles.

Table 7-3: RTM Use Results (Propulsive Power %/Average TS)

Variant	UDDS	HWFET	Towing	Acceleration
Opt	11.1/0.957	1.0/0.992	0.2/0.993	34.2/0.901
Rule	8.8/0.972	0.8/0.995	0.9/0.991	35.4/0.926

The rule-based traction split generally results in less RTM usage, which therefore means less time spent operating under constantly changing traction splits, perhaps offering better continuity in terms of ICE operating points. To demonstrate this theory further, Figure 7-4 plots the traction split for these two variants for a 0-100 km/h acceleration.

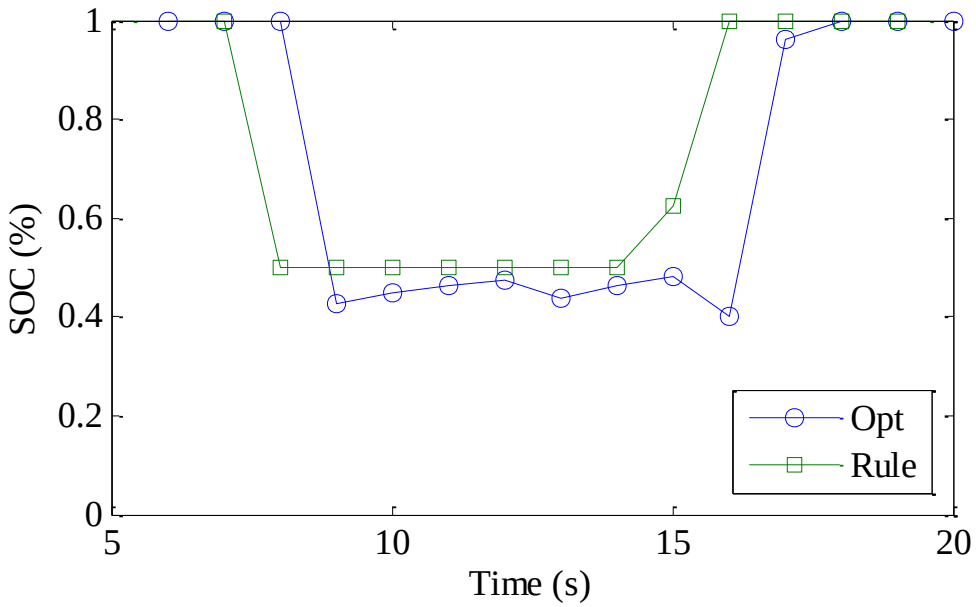

Figure 7-4: TS for 0-100 km/h

The figure not only demonstrates that the traction split throughout the acceleration event is constantly changing in the case of the optimization-based variant, but also illustrates a delay in traction split response time of this variant. This delay in response time could also be a cause of the increased fuel consumption of the optimization-based

implementation versus the rule-based implementation. The slow response (due to the 0.3 second sample time of HOS level 3) means that the optimization-based system may be operating at non-optimal traction splits for periods of time.

The aforementioned variability in traction split as a result of constantly changing optimization outputs could potentially be remedied by modifying the objective function to reduce small changes in traction split, similar to the way in which the power factor was implemented; however, considering the similar results, a rule-based implementation seems a much simpler method to achieve the same goal.

The results for towing also demonstrate the extent to which the front powertrain is more efficient than the rear, as even a significant increase in weight, and the associated increase in frictional forces is not enough to shift the traction split to an intermediary value at cruising speeds. Of note, however, is that the model does not account for the additional drag forces associated with towing a trailer.

It should also be noted that fuel consumption results for acceleration are difficult to compare, as all vehicles do not necessarily meet the aggressive trace exactly; results were simply listed for comparison.

7.2.2. Performance

One of the primary reasons for adding a RTM to the UVic EcoCAR was the improvement in performance. Aside from the fact that the RTM is used heavily in EV-only operation, the addition of several hundred kilograms of weight over the stock vehicle and the down-sizing of the ICE (from the 6-cylinder stock ICE to the 4-cyclinder LE9) meant that more power was needed to meet or improve on the performance

characteristics of the stock vehicle. This is certainly reflected in the acceleration results summarized in Table 7-4.

Table 7-4: Acceleration Results (seconds)

Acceleration	Opt	Rule	FWD
0-100 km/h	6.67	6.65	11.08
80-112 km/h	3.89	3.45	7.89

As expected, the rule- and optimization-based variants significantly outperform the front-wheel drive variant. Interestingly, the rule-based variant performs the best for both cases of acceleration. This makes sense, since the first level of HOS updates only 3 times per second, whereas the traction split rule updates every millisecond; therefore, in general, the rule-based variant will change the traction split more quickly and thus produces more axle torque faster than the optimization-based variant. This phenomenon was illustrated in Figure 7-4.

7.3. In-Vehicle Testing

The UVic EcoCAR Team has access to the University of Victoria Green Vehicle Research and Testing Center, a new facility that includes an ICE dynamometer, four-wheel-drive chassis dynamometer (dynamometer from here on will refer to the chassis dynamometer), and emissions testing equipment.

Figure 7-5: UVic EcoCAR on Chassis Dynamometer

This facility was used for initial in-vehicle testing, though several limitations due to the recent completion of the center must be noted. First, the emissions equipment for the center was unavailable for testing as further set-up and calibration is required. Additionally, the chassis dynamometer has not been fully calibrated and generally applies above-average road load to the vehicle. The results of these limitations are that true fuel consumption data is unavailable and that fuel consumption values will be higher than those obtained using the model. While this is unfortunate, initial testing using the facility is still extremely valuable and can still validate many aspects of the real-time controller, including SOC management, shift execution, ICE operation, and RTM use. Future work, once the facility is fully functional, can most certainly include fuel consumption and emissions measurement.

Both UDDS and HWFET cycles were completed on the dynamometer. However, in this section only figures for the UDDS cycle will be provided, as general results are indicative of both cycles. Data was captured by recording communication on all four of

the vehicle's CAN channels, and through the use of additional dSPACE software that allows for recording of variables internal to the MABX.

Figure 7-6 plots the axle torque over the course of the UDDS cycle for both the simulation and the in-vehicle testing to demonstrate the difference in road load.

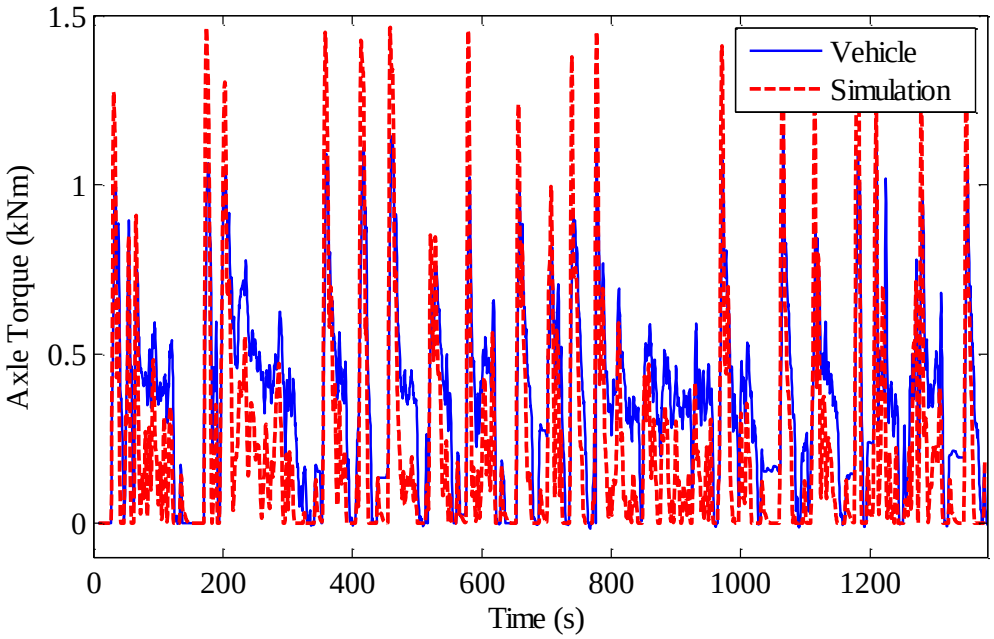

Figure 7-6: Comparison of Simulation and In-Vehicle Axle Torque

As shown, the cruising road load is much higher during in-vehicle testing, but (though it is difficult to see), the axle torque command during acceleration events is much higher in simulation. This can be attributed to a tentative driver, who undoubtedly strayed further from the speed trace during acceleration events than the simulated driver; speed differences were still within allowable/regulated bounds. The same can be said for operation on the HWFET cycle.

Figure 7-7 shows the SOC profile for the UDDS cycle; the CS SOC target was artificially set at 80.7 % for this test.

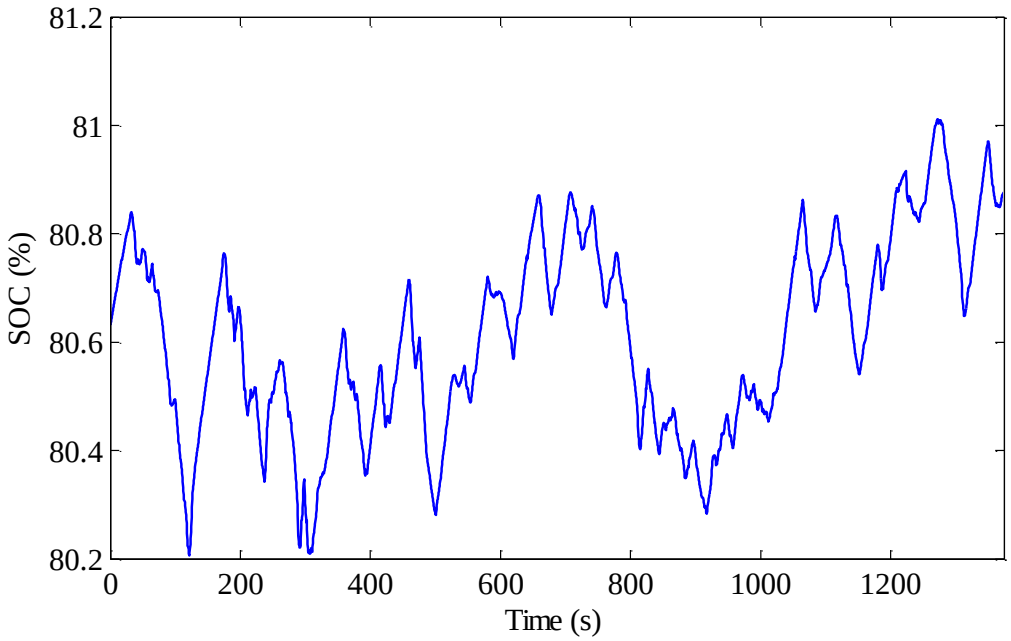

Figure 7-7: In-Vehicle Testing – UDDS SOC

Whereas in the model, the SOC was typically higher than the target on the UDDS cycle, in this case, it is mostly lower. This is most certainly due to the aforementioned higher road load on the dynamometer. The sharp increases in SOC are once again due to the fact that the ICE does not turn off during the many stops throughout the cycle. Despite the high road load, the algorithm still maintained SOC within about 0.5% during UDDS and 0.6% during HWFET.

Figure 7-8 plots shifts throughout the cycle.

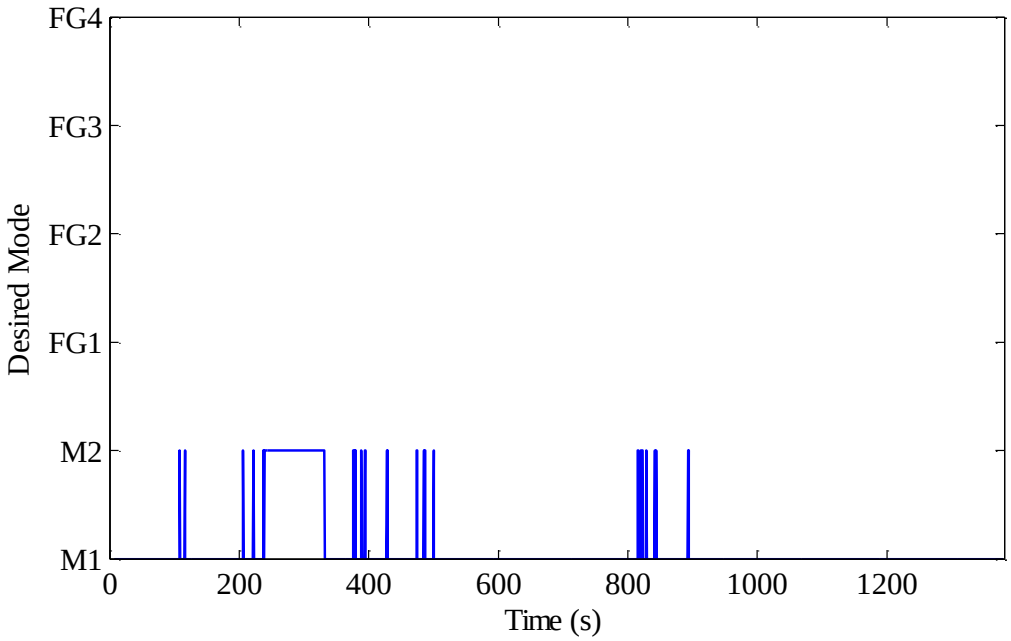

Figure 7-8: In-Vehicle Testing – UDDS Shifts

There were a total of 52 shifts in the UDDS cycle and 41 in the HWFET cycle. It appears that the shift stability issue discovered through simulation is much more problematic when a real driver takes the wheel. This may be due to the reaction of the driver as the ICE changes speed for a synchronous shift, and may also be affected by the higher road load. Either way, this suggests that a more robust gear selection strategy is required, and more in-vehicle testing must be completed in order to tune the strategy.

Anecdotally, it appeared during in-vehicle testing that shifts took much longer to occur in the vehicle as compared to in simulation. This may be a reason for the seemingly failed shifts shown in Figure 7-8 (they met the criteria for successful shifts outlined in §6.2), and further investigation is required.

ICE operation is plotted in Figure 7-9.

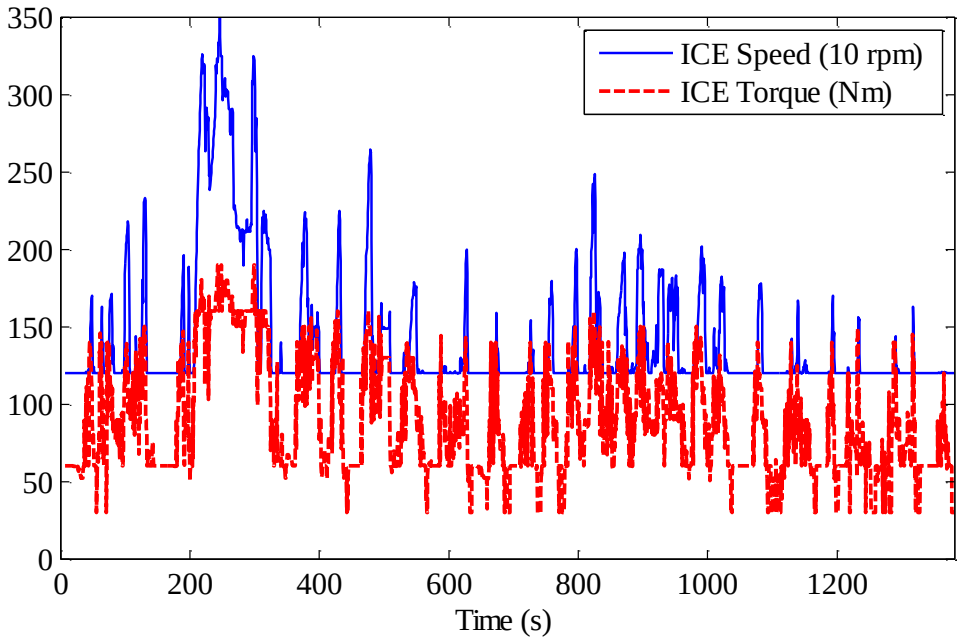

Figure 7-9: In-Vehicle Testing – ICE Operation

ICE speed increases much more frequently here, and ICE torque is higher on average as compared to the modeling results. Again, this makes sense due to the high road load on the dynamometer, and the same occurred throughout the HWFET cycle. These results are very promising, as they demonstrate that efficient ICE operating regions – high speed, high torque – are being selected during high power requests; this is confirmed in Figure 7-10.

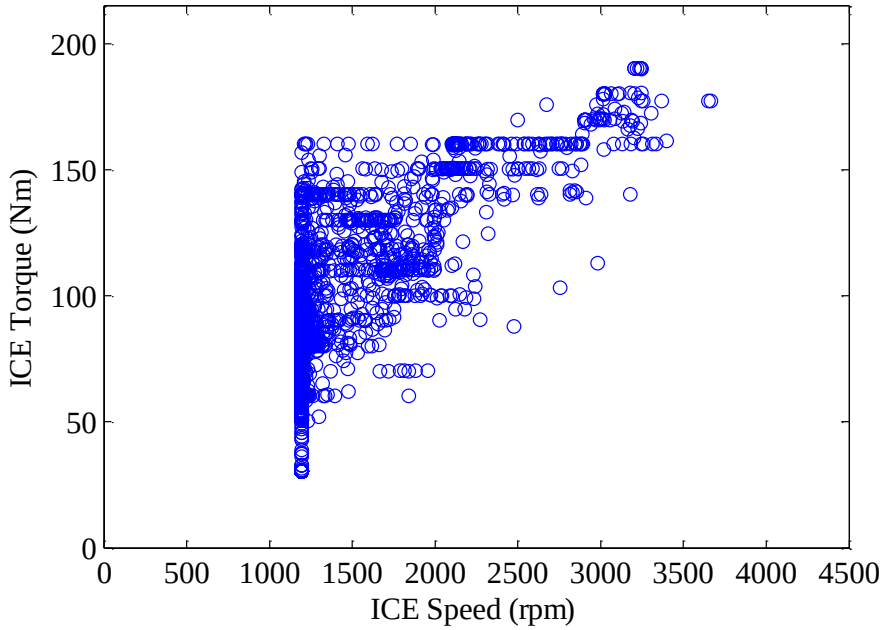

Figure 7-10: In-Vehicle Testing – UDDS Engine Operating Points

There is virtually no operation at high speeds, low torques, where the ICE is inefficient.

Also enlightening is a plot of ICE speed versus vehicle speed, shown in Figure 7-11.

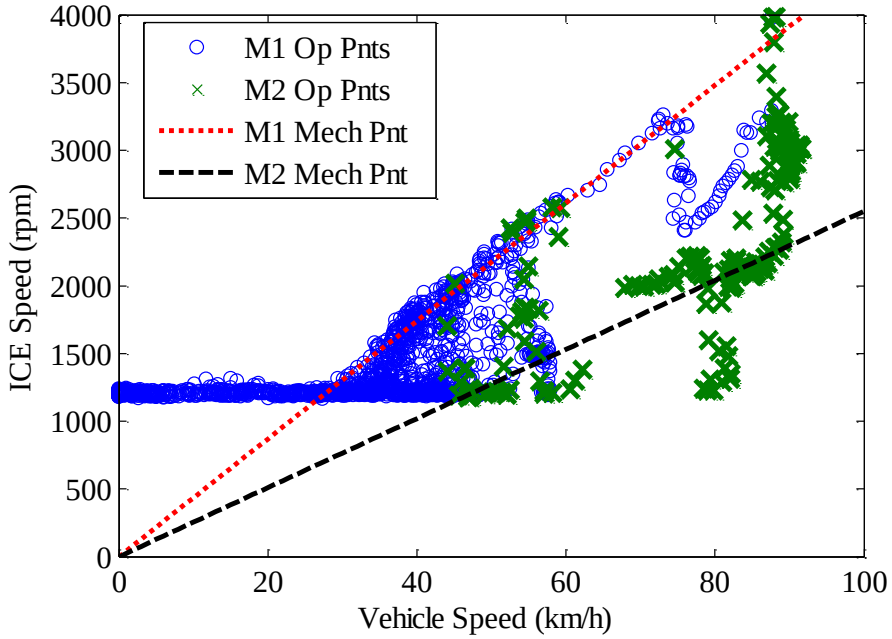

Figure 7-11: In-Vehicle Testing – ICE Operation and Mechanical Points

There is a general trend towards operating at or near the mechanical point, which is also promising. Though the ICE does operate at speeds below the mechanical point, this may be a result of gear shifting, or perhaps, may represent areas where MGB is not absorbing power. In this case, MGA would be drawing power from the ESS and MGB would not be generating power, resulting in no circulating power; refer back to §3.1.3 for a discussion of the mechanical point.

Finally, Figure 7-12 plots the traction split throughout the cycle.

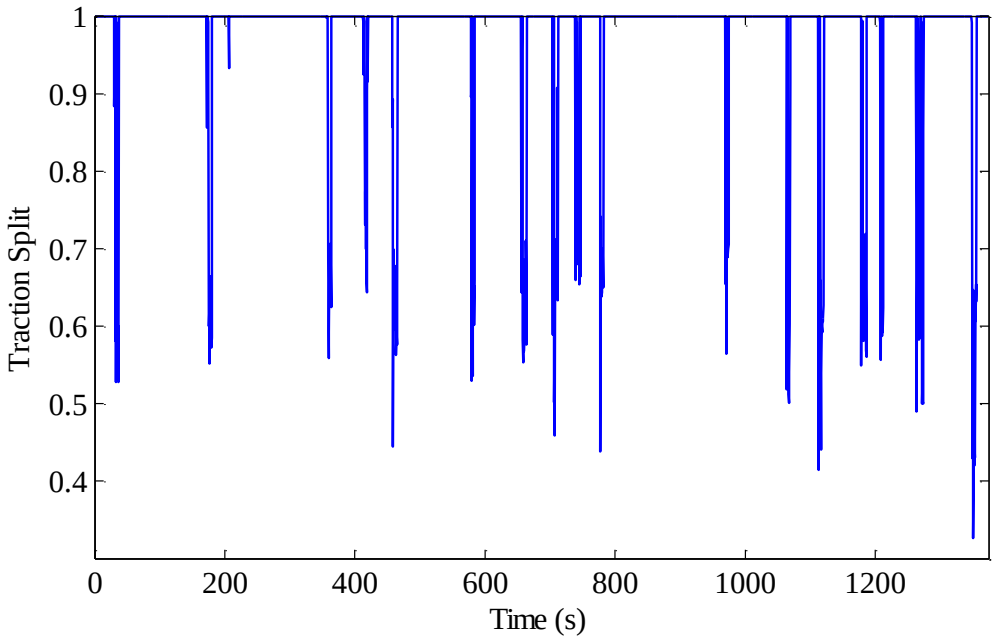

Figure 7-12: In-Vehicle Testing – UDDS Traction Split

In this case, the average traction split was 0.974 and the total propulsive power provided by the RTM was only 3.2% (0.997 and 0.03% for HWFET). This is much lower use than in the simulations, but does in fact make sense. Because in the UDDS cycle, the SOC is lower than the target (which was not the case in the simulations), the dynamic EF biases the objective function towards the use of more ICE power and less ESS power, in order to charge the ESS. Additionally, as shown in Figure 7-6, the driver during in-

vehicle testing did not apply as much axle torque during acceleration as compared to the simulated driver.

Overall, initial in-vehicle testing results are promising, and while there are still some issues to be resolved, this is expected in the vehicle design process, and should be addressed in continuing work at UVic.

7.4. Challenges in Control of a 'Plus' Architecture

It is now worth taking a step back to examine why control of the 2-Mode Plus architecture results in operation that is heavily biased to the front powertrain. Section 6.1.4 already touched on the fact that the size and gear ratio of the UVic RTM are not ideal to promote efficient RTM operation. However, there is an addition nuance to the 'Plus' architecture that makes it inherently conducive to front powertrain operation. Mode 1 will be used as an example.

Recall from Chapter 3 that in Mode 1, MGA acts as a generator and controls ICE speed, while MGB operates in parallel to the ICE, sourcing or absorbing electric power as needed. Recall also that ICE power that is not absorbed by MGA is transferred through the mechanical power path to the road; thus, if MGB operated at zero torque, the vehicle could still be propelled using ICE power alone.

In the 2-Mode plus architecture, the power absorbed by MGA could potentially be used by either MGB or the RTM, or a combination of these MGs, as shown in the simplified diagram of Figure 7-13.

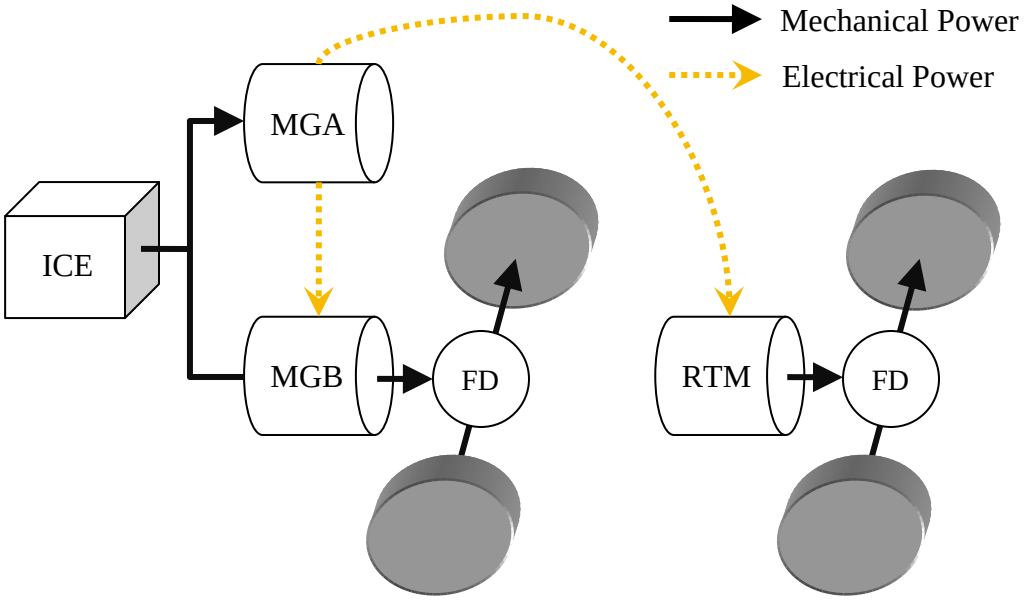

Figure 7-13: Powerflow in 2-Mode Plus Architecture

MGB, though, is already a quite efficient MG, having been designed from the ground up and sized appropriately for its task. Thus, the RTM must be equally or more efficient *under typical driving conditions* to warrant its usage over MGB; it has already been shown that this is not the case in UVic EcoCAR. In addition to this, traction splits that result in values of total front axle torque that are less than the axle torque provided by the ICE through the transmission's mechanical power path result in the use of MGB as a generator in addition to MGA, as shown in Figure 7-14.

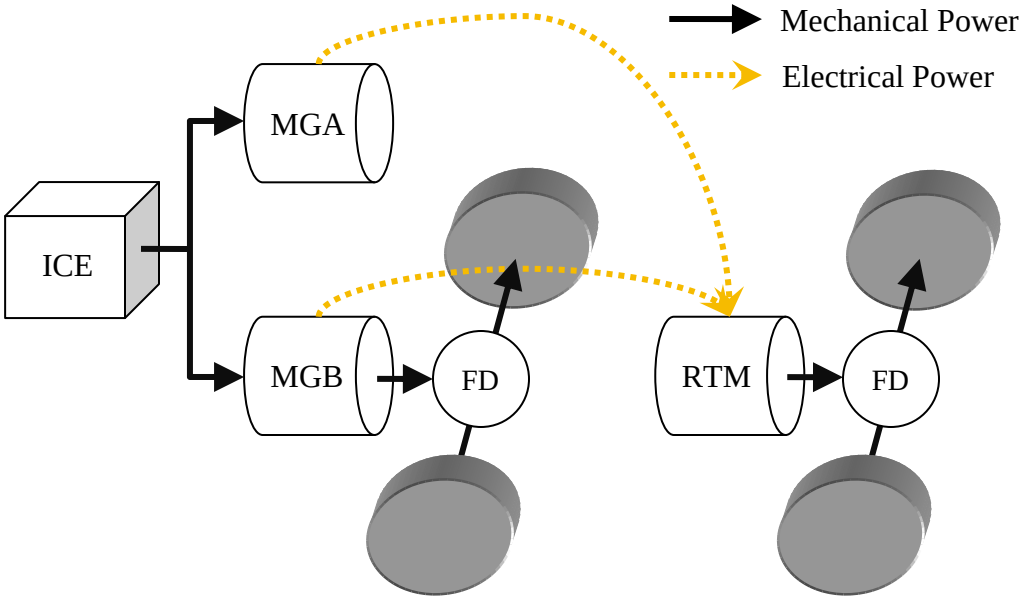

Figure 7-14: Circulating Power in 2-Mode Plus Architecture

There is no instance in which re-circulating power in this way to achieve a given axle torque could be more efficient than simply allowing the mechanical ICE power to reach the road.

Combined with the fact that high levels of ICE power relative to propulsive power are generally desired to achieve full performance, reduce electrical losses and ESS degradation, and/or improve consumer acceptability, it is not surprising that the RTM is so seldom used in the current configuration. In fact, the same may be said of any 'plus' architecture (aside from series) that has electric drive components operating on the front axle. A better method to achieve the high levels of electric power needed for EV driving without having to include a large RTM that remains essentially unused in CS mode may be to increase the size of a drive MG on the front axle. This solution may depend on the type and size of the vehicle, packaging considerations, and component availability among other things, but may warrant further consideration. Lending weight to this solution, to

achieve full EV performance with the Chevy Volt's 4ET50 transmission – based on the 2-Mode transmission, but with modifications – GM did just this, specifying a larger drive MG on the front axle [52]; the Volt, though, is a mid-sized passenger car which requires smaller MGs for full propulsion.

The UVic EcoCAR, then, presents an interesting situation given these findings. This large RTM was selected as essentially the only feasible method to provide fully functional electric operation in CD mode (the 2-Mode was not capable of providing enough all-electric power), and thus still serves a very important role in the architecture as a whole. In practice, therefore, the level of RTM utilization in the vehicle (considering both CD and CS modes) will vary based on the distance driven on a daily basis.

It is assumed based on the considerations above that even a RTM more favourable in size or with a more ideal gear ratio may not result in higher RTM use under normal circumstances. This is examined in the following section.

7.5. Possible Improvements to the 2-Mode Plus Architecture

To determine the effects of gear ratio and motor size on RTM use and overall efficiency, the optimization-based model variant was first examined using several different FD ratios through both the HWFET and UDDS drive cycles. The results are summarized in Table 7-5.

Table 7-5: FC and RTM Use versus Final Drive Ratio

Rear Final Drive	UDDS		HWFET	
	FC (Lge/100km)	RTM Use (%)	FC (Lge/100km)	RTM Use (%)
4.0	7.763	5.34	5.830	0.47
4.5	7.774	4.66	5.836	0.36
5.0	7.783	3.71	5.837	0.17
5.5	7.793	6.20	5.841	0.13
6.0	7.800	8.44	5.843	0.24
6.5	7.816	6.92	5.844	0.19
7.0	7.823	9.94	5.856	0.28
7.5	7.834	9.15	5.862	0.26

Reducing the final drive ratio does marginally improve fuel consumption for both drive cycles, but RTM use increases only marginally during highway driving and actually decreases significantly during city driving. In the case of city driving, this decrease in RTM use makes sense, since decreasing the final drive ratio decreases the relative speed of the RTM throughout the cycle. This means that at low vehicle speeds, RTM operation can be much less efficient than at similar vehicle speeds with a high ratio. This is demonstrated in Figure 7-15, which plots RTM operation at a FD ratio of 4.0 for the UDDS cycle.

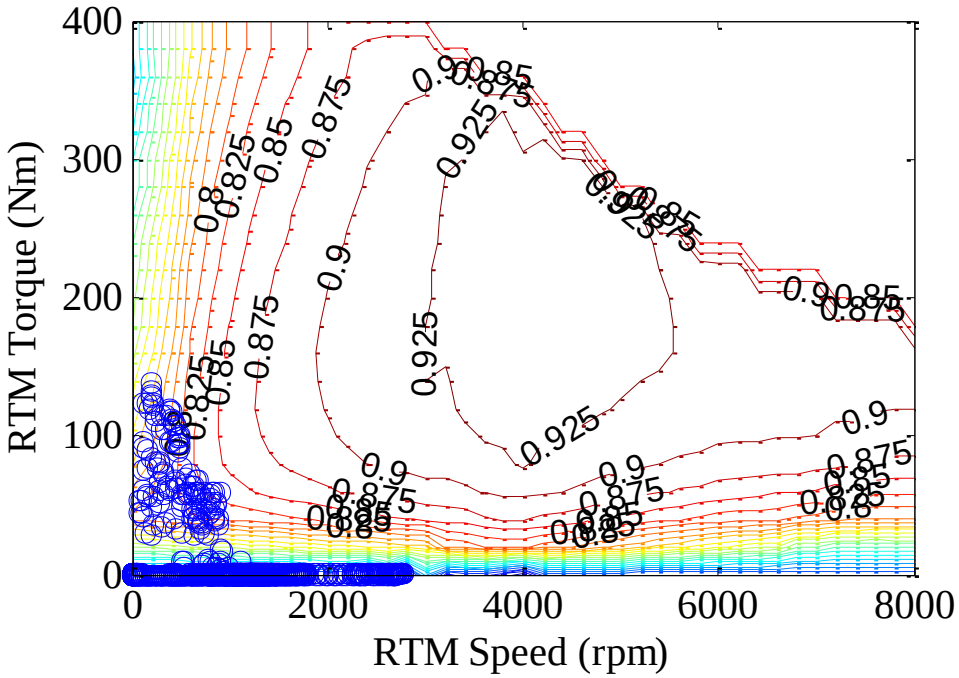

Figure 7-15: RTM Operating Points – UDDS Cycle with Rear FD of 4.0

Compared to the operating points shown in Figure 6-9, these points are located in much less efficient areas as a result of the decrease in FD ratio.

The discussion in §7.4 also warrants examining the effects of different motor sizes on RTM use and vehicle fuel consumption. Two different MGs were used in this analysis: a MG identical to MGB, and a 30 kW motor based on the 2004 model year Toyota Prius taken from PSAT (version 6.2 SP1). Both motor variants were run through the same simulations as the original UVic EcoCAR RTM, and the results are summarized in Table 7-6 and Table 7-7.

Table 7-6: FC and RTM Use versus Final Drive Ratio - MGB

Rear Final Drive	UDDS		HWFET	
	FC (Lge/100km)	RTM Use (%)	FC (Lge/100km)	RTM Use (%)
4.0	7.790	2.57	5.823	5.53
4.5	7.794	4.44	5.815	5.53
5.0	7.802	1.80	5.835	2.77
5.5	7.804	0.58	5.849	1.28
6.0	7.814	2.92	5.862	5.14
6.5	7.816	3.86	5.868	4.67
7.0	7.814	3.47	5.865	5.17
7.5	7.813	4.52	5.868	3.69

Table 7-7: FC and RTM Use versus Final Drive Ratio – Prius MG

Rear Final Drive	UDDS		HWFET	
	FE (Lge/100km)	RTM Use (%)	FC (Lge/100km)	RTM Use (%)
4.0	7.732	2.94	5.806	1.18
4.5	7.742	4.22	5.809	1.68
5.0	7.744	3.55	5.808	1.68
5.5	7.757	2.28	5.810	1.31
6.0	7.767	5.67	5.812	1.52
6.5	7.774	4.95	5.814	1.84
7.0	7.785	6.98	5.817	1.78
7.5	7.789	6.32	5.819	2.14

As predicted in the previous section, RTM usage did not rise; instead, it fell with the use of smaller motors, while fuel consumption changes across a given FD ratio for MG variants were negligible. It appears that using a small MG might not provide enough incentive in terms of relatively efficient high-power operation to warrant higher levels of use. Even with a RTM identical to MGB, meaning that at the same speed (though speeds are different at a given vehicle speed due to different front and rear gear ratios) electrical power consumption and losses are identical for both front and rear MGs, the front powertrain was used for the vast majority of the cycle. This undoubtedly relates to the fact that heavily rear-biased traction splits can result in inefficient power circulation.

CHAPTER 8 Summary and Future Work

The primary objective of this thesis was the development and application of a real-time, optimization-based control system to an all-wheel drive E-REV powertrain architecture based on GM's front-wheel drive 2-Mode transmission. The flexibility and complexity of this vehicle, due to its ECVT and AWD capabilities, necessitated the development of an equally complex control system capable of maximizing vehicle efficiency. The intent of the control development process was optimization from a system perspective, which included not only the selection of appropriate ICE/transmission operating states, but an appropriate traction split between front and rear axles.

Work was based on a specific vehicle under development at the University of Victoria through the EcoCAR Challenge program, and summarized primary steps in the design and implementation of this real-time control system: its physical integration and operation in relation to existing vehicle components; the structure and operation of various software modules within the controller; steps taken through the MBD process; development of the required real-time optimization algorithms; tuning of the controller through simulation; and finally, preliminary in-vehicle testing of the control strategy. The end result of this work was the fundamental basis of a *functional* real-time control system for the vehicle, and several insights into the complexities of hybrid vehicle powertrain architecture selection, both of which should be of value in ongoing hybrid vehicle research at UVic.

The real-time control system was designed with the flexibility to tune levels of ICE use and ESS power use, allowed for the inclusion of a four-wheel drive traction control system (while still ensuring optimal ICE operation), and left adequate controller

resources for future additions to the control system, if necessary. Results also indicated that a rule-based traction split system may be sufficient to replace an optimization-based system, which warrants further examination and perhaps in-vehicle testing.

From an architectural standpoint, an important point was revealed regarding the best way to include electric torque capability for EV operation: increasing the size of a single MG may in the end be more efficient than including a RTM to achieve the same goal. This point was not initially obvious to the UVic EcoCAR Team during architecture selection – perhaps due to the components available/examined during the selection process – but was revealed through the relatively 'opaque' process of optimization.

8.1. Research Contributions

Real-time optimization represents the cutting edge in terms of hybrid vehicle control strategies, and this thesis provided insight into the challenges associated with real-time optimization-based control from the algorithm development stage, through modeling and simulation, to implementation in the vehicle. Two key areas in the field were examined through a case study of the UVic EcoCAR vehicle. First, a method to reliably determine the global optimum solution of a three DOF optimization problem in real-time was discussed, developed, and implemented. Second, drivability, logistical, and component longevity issues in the application of real-time optimization-based control were examined, and potential solutions developed and tested. The successful in-vehicle implementation of the algorithm added significant weight to this thesis, and presented several challenges and opportunities for future work.

8.2. Future Work and Challenges

Algorithm development represents only one phase of vehicle development, and from the perspective of the EcoCAR vehicle, much work can be done and much can still be learned:

- Continuing work on the vehicle should focus primarily on increasing operational capacity. For example, the use of fixed gears or the resolution of the ICE idle-stop issues would improve vehicle operation and perhaps reveal further topics for investigation.
- An alternative or improved method for shifting can be investigated, implemented, and tested in the vehicle.
- Further testing, including in the vehicle, of rule- and optimization-based traction split systems can be performed to assess effects on fuel consumption and drivability.
- Alternative and perhaps dynamic implementations of the power factor (§6.3), and more advanced dynamic implementations of the EF (§6.4) could be investigated through further algorithm development, simulation, and in-vehicle testing.
- Finally, resolving initial issues with new equipment in the UVic Hybrid Vehicle Center can lead to further and more revealing testing through the use of emissions equipment.

From a broader perspective, the work completed in this thesis sets the foundation for possible larger studies that could encompass topics such as:

- The use of further optimization and/or drive pattern recognition in order to modify control system parameters (such as the power factor or EF) on-the-fly.
- The implementation of GPS technology to reveal information regarding the future of the current drive cycle, so as to allow for true optimal control.
- The training of neural network- or fuzzy logic-based systems using the current optimization algorithms.

Notably, UVic has been accepted into EcoCAR 2: Plugging into the Future, the next iteration of the EcoCAR challenge that runs from September 2011 to the summer of 2014. It is hoped that the work done in this thesis provides a solid foundation upon which future EcoCAR Team members, as well as other researchers at UVic, can build, perhaps taking into consideration the future work suggested above.

Bibliography

[1] U.S. Energy Information Administration. (2010). Annual Energy Review 2009. [Online]. Available: http://www.eia.gov/totalenergy/data/annual/pdf/aer.pdf

[2] U.S. Energy Information Administration. (2011). Monthly Energy Review - August 2011. [Online]. Available: http://www.eia.gov/totalenergy/data/monthly/pdf/mer.pdf

[3] Intergovernmental Panel on Climate Change. (2008). Climate Change 2007: Synthesis Report; Causes of Change. [Online]. Available: http://www.ipcc.ch/publications_and_data/ar4/syr/en/spms2.html

[4] J. Wise, "A Real-Time Hybrid Vehicle Control Strategy and Testing Platform," M.A.Sc, Department of Mechanical Engineering, University of Victoria, Victoria, British Columbia, Canada, 2011.

[5] M. Ehsani, *et al.*, "Hybrid Electric Vehicles: Architecture and Motor Drives," *Proceedings of the IEEE*, vol. 95, pp. 719-728, 2007.

[6] J. D. Wishart, *et al.*, "Review of multi-regime hybrid vehicle powertrain architecture," *Int. J. Electric and Hybrid Vehicles*, 2008.

[7] V. Wouk, "Hybrids: then and now," *Spectrum, IEEE*, vol. 32, pp. 16-21, 1995.

[8] J. M. Miller, "Hybrid electric vehicle propulsion system architectures of the e-CVT type," *IEEE Transactions on Power Electronics*, vol. 21, pp. 756-767, 2006.

[9] L. Y. Zhou, *et al.*, "Design, Modeling, and Hardware Implementation of a Next Generation Extended Range Electric Vehicle," *SAE Publication*, 2010.

[10] S&T Consultants Inc. *GHGenius - A model for life cycle assessment of transportation fuel* Available: http://www.ghgenius.ca/

[11] U.S. Department of Transportation. *National Household Travel Survey*. Available: http://npts.ornl.gov/

[12] SAE, "J2841 - Utility Factor Definitions for Plug-In Hybrid Electric Vehicles Using 2001 U.S. DOT National Household Travel Survey Data," 2009.

[13] SAE, "J1711 - Recommended Practice for Measuring the Exhaust Emissions and Fuel Economy of Hybrid-Electric Vehicles, Including Plug-in Hybrid Vehicles," ed, 2010.

[14] US Environmental Protection Agency. *Dynamometer Driver's Aid*. Available: http://www.epa.gov/nvfel/testing/dynamometer.htm

[15] Argonne National Laboratory. (2010). *Powertrain System Analysis Toolkit (PSAT)*. Available: http://www.transportation.anl.gov/modeling_simulation/PSAT/index.html

[16] F. R. Salmasi, "Control strategies for hybrid electric vehicles: evolution, classification, comparison, and future trends," *IEEE Transactions on Vehicular Technology*, vol. 56, pp. 2393-404, 2007.

[17] D. A. Crolla, *et al.*, "Controller design for hybrid vehicles - state of the art review," in *2008 IEEE Vehicle Power and Propulsion Conference (VPPC), 3-5 Sept. 2008*, Piscataway, NJ, USA, 2008, p. 6 pp.

[18] S. G. Wirasingha and A. Emadi, "Classification and review of control strategies for plug-in hybrid electric vehicles," in *2009 IEEE Vehicle Power and Propulsion Conference (VPPC), 7-10 Sept. 2009*, Piscataway, NJ, USA, 2009, pp. 907-14.

[19] Y. Cheng, *et al.*, "Global modeling and control strategy simulation for a hybrid electric vehicle using electrical variable transmission," in *Vehicle Power and Propulsion Conference, 2008. VPPC '08. IEEE*, 2008, pp. 1-5.

[20] S. Chen, *et al.*, "Realization of an energy management strategy for a series-parallel hybrid electric vehicle," in *Vehicle Power and Propulsion Conference, 2008. VPPC '08. IEEE*, 2008, pp. 1-6.

[21] MathWorks Inc. (2011, August 2011). Fuzzy Logic Toolbox User's Guide. Available: http://www.mathworks.com/help/toolbox/fuzzy/fuzzy_ug_collection.html

[22] R. Chen, *et al.*, "The application of fuzzy-neural network on control strategy of hybrid vehicles," in *Control Conference, 2008. CCC 2008. 27th Chinese*, 2008, pp. 281-284.

[23] H. Hannoun, *et al.*, "Energy management strategy for a parallel hybrid electric vehicle using fuzzy logic," Taormina, Italy, 2006, pp. 230-234.

[24] A. S. Sarvestani and A. A. Safavi, "A novel optimal energy management strategy based on fuzzy logic for a Hybrid Electric Vehicle," in *Vehicular Electronics and Safety (ICVES), 2009 IEEE International Conference on*, 2009, pp. 141-145.

[25] L. Hyeoun-Dong and S. Seung-Ki, "Fuzzy-logic-based torque control strategy for parallel-type hybrid electric vehicle," *IEEE Transactions on Industrial Electronics*, vol. 45, pp. 625-32, 1998.

[26] Y. Lianghui, *et al.*, "Research of fuzzy logic control strategy for engine start/stop in dual-clutch hybrid electric vehicle," in *Fuzzy Systems and Knowledge Discovery (FSKD), 2010 Seventh International Conference on*, 2010, pp. 912-917.

[27] T. A. Anderson, *et al.*, "Design and optimization of a fuzzy-rule based hybrid electric vehicle controller," in *Vehicle Power and Propulsion Conference, 2008. VPPC '08. IEEE*, 2008, pp. 1-7.

[28] L. V. Perez, *et al.*, "Optimization of power management in an hybrid electric vehicle using dynamic programming," *Mathematics and Computers in Simulation*, vol. 73, pp. 244-254, 2006.

[29] M. Montazeri-Gh, *et al.*, "Application of genetic algorithm for optimization of control strategy in parallel hybrid electric vehicles," *Journal of the Franklin Institute*, vol. 343, pp. 420-435, 2006.

[30] O. Kyoungcheol, *et al.*, "Optimization of control strategy for a single-shaft parallel hybrid electric vehicle," *Proceedings of the Institution of Mechanical Engineers, Part D (Journal of Automobile Engineering)*, vol. 221, pp. 555-65, 2007.

[31] A. Piccolo, *et al.*, "Optimisation of energy flow management in hybrid electric vehicles via genetic algorithms," Como, 2001, pp. 434-439.

[32] L.-C. Fang and S.-Y. Qin, "Concurrent Optimization for Parameters of Powertrain and Control System of Hybrid Electric Vehicle Based on Multi-Objective Genetic Algorithms " presented at the SICE-ICASE International Joint Conference, Bexo, Busan, Korea, 2006.

[33] Y. Shichun, *et al.*, "Optimization of Fuzzy Controller Based on Genetic Algorithm," in *Intelligent System Design and Engineering Application (ISDEA), 2010 International Conference on*, 2010, pp. 21-28.

[34] X. Chang-jun, *et al.*, "Control strategy of hybrid power system for Fuel Cell Electric Vehicle based on neural network optimization," in *Automation and Logistics, 2008. ICAL 2008. IEEE International Conference on*, 2008, pp. 753-757.

[35] G. Paganelli, *et al.*, "Equivalent consumption minimization strategy for parallel hybrid powertrains," Birmingham, AL, USA, 2002, pp. 2076-81.

[36] S. Delprat, *et al.*, "Optimal control of a parallel powertrain: from global optimization to real time control strategy," in *Vehicular Technology Conference, 2002. VTC Spring 2002. IEEE 55th*, 2002, pp. 2082-2088 vol.4.

[37] A. Sciarretta, *et al.*, "Optimal control of parallel hybrid electric vehicles," *Control Systems Technology, IEEE Transactions on*, vol. 12, pp. 352-363, 2004.

[38] C. Musardo, *et al.*, "A-ECMS: An Adaptive Algorithm for Hybrid Electric Vehicle Energy Management," in *Decision and Control, 2005 and 2005*

European Control Conference. CDC-ECC '05. 44th IEEE Conference on, 2005, pp. 1816-1823.

[39] J. Meisel, "Kinematic Study of the GM Front-Wheel Drive Two-Mode Transmission and the Toyota Hybrid System THS-II Transmission," presented at the 2011 SAE World Congress, Detroit, MI, 2011.

[40] J. Waldner, *et al.*, "Developemnt and Testing of an Advanced Extended Range Electric Vehicle," presented at the 2011 SAE World Congress, Detroit, MI, 2011.

[41] dSPACE Inc. *dSPACE MicroAutoBox II* Available: http://www.dspaceinc.com/en/inc/home/products/hw/micautob.cfm

[42] J. Ferreira, "MDAI: Model based design in automobile industry," in *Industrial Informatics, 2009. INDIN 2009. 7th IEEE International Conference on*, 2009, pp. 434-439.

[43] P. Struss and C. Price. (2003) Model-Based Systems in the Automotive Industry. *AI Magazine*. Available: http://www.aaai.org/ojs/index.php/aimagazine/article/view/1728

[44] D. H. Stamatis, *Failure Mode and Effect Analysis: FMEA from Theory to Execution*, 2nd ed.: ASQ Quality Press, 2003.

[45] J. R. Anstrom, *et al.*, "Simulation and field-testing of hybrid ultra-capacitor/battery energy storage systems for electric and hybrid-electric transit vehicles," Austin, TX, United States, 2005, pp. 491-497.

[46] UQM Technologies Inc. *UQM® PowerPhase® Hybrid Electric Propulsion Systems*. Available: http://www.uqm.com/hybrid%20systems.html

[47] A123 Systems Inc. *AMP20 Prismatic Pouch Cell*. Available: http://www.a123systems.com/products-cells-prismatic-pouch-cell.htm

[48] B. Yann Liaw, *et al.*, "Modeling of lithium ion cells--A simple equivalent-circuit model approach," *Solid State Ionics*, vol. 175, pp. 835-839, 2004.

[49] H. Yang, *et al.*, "Development of Two-Mode Hybrid Powertrain with Enhanced EV Capability," presented at the 2011 SAE World Congress, Detroit, MI, 2011.

[50] US Department of Energy. *Fuel Economy of 2009 Saturn VUE* [Online]. Available: http://www.fueleconomy.gov/feg/bymodel/2009_Saturn_Vue.shtml

[51] US Environmental Protection Agency. *EPA's Fuel Economy Programs* [Online]. Available: http://www.epa.gov/fueleconomy/420f09067.htm

[52] M. A. Miller, *et al.*, "The GM "Voltec" 4ET50 Multi-Mode Electric Transaxle," presented at the 2011 SAE World Congress, Detroit, MI, 2011.